E-ISSN: 2147-1959

MIRT

Molecular Imaging and Radionuclide Therapy

June 2025 Volume 34 Issue 2 www.tsnm.org

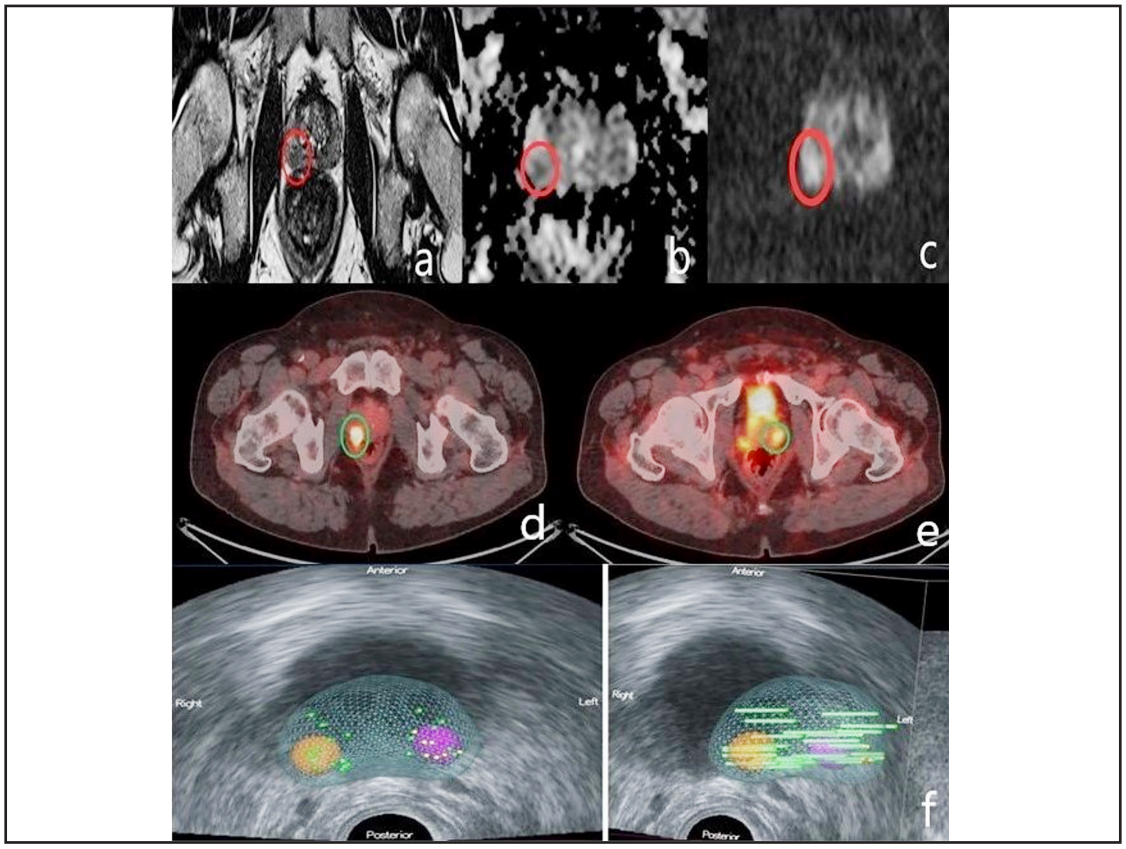

"Official Journal of the Turkish Society of Nuclear Medicine"

galenos yayınevi

TURKISH SOCIETY OF NUCLEAR MEDICINE 1975

MIRT

Molecular Imaging and Radionuclide Therapy

MIRT

Molecular Imaging and Radionuclide Therapy

Turkish Society of Nuclear Medicine
Cinnah Caddesi Pilot Sokak No: 10/12 Çankaya 06650 Ankara, Türkiye **Phone:** +90 312 441 00 45 **Fax:** +90 312 441 12 95 **Web:** www.tsnm.org **E-mail:** dernekmerkezi@tsnm.org
"Formerly Turkish Journal of Nuclear Medicine"

Reviewing the articles' conformity to the publishing standards of the Journal, typesetting, reviewing and editing the manuscripts and abstracts in English, creating links to source data, and publishing process are realized by Galenos.

Publisher Contact
Address: Molla Gürani Mah. Kaçamak Sk. No: 21/1 34093 İstanbul, Türkiye
Phone: +90 (530) 177 30 97 / +90 (539) 307 32 03
E-mail: info@galenos.com.tr/yayin@galenos.com.tr
Web: www.galenos.com.tr
Publisher Certificate Number: 14521

Online Publication Date: June 2025
ISSN: 2146-1414 **E-ISSN:** 2147-1959
International scientific journal published quarterly.

MIRT

Molecular Imaging and Radionuclide Therapy

Please refer to the journal's webpage **(https://mirt.tsnmjournals.org/)** for "Aims and Scope", "Instructions to Authors" and "Ethical Policy".

The editorial and publication process of Molecular Imaging and Radionuclide Therapy are shaped in accordance with the guidelines of ICMJE, WAME, CSE, COPE, EASE, and NISO. The journal is in conformity with the Principles of Transparency and Best Practice in Scholarly Publishing.

Molecular Imaging and Radionuclide Therapy is indexed in **Pubmed, Pubmed Central (PMC), Emerging Sources Citation Index (ESCI), TUBITAK-ULAKBIM, Scopus, Gale/Cengage Learning, EBSCO databases, ProQuest Health & Medical Complete, CINAHL, Embase, J-Gate, IdealOnline, Türkiye Atıf Dizini-Turkiye Citation Index, Turk Medline, Hinari, GOALI, ARDI, OARE, AGORA** and **CNKI**.

The journal is published electronically.

Owner: Murat Fani Bozkurt on Behalf of Turkish Society of Nuclear Medicine

Responsible Manager: Murat Fani Bozkurt

MIRT
Molecular Imaging and Radionuclide Therapy

CONTENTS

Original Articles

Interesting Images

MIRT
Molecular Imaging and Radionuclide Therapy

CONTENTS

Case Report

Original Article

Mol Imaging Radionucl Ther 2025;34:90-96 *DOI:10.4274/mirt.galenos.2025.93797*

The Effect of GLUT-1-XbaI G>T and HaeIII T>C Polymorphisms on ^{18}F-FDG Uptake Rates

GLUT-1-XbaI G>T ve HaeIII T>C Polimorfizmlerinin ^{18}F-FDG Alım Oranları Üzerindeki Etkisi

Melih Kısaarslan[1], Yasemin Adalı[1], Veli Kaan Aydın[1], Yasemin Berberoğlu[1], Doğangün Yüksel[2], Aylin Köseler[1]

[1]*Pamukkale University Faculty of Medicine, Department of Biophysics, Denizli, Türkiye*
[2]*Pamukkale University Faculty of Medicine, Department of Nuclear Medicine, Denizli, Türkiye*

Abstract

Objectives: To investigate the effects of glut polymorphisms on ^{18}Fluorine-fluorodeoxyglucose (^{18}F-FDG) uptake rates.

Methods: The ^{18}F-FDG positron emission tomography/computed tomography images and mass lesion metabolism standard uptake value maximum (SUV_{max}) results of the patients were evaluated. Glucose transporter protein-1 (GLUT-1)-XbaI G>T (rs2754218) and HaeIII T>C (rs1385129) polymorphisms and their effects on ^{18}F-FDG uptake rates were investigated using DNA obtained from peripheral blood.

Results: When the XbaI G>T genotype distribution of the patients was examined, the XbaI G/G genotype was found to be 87%, the XbaI G/T genotype 12%. The XbaI T/T phenotype was detected in only one patient (1%). In the HaeIII T>C genotype distribution, the HaeIII C/C genotype was found as 54%, the HaeIII T/C genotype as 31%, and the HaeIII T/T genotype as 15%. When the XbaI and HaeIII genotypes were examined together, the number of polymorphic genotypes was significantly higher in the lung and bronchial tumor groups compared to other cancer types.

Conclusion: The presence of polymorphism in at least one of the two gene regions, in the lung-bronchial tumor group and the high SUV_{max} value in this patient group, may indicate a change in the involvement rates.

Keywords: Glucose transporter protein-1 polymorphism, ^{18}Fluorine-fluorodeoxyglucose, positron emission tomography imaging, glucose transporter protein-1-XbaI G>T (rs2754218), HaeIII T>C (rs1385129)

Öz

Amaç: Glut polimorfizmlerinin ^{18}Flor-florodeoksiglukoz (^{18}F-FDG) alım oranları üzerindeki etkisinin araştırılmasıdır.

Yöntem: Hastaların pozitron emisyon tomografisi/bilgisayarlı tomografi görüntüleri ve kitle lezyon metabolizması standart alım değeri maksimum (SUV_{maks}) sonuçları değerlendirildi. Periferik kandan alınan DNA ile hastalarda glikoz taşıyıcı protein-1 (GLUT-1)-XbaI G>T (rs2754218) ve HaeIII T>C (rs1385129) polimorfizmleri ve ^{18}F-FDG tutulum oranlarına etkileri araştırıldı.

Bulgular: Hastaların XbaI G>T genotip dağılımına bakıldığında, XbaI G/G genotipi %87; XbaI G/T genotipi %12 olarak bulundu. XbaI T/T fenotipi sadece 1 hastada (%1) tespit edildi. HaeIII T>C genotip dağılımında, HaeIII C/C genotipi %54; HaeIII T/C genotipi %31; HaeIII T/T genotipi %15 olarak bulundu. XbaI ve HaeIII genotipleri birlikte incelendiğinde, polimorfik genotip sayısının akciğer ve bronşiyal tümör gruplarında diğer kanser tiplerine göre anlamlı derecede yüksek olduğu görülmüştür.

Address for Correspondence: Aylin Köseler, Pamukkale University Faculty of Medicine, Department of Biophysics, Denizli, Türkiye
E-mail: akoseler@pau.edu.tr **ORCID ID:** orcid.org/0000-0003-4832-0436
Received: 10.12.2024 **Accepted:** 09.03.2025 **Publication Date:** 03.05.2025

Cite this article as: Kısaarslan M, Adalı Y, Aydın VK, Berberoğlu Y, Yüksel D, Köseler A. The effect of GLUT-1-XbaI G>T and HaeIII T>C polymorphisms on ^{18}F-FDG uptake rates. Mol Imaging Radionucl Ther. 2025;34:90-96.

Öz

Sonuç: Akciğer-bronşiyal tümör grubunda hastalardaki iki gen bölgesinden en az birinde polimorfizmin olması ve bu hasta grubunda SUV_{maks} değerinin yüksek olması tutulum oranlarında bir değişikliğe işaret edebilir.

Anahtar kelimeler: Glikoz taşıyıcı protein-1, ^{18}Flor-florodeoksiglukoz, pozitron emisyon tomografisi görüntüleme, glikoz taşıyıcı protein-1-XbaI G>T (rs2754218), HaeIII T>C (rs1385129)

Introduction

Glucose transporter protein-1 (GLUT-1) is the most widely distributed GLUT isoform in the human body. It is expressed on the surface of almost all types of cells. Glucose transport via GLUT-1 is driven by a gradient across the cell membrane. Glucose transporters comprise a family of facilitative transporters that are divided into three classes. GLUT-1 is a member of class 1 and is highly expressed in glomeruli, mesangial cells, endothelial cells, and podocytes. It is also insulin-independent (1).

The *GLUT-1* gene (SLC2A1) (rs841853) is located on chromosome 1p34.2 and contains 10 exons and 9 introns. Single nucleotide polymorphisms are variations in DNA sequence that occur when a single nucleotide in the genome differs between members of a species. This small variance in DNA sequence can affect the development of certain diseases or the response to pathogens, drugs, or other agents. Accordingly, single nucleotide polymorphisms of the *GLUT-1* gene, located on chromosome 1p35-p31.3, are known to have potential functional effects on diabetic nephropathy, vascular calcifications, renal carcinoma risk, and the uptake of 2-(^{18}F) ^{18}Fluorine-fluorodeoxyglucose (^{18}F-FDG) related to cancer risk (2).

Positron emission tomography/computed tomography (PET/CT) imaging, which detects the glucose analog ^{18}F-FDG, provides the opportunity to obtain both anatomical and metabolic information about a tumor. ^{18}F-FDG accumulates in tumor cells because rapidly growing cancer cells have the ability to increase glucose metabolism. A positive correlation has been shown between tumor ^{18}F-FDG uptake and tumor aggressiveness (3).

GLUT-1 is a key rate-limiting molecule in the transport and metabolism of glucose in cancer cells. It is also expressed in several human carcinomas. The upregulation of GLUT-1 suggests that it plays a crucial role in tumor biology. Therefore, it is hypothesized that increased expression of GLUT-1 in human carcinomas indicates improved metabolism and energy utilization, as well as more aggressive behavior. High protein expression of GLUT-1 has been observed in most urothelial carcinomas, which is related to tumor stages and grades, as well as poor tumor differentiation prognosis (4). The uptake mechanism and biochemical pathway of ^{18}F-FDG have been extensively studied both *in vitro* and *in vivo*. The transport of ^{18}F-FDG across the cell membrane via glucose transport proteins and intracellular phosphorylation by hexokinase has been identified as key steps (5).

^{18}F-FDG PET/CT is an imaging modality capable of detecting functional tumor tissue. This is made possible by the increased glucose metabolism characteristic of tumors. Images obtained through this method are superimposed with CT images, allowing for both visual and quantitative assessment, thus providing anatomical and metabolic information about the tumor.

The standardized uptake value (SUV) in tumor tissue is adjusted for the given dose and the patient's weight, reflecting the average activity. ^{18}F-FDG enters the cell via facilitated diffusion with the help of GLUT transporters (6). It is then phosphorylated by the enzyme hexokinase into ^{18}F-FDG-6-phosphate, leading to its accumulation within the cell. Cancer cells exhibit increased GLUT-1 expression. Polymorphisms can influence gene expression and protein function (7). This study aimed to investigate the impact of GLUT-1-XbaI G>T (rs2754218) and HaeIII T>C polymorphisms on ^{18}F-FDG uptake.

Materials and Methods

Data Sampling

Our study included patients who applied to Pamukkale University Faculty of Medicine, Department of Nuclear Medicine, PET/CT unit for ^{18}F-FDG oncological whole-body PET/CT due to malignancy investigation. These patients had a preliminary diagnosis or were diagnosed with cancer, had not received any treatment, and were going to undergo ^{18}F-FDG PET for the first time. Patients with a definite pathological diagnosis of cancer constituted the study group. The control group will consist of those reported as normal on the ^{18}F-FDG PET/CT study or those reported as benign by pathology, even if there are abnormal uptake findings.

This study included 100 patients and 100 healthy individuals in the control group. PET/CT images of the patients were evaluated to assess mass lesion metabolism and the presence of metastatic foci. This was a prospective case-control study, and its protocol was approved by the Pamukkale University Non-Interventional Clinical Research

Ethics Committee (number: E-60116787-020-5047, date: 05.01.2021). All procedures carried out on patients were in accordance with the Helsinki Declaration.

^{18}F-FDG PET/CT Procedure

All patients were instructed to fast for 4 hours prior to the intravenous administration of ^{18}F-FDG. Before ^{18}F-FDG injection, the blood glucose levels of all patients are checked, and 3.7 MBq/kg ^{18}F-FDG is administered intravenously to patients with blood glucose levels below 160 mg/dL. Whole-body PET/CT scans were acquired approximately 45-60 minutes after injection using a PET/CT unit (Gemini TF TOF PET/CT; Philips, Cleveland, OH, USA). The system consists of a full-ring dedicated PET scanner and a 2-slice spiral CT scanner.

The imaging protocol involved patient preparation with 1,500 mL of water-based oral contrast agent, and intravenous injection of 140 mL of contrast medium (Ultravist 300; Schering AG). A CT scan (100 mA at 130 kV) was acquired first, followed by a PET scan (3 dimensions, emission time, 4-6 min/bed position depending on body weight). A pulmonary gating technique in both PET and CT scans was used to avoid artifacts caused by breathing. Standardized uptake value was determined in tumor tissue as a measure of ^{18}F-FDG uptake using a region of interest technique. PET images, non-contrast low-dose CT images, and PET/CT fusion images are examined with visual and semiquantitative SUV_{max} values.

GLUT-1 Genotyping

DNA samples were isolated from the peripheral blood of the patients immediately before the PET/CT scan and stored at -20 °C. GLUT-1-XbaI G>T (rs2754218) and HaeIII T>C (rs1385129) polymorphisms were determined from the extracted genomic DNA using the standard phenol-chloroform method. The primers used in both polymerase chain reaction amplification and DNA sequencing are listed in Table 1 (4,8).

Statistical Analysis

This study utilized a power analysis to determine the required sample size, aiming for a medium-high effect size (f=0.4), with 95% confidence and 90% power. As a result of the analysis, it was found that at least 84 participants were needed for the patient group. To account for a possible 15% loss of data, 100 patients were included in the study, while the control group was also formed with 100 patients. Data analysis was performed using SPSS 25 software. Continuous variables were presented as mean ± standard deviation, while categorical variables were presented as counts and percentages. Genotype data frequency analysis was employed to determine the distribution of patient genotypes. One-way ANOVA was used to compare differences among more than two independent groups when the assumptions for parametric tests were met. The Mann-Whitney U test was used for group comparisons when parametric assumptions were not met. Spearman correlation analysis was used to examine the relationships between continuous variables. Fisher's exact test was used to assess differences between categorical variables. A p-value of less than 0.05 was considered statistically significant for all analyses.

Results

The DNA sequence analysis results of the GLUT-1 XbaI G>T(rs2754218) polymorphism are shown in Figure 1.

The DNA sequence analysis result of the GLUT-1 HaeIII T>C (rs1385129) polymorphism is shown in Figure 2.

When the XbaI G>T genotype distribution was examined, the XbaI G/G genotype was seen at a rate of 87%, and the XbaI G/T genotype was seen at a rate of 12%. The XbaI T/T genotype was detected in only 1 patient (1%). In the HaeIII T/C genotype distribution, C/C genotype was detected at 54%, T/C genotype at 31%, and T/T genotype at 15% (Table 2).

SUV_{max} Primer values were determined as 11.65±12.7 in the melanoma group, 11.09±5.48 in the lung-bronchial tumors group, 10.73±3 in the urogenital tumors group, 2.15±4.8 in the gastrointestinal system (GIS) tumors group, and 5.26±2.19 in the breast cancer group. PET/CT images and SUV_{max} values of the patients with lung-bronchial cancer diagnosis are shown in Figure 3 (Table 3).

When the cancer types were examined according to the system in which the cancer was seen, the patient group was divided into subgroups as melanoma, lung-bronchial

Table 1. PCR and DNA sequencing primers

	Primers	PCR product
GLUT-1 G>T (rs2754218)	**F:** 5'-TGC AAC CCA TGA GCT AAC AA-3' **R:** 5'-GAA CCC AGC ACT CTG TAG CC-3'	305 bp
GLUT-1 T>C (rs1385129)	**F:** 5'-CTC CCA GAC ACG CCT ATA ACA GT-3' **R:** 5'-GGC TGG TGT CCA TAA GCC AAC G-3'	173 bp

PCR: Polymerase chain reaction, GLUT-1: Glucose transporter protein-1

tumors, urogenital tumors, GIS tumors, breast cancer and other. While the XbaI G/G genotype was found in all patients with melanoma, urogenital tumors, GIS tumors, breast cancer, and other cancer subgroups, the XbaI G/G, G/T, and T/T genotypes were seen in lung-bronchial tumors. In melanoma and urogenital tumors, the HaeIII C/C genotype was seen, while in other tumor types, all genotypes were detected (Table 4).

In addition, XbaI and HaeIII genotypes were evaluated together, and the relationship between cancer types and both genotypes was examined. It was shown that the number of polymorphic genotypes was significantly higher, especially in the lung and bronchial tumor group, compared to other cancer types.

The relationship between XbaI and HaeIII genotypes, and SUV is shown in Table 5. The genotypes with the highest SUV_{max} values were identified to be XbaI G/G and HaeIII C/C and XbaI G/T and HaeIII T/T.

Finally, Table 6 demonstrates the age distribution of the patients, revealing a mean age of 57.8 years with a range between 20 and 87 years. Table 7 presents the gender

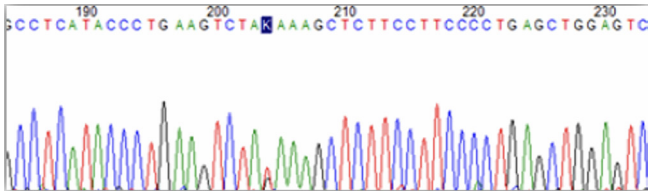

Figure 1. K indicates that the G>T nucleotide change in the sequence analysis is inherited in heterozygous form

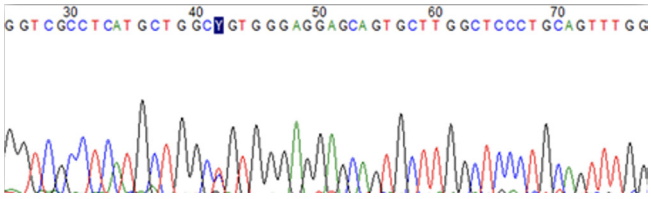

Figure 2. Y indicates that the C>T nucleotide change in the sequence analysis was inherited in a heterozygous form

Table 2. Genotype distributions of patient and control groups

	Patients genotype n (%)	Control genotype n (%)
GLUT-1 XbaI G>T (rs2754218)	**G/G** 87 (87%) **G/T** 12 (12%) **T/T** 1 (1%)	**G/G** 87 (87%) **G/T** 13 (13%)
GLUT-1 HaeIII T>C (rs1385129)	**C/C** 54 (54%) **T/C** 31 (31%) **T/T** 15 (15%)	**C/C** 48 (48%) **T/C** 42 (42%) **T/T** 10 (10%)

GLUT-1: Glucose transporter protein-1

Table 3. Cancer types and SUV_{max} results of PRIMARY tumor

Type of cancer	SUV_{max} (mean ± standard deviation)
Melanoma	11.65±12.7
Lung-bronchial tumors	11.09±5.48
Urogenital tumors	10.73±3
GIS tumors	2.15±4.8
Breast cancer	5.26±2.19
Other	9.75±5.38

SUV_{max}: Maximum standardized uptake value, GIS: Gastrointestinal system

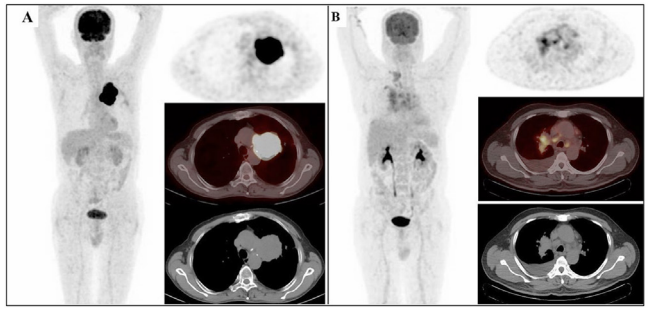

Figure 3. PET/CT images of patients with lung-bronchial cancer
PET/CT images of a 70-year-old male showing the left lung. SUV_{max}: 7.56. (XbaI G>T genotype: G/G; HaeIII T>C genotype: C/C)
B: PET/CT images of a 53-year-old male on the right lung. SUV_{max}: 10.37. (XbaI G>T genotype: G/T; HaeIII T>C genotype: T/C)
PET/CT: Positron emission tomography/computed tomography, SUV_{max}: Maximum standardized uptake value

Table 4. Cancer types and GLUT-1 genotype result

	GLUT-1 XbaI G>T (rs2754218) genotype n (%)	GLUT-1 HaeIII T>C (rs1385129) genotype n (%)
Melanoma	**G/G** 4 (100%) **G/T** **T/T**	**C/C** 4 (100%) **T/C** **T/T**
Lung-bronchial tumors	**G/G** 24 (64,86%) **G/T** 12 (32,43%) **T/T** 1 (2,70%)	**C/C** 10 (27,77%) **T/C** 15 (41,66%) **T/T**
Urogenital tumors	**G/G** 17 (100%) **G/T** **T/T**	**C/C** 17 (100%) **T/C** **T/T**
GIS tumors	**G/G** 15 (100%) **G/T** **T/T**	**C/C** 11 (73,33%) **T/C** 4 (26,67%) **T/T**
Breast cancer	**G/G** 16 (100%) **G/T** **T/T**	**C/C** 8 (34,78%) **T/C** 6 (26,09%) **T/T** 9 (39,13%)
Other	**G/G** 11 (100%) **G/T** **T/T**	**C/C** 4 (25%) **T/C** 6 (37,5%) **T/T** 6 (37,5%)

distribution, indicating that 46% of the patients were female and 54% were male. Table 8 summarizes the distribution of patients' diagnoses based on International Classification of Diseases codes, with lung-related abnormalities (R91) being the most common diagnosis (22%).

Discussion

PET/CT, a non-invasive imaging technique widely accepted worldwide, provides exceptional benefits in oncology patient follow-up, helping to reduce mortality and morbidity in cancer patients. The level of ^{18}F-FDG uptake, which generally reflects tumor aggressiveness, indicates viable tumor tissue and increased glucose metabolism. The accumulation of ^{18}F-FDG in tumors demonstrates the known natural behavior of tumors.

The most commonly used radiopharmaceutical in PET/CT is ^{18}F-FDG, a glucose derivative. ^{18}F-FDG, a glucose analog, is taken up by living cells in the first step of the normal glucose pathway. It is used in cancer diagnosis due to the increased glycolytic activity in neoplastic cells. The rate of glucose metabolism is consistent with the rate of ^{18}F-FDG uptake.

Glucose transporters, chiefly GLUT-1, play critical roles in the import and metabolism of glucose and auxiliary substrates (9,10,11). and are significantly overexpressed in many cancers, including brain, breast, cervical, colorectal, cutaneous, endometrial, esophageal, hepatic, lung, oral, ovarian, pancreatic, prostate, and renal cancers. The cellular uptake mechanism of ^{18}F-FDG has been studied both *in vitro* and *in vivo*. Studies have shown that polymorphisms in the GLUT-1 transporter protein affect the cellular uptake of ^{18}F-FDG. These polymorphisms have been identified as GLUT-1-XbaI G>T (rs2754218), HpyCH4V A>T (rs710218), and HaeIII T>C (rs1385129). Polymorphisms in the *GLUT-1* gene have been associated with increased ^{18}F-FDG uptake, accelerated tumor growth, and breast cancer.

Numerous studies have investigated the influence of the GLUT-1-XbaI G>T polymorphism (rs2754218) on ^{18}F-FDG uptake, with a primary focus on various cancer types. Relevant studies have reported the association between

Table 5. Association between XbaI and HaeIII genotypes and SUV_{max} values of PRIMARY tumor

Genotype	SUV_{max} mean ± standard deviation
XbaI G/G & HaeIII C/C	10.89±5.85
XbaI G/T & HaeIII T/T	10.65±6.75
XbaI G/T & HaeIII T/C	9.54±5.02
XbaI T/T & HaeIII T/T	
XbaI G/G & HaeIII T/T	4.28±3.48
XbaI G/G & HaeIII T/C	6.81±2.67

SUV_{max}: Maximum standardized uptake value

Table 6. Characteristic analysis of the patient (age)

	n	Mean	SD	Min.	Max.
Age	100	57.8	13.37	20	87

SD: Standard deviation, Min.: Minimum, Max.: Maximum, n: Number

Table 7. Characteristic analysis of the patient (gender)

Gender	n	%
Female	46	46%
Male	54	54%

Table 8. Patients' diagnosis statement

ICD code	Diagnosis description	n	%
C04	Base of tongue CA	1	1.00
C09	Tonsil CA	1	1.00
C15	Esophagus CA	1	1.00
C16	Stomach CA	1	1.00
C18	Colon CA	4	4.00
C21	Anus and anal canal CA	1	1.00
C22	Liver and intrahepatic bile duct CA	1	1.00
C25	Pancreas CA	4	4.00
C32	Larynx CA	7	7.00
C34	Bronchus and lung CA	8	8.00
C38	Heart, mediastinum and pleura CA	1	1.00
C43	Skin malignant melanoma	4	4.00
C45	Mesothelioma	1	1.00
C49	Connective and soft tissue CA	1	1.00
C50	Breast CA	16	16.00
C53	Cervix uteri CA	3	3.00
C54.1	Endometrium CA	1	1.00
C56	Ovary CA	1	1.00
C61	Prostate CA	1	1.00
C62	Testis CA	1	1.00
C64	Kidney CA (excluding renal pelvis)	7	7.00
C67	Bladder CA	2	2.00
C80	Malignant neoplasm, unspecified site	7	7.00
D37.4	Colon, uncertain behavior neoplasm	1	1.00
K62	Other diseases of anus and rectum	1	1.00
M79	Other soft tissue disorders	1	1.00
R91	Lung, diagnostic A.B	22	22.00

ICD: International Classification of Disease, CA: Cancer

the societal T allele and high ^{18}F-FDG in ethnic studies, claiming that this allele could increase the capability for glucose transport and hence increased tumor activity. Conversely, the investigations on GLUT-1 HaeIII T>C polymorphism have not been exhaustive, and some studies have speculated that the C allele may be related to lower ^{18}F-FDG uptake (9,11,12).

In our study, the XbaI G/G genotype was observed in 87% of the patients, while the XbaI G/T genotype was found in 12%. Only one patient (1%) had the XbaI T/T genotype. For the HaeIII T>C genotype distribution, the HaeIII C/C genotype was detected in 54%, HaeIII T/C genotype in 31%, and HaeIII T/T genotype in 15%.

The genotype distributions in both gene regions varied according to cancer types (p=0.0001). There was no statistically significant difference in SUV_{max} values between the XbaI and HaeIII genotypes (p-values: p=0.89 and p=0.541, respectively). Cancer types were categorized based on the affected system, the patient group was divided into subgroups: melanoma, lung and bronchial tumors, urogenital tumors, GIS tumors, breast cancer, and others. All patients in the melanoma, urogenital tumors, GIS tumors, breast cancer, and other cancer subgroups had the XbaI G/G genotype. However, in lung-bronchial tumors, the XbaI G/T genotype was observed at a rate of 32.43%.

XbaI and HaeIII genotypes were evaluated together to examine their relationship with cancer types was observed that the number of polymorphic genotypes was significantly higher in the lung-bronchial tumor group compared to other cancer types. Particularly, patients in the lung-bronchial tumor group had mutations in at least one of the two gene regions.

However, ^{18}F-FDG uptake intensity varies depending on tumor histopathology. While epidermal and adenocarcinomas, such as small cell lung cancer, show a high degree of uptake, tumors like bronchoalveolar and carcinoid tumors, which have dense mucinous content or are slow-growing, may not show pathological levels of ^{18}F-FDG uptake.

This study investigated the relationship between GLUT-1 polymorphisms (specifically GLUT-1-XbaI G>T and HaeIII T>C), ^{18}F-FDG uptake rates, and cancer types. Here's a breakdown of the findings:

Genotype Distribution Varies by Cancer Type: The distribution of GLUT-1-XbaI G>T and HaeIII T>C genotypes differed significantly among various cancer types. Notably, the XbaI G/T genotype was more prevalent in lung-bronchial tumors compared to other cancer types.

No Significant Difference in SUV_{max} values Based on Genotype Alone: No statistically significant difference was found in SUV_{max} values when comparing groups based solely on XbaI or HaeIII genotypes.

High Prevalence of Polymorphisms in Lung and Bronchial Tumors: A significantly higher number of patients with lung-bronchial tumors exhibited polymorphisms in at least one of the two *GLUT-1* gene regions compared to other cancer types.

Conclusion

Though the study has failed to establish a proper correlation between specific genotypes and SUV_{max} values, a high prevalence of GLUT-1 polymorphisms in lung-bronchial tumor patients with high SUV_{max} values may highlight a possible relation, requiring further research. There is a complex relationship between genetic variation, glucose metabolism, and uptake of ^{18}F-FDG in cancer.

Potential Consequences: Further studies will be needed to unravel the consequences of such results. If, in the near future, more associations between GLUT-1 variations and ^{18}F-FDG uptake in specific cancers are developed, then this would imply the following: a) Personalized medicine: Treatment strategies could be developed with a focus on the unique properties of each individual's genome. b) Diagnostic precision: It could allow for more accurate interpretation of ^{18}F-FDG PET/CT scans for certain malignancies. c) Drug development: Interference with GLUT-1 may also represent a potential therapeutic approach for drugs under development.

Ethics

Ethics Committee Approval: The protocol was approved by the Pamukkale University Non-Interventional Clinical Research Ethics Committee (number: E-60116787-020-5047, date: 05.01.2021).

Informed Consent: This was a prospective case-control study.

Footnotes

Authorship Contributions

Surgical and Medical Practices: M.K., D.Y., Concept: D.Y., A.K., Design: D.Y., A.K., Data Collection or Processing: V.K.A., D.Y., A.K., Analysis or Interpretation: M.K., V.K.A., Y.B., D.Y., A.K., Literature Search: Y.A., D.Y., A.K., Writing: Y.A., Y.B., A.K.

Conflict of Interest: No conflict of interest was declared by the authors.

Financial Disclosure: This study was supported by pamukkale University Scientific Research Projects Coordination Unit through project numbers 2021SABE010.

References

1. Zhao FQ, Keating A. Functional properties and genomics of glucose transporters. Curr Genomics. 2007;8:113-128.
2. Hodgkinson AD, Millward BA, Demaine AG. Polymorphisms of the glucose transporter (GLUT1) gene are associated with diabetic nephropathy. Kidney Int. 2001;59:985-989.
3. Xu C, Yang X, Wang Y, Ding N, Han R, Sun Y, Wang Y. An analysis of the polymorphisms of the GLUT1 gene in urothelial cell carcinomas of the bladder and its correlation with p53, Ki67 and GLUT1 expressions. Cancer Gene Ther. 2017;24:297-303.
4. Ng DPK, Canani L, Araki SI, Smiles A, Moczulski D, Warram JH, Krolewski AS. Minor effect of GLUT1 polymorphisms on susceptibility to diabetic nephropathy in type 1 diabetes. Diabetes. 2002;51:2264-2269.
5. Grabellus F, Sheu SY, Bachmann HS, Lehmann N, Otterbach F, Heusner TA, Antoch G, Bockisch A, Kimmig R, Schmid KW, Stahl AR. The XbaI G>T polymorphism of the glucose transporter 1 gene modulates 18F-FDG uptake and tumor aggressiveness in breast cancer. J Nucl Med. 2010;51:1191-1197.
6. Beaulieu S, Kinahan P, Tseng J, Dunnwald LK, Schubert EK, Pham P, Lewellen B, Mankoff DA. SUV varies with time after injection in 18F-FDG PET of breast cancer: characterization and method to adjust for time differences. J Nucl Med. 2003;44:1044-1050.
7. Bertholee D, Maring JG, van Kuilenburg AB. Genotypes affecting the pharmacokinetics of anticancer drugs. Clin Pharmacokinet. 2017;56:317-337.
8. Rufino M, Hernánde Dz, Barrios Y, Salido E. The GLUT-1 XbaI gene polymorphism is associated with vascular calcifications in nondiabetic uremic patients. Nephron Clin Pract. 2008;108:182-187.
9. Suwannakul N, Armartmuntree N, Thanan R, Midorikawa K, Kon T, Oikawa S, Kobayashi H, Ma N, Kawanishi S, Murata M. Targeting fructose metabolism by glucose transporter 5 regulation in human cholangiocarcinoma. Genes Dis. 2021;9:1727-1741.
10. Nomura N, Verdon G, Kang HJ, Shimamura T, Nomura Y, Sonoda Y, Hussien SA, Qureshi AA, Coincon M, Sato Y, Abe H, Nakada-Nakura Y, Hino T, Arakawa T, Kusano-Arai O, Iwanari H, Murata T, Kobayashi T, Hamakubo T, Kasahara M, Iwata S, Drew D. Structure and mechanism of the mammalian fructose transporter GLUT5. Nature. 2015;526:397-401.
11. Tanasova M, Fedie JR. Molecular tools for facilitative carbohydrate transporters (Gluts). Chembiochem. 2017;18:1774-1788.
12. Douard V, Ferraris RP. Regulation of the fructose transporter GLUT5 in health and disease. Am J Physiol Endocrinol Metab. 2008;295:E227-E237.

Original Article

Mol Imaging Radionucl Ther 2025;34:97-106 *DOI:10.4274/mirt.galenos.2025.85429*

A Comprehensive Diagnostic Assessment of Thyroid Nodules Utilizing Scintigraphy and Telomere Lengths (T/S ratios)

Tiroid Nodüllerinin Sintigrafi ve Telomer Uzunluğu (T/S oranı) ile Kapsamlı Tanısal Değerlendirmesi

Fulya Koç Öztürk[1], Semra Usta Özdemir[1], Ersen Karakılıç[2], Fatma Sılan[3]

[1]*Çanakkale Onsekiz Mart University Faculty of Medicine, Department of Nuclear Medicine, Çanakkale, Türkiye*

[2]*Çanakkale Onsekiz Mart University Faculty of Medicine, Department of Internal Medicine, Division of Endocrinology and Metabolism, Çanakkale, Türkiye*

[3]*Çanakkale Onsekiz Mart University Faculty of Medicine, Department of Medical Genetics, Çanakkale, Türkiye*

Abstract

Objectives: This study aims to evaluate the effectiveness and role of telomere length measurements in leukocytes, plasma free cell DNA (cfDNA), and biopsy cells, along with technetium-99m (Tc-99m) methoxyisobutylisonitrile (MIBI) scintigraphy, as non-invasive methods for diagnosing malignant thyroid lesions.

Methods: Data from 128 patients, who underwent ultrasound, Tc-99m MIBI scintigraphy, and fine-needle biopsy with a preliminary diagnosis of malignant thyroid nodules, were analyzed. In 98 patients, telomere lengths in leukocytes (from blood), cfDNA (from plasma), and biopsy cells were measured using the quantitative polymerase chain reaction method, and the relative telomere/single copy gene (T/S) ratio was calculated. Based on cytological examination results, patients were categorized into three groups: malignant, benign, and suspicious. Group differences were analyzed using the Kruskal-Wallis and Chi-square tests, and correlations between variables were examined with Spearman correlation analysis.

Results: The sensitivity, specificity, positive predictive value, negative predictive value, and accuracy of Tc-99m MIBI scintigraphy for diagnosing malignant thyroid nodules were 64.70%, 79.16%, 29.72%, 83.51%, and 67.96%, respectively. While these results align with the literature, the positive predictive value was notably lower. No significant differences were observed in telomere lengths (T/S ratios) in leukocytes, plasma, or tissue between the groups.

Conclusion: Tc-99m MIBI scintigraphy demonstrates reasonable diagnostic accuracy for identifying malignancy in thyroid nodules. Contrary to limited reports, telomere length measurements may not be a reliable method for predicting thyroid malignancy. Larger studies are needed to further explore these findings.

Keywords: Thyroid cancer, technetium-99m methoxyisobutylisonitrile scintigraphy, cell DNA, liquid biopsy, circulating tumor DNA, telomere

Öz

Amaç: Bu çalışma, lökositlerde, plazma serbest hücre DNA'sında (cfDNA) ve biyopsi hücrelerinde telomer uzunluğu ölçümleri ile teknesyum-99m (Tc-99m) metoksiizobütilizonitril (MIBI) sintigrafisinin, kötü huylu tiroid lezyonlarının teşhisinde non-invaziv yöntemler olarak etkinliğini ve rolünü değerlendirmeyi amaçlamaktadır.

Yöntem: Malign tiroid nodülleri ön tanısı konulan ve ultrason, Tc-99m MIBI sintigrafisi ve ince iğne biyopsisi uygulanan 128 hastanın verileri analiz edilmiştir. Doksan sekiz hastada, lökositlerde (kandan), cfDNA'da (plazmadan) ve biyopsi hücrelerinde telomer uzunlukları kantitatif polimeraz

Address for Correspondence: Semra Usta Özdemir, Çanakkale Onsekiz Mart University Faculty of Medicine, Department of Nuclear Medicine, Çanakkale, Türkiye

E-mail: drsemrausta@gmail.com **ORCID ID:** orcid.org/0000-0003-1302-9630

Received: 19.10.2024 **Accepted:** 02.02.2025 **Epub:** 26.05.2025 **Publication Date:** 03.05.2025

Cite this article as: Koç Öztürk F, Usta Özdemir S, Karakılıç E, Sılan F. A comprehensive diagnostic assessment of thyroid nodules utilizing scintigraphy and telomere lengths (T/S ratios). Mol Imaging Radionucl Ther. 2025;34:97-106.

zincir reaksiyonu yöntemiyle ölçülmüş ve göreceli telomer/tek kopya gen (T/S) oranı hesaplanmıştır. Sitolojik inceleme sonuçlarına göre hastalar; kötü huylu, iyi huylu ve şüpheli olmak üzere üç gruba ayrılmıştır. Gruplar arası farklar Kruskal-Wallis ve ki-kare testleriyle analiz edilmiş, değişkenler arasındaki korelasyonlar Spearman korelasyon analizi ile değerlendirilmiştir.

Bulgular: Tc-99m MIBI sintigrafisinin kötü huylu tiroid nodüllerini teşhis etmedeki duyarlılık, özgüllük, pozitif öngörü değeri, negatif öngörü değeri ve doğruluk oranları sırasıyla %64,70, %79,16, %29,72, %83,51 ve %67,96 olarak bulunmuştur. Bu sonuçlar literatürle uyumlu olmakla birlikte, pozitif öngörü değerinin belirgin şekilde düşük olduğu gözlemlenmiştir. Lökosit, plazma veya doku örneklerindeki telomer uzunlukları (T/S oranları) açısından gruplar arasında anlamlı bir fark bulunmamıştır.

Sonuç: Tc-99m MIBI sintigrafisi, tiroid nodüllerinde malignitenin tespitinde makul bir tanısal doğruluk sunmaktadır. Ancak sınırlı raporlara rağmen, telomer uzunluğu ölçümlerinin tiroid malignitesini öngörmede güvenilir bir yöntem olmayabileceği anlaşılmaktadır. Bu bulguların daha kapsamlı çalışmalarla araştırılması gerekmektedir.

Anahtar kelimeler: Tiroid kanseri, teknesyum-99m metoksi izobütilizonitril sintigrafi, hücre DNA'sı, sıvı biyopsi, dolaşan tümör DNA'sı, telomer

Introduction

It is crucial to determine the functional status of the detected thyroid nodules and whether they are malignant. For this purpose, thyroid function tests, ultrasound (US) findings, and scintigraphic evaluations are conducted on patients (1,2).

Although thyroid function tests provide valuable information about the functional status of the thyroid gland and nodules, they do not indicate the presence of malignancy. US imaging can assess the size, echogenicity, structure, presence of micro- and macro-calcifications, margin irregularity, peripheral halo, shape, and vascularity, of nodules. Among these features, hypoechogenicity, microcalcifications, and irregular margins are the characteristics most strongly associated with malignancy (3,4,5). Additionally, thyroid US can evaluate the presence of pathological lymph nodes in the neck or signs of invasion in surrounding tissues. However, no US finding alone is sufficiently sensitive and specific for detecting malignancy (5).

Another method used to assess the malignancy potential of thyroid nodules is thyroid scintigraphy. In thyroid scintigraphy with technetium-99m (Tc-99m) methoxyisobutylisonitrile (MIBI), uptake rates and washout levels can provide insights into the presence of malignancy in nodules (6). Tc-99m MIBI is a tracer used to detect P-glycoprotein (Pgp) function and inhibition *in vivo*, which is associated with the multidrug resistance mechanism in tumors. The multidrug resistance (MDR1) Pgp affects the uptake of MIBI in tumor cells, making it a preferred agent for differentiating benign from malignant thyroid nodules (6). Studies have shown that the likelihood of malignancy increases in hypofunctioning nodules with MIBI uptake, while nodules without uptake are generally benign. In another study, 35% of nodules showing uptake with Tc-99m MIBI were found to be malignant (7).

In recent years, liquid biopsy has emerged as an important innovation in distinguishing between benign and malignant thyroid nodules (8). Liquid biopsy enables the non-invasive detection of biological markers, such as cell-free DNA (cfDNA) released by tumors, in body fluids like blood. cfDNA can provide crucial insights into the presence of malignancies. These biomarkers reflect the genetic characteristics and mutations of the tumor, and can be used for cancer diagnosis, prognostic evaluation, monitoring treatment response, and determining those at high risk (9,10). Telomeric DNA lengths are a significant parameter in cancer biology, as changes in telomere length have been shown to be associated with tumor formation and progression. Telomeres are protective structures located at the ends of chromosomes that delay cellular aging and apoptosis. The majority of cancer cells express the enzyme telomerase, which lengthens telomeres, granting the cells immortality. In particular, the telomerase enzyme is upregulated in many malignancies, including thyroid cancer. Therefore, telomere length and telomerase activity are being explored as potential biomarkers for cancer diagnosis. The release of cfDNA into the bloodstream is related to increased cell death and tumor microcirculation associated with cancer cells. However, it has also been shown that cfDNA can increase in other conditions, such as trauma, inflammation, and myocardial infarction, so the specificity of cfDNA measurements for cancer must be interpreted with caution (11,12).

Traditional methods used to detect malignancy in thyroid nodules, such as fine-needle aspiration biopsy (FNAB), are invasive techniques. However, since these methods take samples from only specific parts of the tumor tissue, they may not fully reflect tumor heterogeneity (13,14). This can lead to ambiguous or uncertain results.

For these reasons, our study aims to investigate the diagnostic accuracy and role of non-invasive methods, including Tc-99m MIBI scintigraphy and telomere length measurements (a form of liquid biopsy), in detecting malignant thyroid lesions.

Materials and Methods

Study Population

A total of 128 patients were included in the study, who underwent Tc-99m MIBI thyroid-tumor scan scintigraphy at the nuclear medicine clinic due to suspected malignancy, FNAB in the endocrinology clinic, and cfDNA and telomere length measurements in blood, plasma, and biopsy samples in the medical genetics laboratory. While all patients underwent scintigraphy and biopsy, telomere lengths were measured in 98 of them. Patients with thyroiditis and insufficient biopsy material were excluded from the study.

The groups were formed based on the Bethesda classification (I: Non-diagnostic/unsatisfactory, II: Benign (colloid and follicular cells), III: atypia of undetermined significance/follicular lesion of undetermined significance (AUS/FLUS) (follicular or lymphoid cells with atypical features), IV: Suspicious for malignancy, VI: Malignant).

Patients with a Bethesda Class I diagnosis were excluded from the study. Those with a Bethesda Class II diagnosis were categorized as the benign group. Patients in Bethesda Classes III, IV, and V were grouped into the suspicious group. Lastly, those with a Bethesda Class VI diagnosis were classified as the malignant group.

All participants were informed about the study prior to the collection of blood and biopsy samples, and they were included after obtaining signed consent forms. This study received ethical approval from the Çanakkale Onsekiz Mart University Rectorate Clinical Research Ethics Committee (date: 12/03/2020, decision no: 2020-04).

Technetium-99m Methoxyisobutylisonitrile Scintigraphy

The Tc-99m MIBI scintigraphies were obtained using a dual-head gamma camera system (Infinia, General Electric Medical Systems, Milwaukee, Wisconsin, USA) with a low-energy, parallel-hole, high-resolution collimator, a 20% window width, and a 140 KeV photopeak of Tc-99m. Early planar, 15-minute single photon emission computed tomography and 2-hour planar imaging were performed after the injection (0.31 mCi/kg sestamibi). The Tc-99m MIBI scintigraphy images were evaluated by two nuclear medicine experts. Lesions were categorized as "isoactive" if their uptake was equal to or greater than the background activity and/or thyroid tissue uptake, and "hyperactive" if the lesion's uptake was greater than the background activity and/or thyroid tissue activity.

Measurement of Telomere Length by Quantitative Polymerase Chain Reaction Method

Preparation of Standards

In all studies, DNA obtained from a venous blood sample taken from a healthy young individual was used as a calibrator. In studies normalized with the calibrator, a standard curve is not necessary for each experiment. Since the target/reference gene ratios of the samples were normalized with the calibrator target/reference gene ratio, the results are only affected by the different polymerase chain reaction (PCR) efficiencies of the target and reference genes. To mitigate this effect, the PCR efficiency can be adjusted to 2 during analysis.

Inclusion of Samples in Telomere and Betaglobulin Polymerase Chain Reaction Analysis

Primers synthesized by HPLC were diluted to 100 pmol/µL as main stocks, and intermediate stocks of 10 pmol/µL were prepared and stored at -20 °C for PCR. The samples were subjected to PCR using telomere and beta-globin primers. The samples were analyzed using the Light Cycler 2.0 (Roche) device. The quantification process was performed on the real-time PCR (Roche Light Cycler 2.0) device. Samples were analyzed in duplicate.

Quantitative Assessment of Telomere Length

When PCR efficiency is assumed to be 100%, the telomere/single copy gene (T/S) ratio is calculated as follows:

T/S ratio= [2 Ct(telomer) / 2 Ct(beta globin)]-1= [2 [Ct(telomer)-Ct(beta globin)]]-1= 2-ΔCt

ΔCt=[Ct(telomer)-Ct(beta globin)]

Relatif T/S ratio=2-(ΔCt1- ΔCt2)= 2-ΔΔCt

ΔΔCt= ΔCtT-ΔCt calibrator

Statistical Analysis

The study data were transferred into SPSS 26.0 for electronic analysis. Data control and analyses were conducted using this program. For the presentation of descriptive statistics, percentages, means, standard deviation, median, minimum, and maximum (min.-max.) values were used. Statistical evaluations included Chi-square, Kruskal-Wallis, and Spearman correlation analyses. Receiver operating characteristic (ROC) curve analysis was performed to determine the cutoff points for the relative T/S ratio values of whole blood, plasma, and tissue in detecting malignancy, and the graphs were presented. A p-value of <0.05 was considered statistically significant.

Results

Descriptive Findings

A total of 128 patients, including 101 women (79%) and 27 men (21%) aged between 19 and 85 years (mean age 52.66±13.14), were included in our study. All patients had results from Tc-99m MIBI thyroid scintigraphy and thyroid biopsies, while the telomere lengths in blood, plasma, and tissue could be measured genetically in 98 patients (Table 1).

According to the pathology results, the average age (min.-max.) and gender distribution of the cases were divided into 3 groups. No statistically significant difference was found between the groups regarding age (p=0.544) and gender (p=0.083) (Table 1).

Comparison of Ultrasonographic Features of Thyroid Nodules

When comparing the nodule diameters among these three groups, no significant difference was found (p=0.456) (Table 1). Our study population consisted of patients categorized into Thyroid Imaging Reporting and Data System (TIRADS) categories 3, 4, and 5 according to current guidelines indicating the need for biopsy. When the distribution of TIRADS categories in the benign, suspicious, and malignant groups was examined, it was found that the benign group had the highest proportion of TIRADS 3 (54.16%), the suspicious group had the highest proportion of TIRADS 4 (40%), and the malignant group had the highest proportion of TIRADS 5 (70.58%), which is a clinically expected result. As the risk of malignancy increases within the TIRADS categories, the likelihood of obtaining a malignant pathological result also increases. Statistical evaluation revealed that this difference is significant (p=0.001, Table 1).

Among the patients evaluated as TIRADS 3-4-5 on US who were underwent biopsy, the cytological results obtained according to the Bethesda classification showed that 96 patients had benign results, 11 patients had AUS/FLUS, 3 patients had follicular neoplasia or suspicion, (including Hurthle cell type), 1 patient had suspicion of malignancy, and malignancy was reported in 17 patients (Table 2). Of the 17 cases with thyroid malignancy identified, 14 were papillary carcinoma, 2 were follicular variant papillary carcinoma, and 1 was primary thyroid lymphoma based on histopathological type.

Comparison of Technetium-99m Methoxyisobutylisonitrile Scintigraphy Results

The power and effectiveness of Tc-99m MIBI thyroid scintigraphy, performed to investigate the presence of malignancy in thyroid nodules, were statistically evaluated. The specificity of Tc-99m MIBI thyroid scintigraphy in detecting benign nodules was calculated as 79.16%, and the negative predictive value was 83.51%. The sensitivity

Table 1. The demographic and clinical characteristics of the study group patients

Clinical characteristics	Study group (n=128)			
	Benign group (n=96)	Suspicious group (n=15)	Malignant group (n=17)	p-value
Age (mean ± SD)	53.46±12.72	49.53±15.13	50.88±13.95	0.544
(Min.-max.)	(19-85)	(19-77)	(20-77)	
Gender (%)				
Female	78 (81.25)	13 (86.66)	10 (58.82)	0.083
Male	18 (18.75)	2 (13.33)	7 (41.17)	
Nodule size				
Mean (mm)	22.04±10.43	18.73±9.04	22.29±15.54	0.456
(Min.-max.)	(5.0-48.0)	(5.0-35.0)	(10.0-60.0)	
TIRADS				
3 n (%)	52 (54.16)	6 (40.0)	2 (11.76)	0.001
4 n (%)	23 (23.95)	5 (33.33)	3 (17.64)	
5 n (%)	21 (21.87)	4 (26.66)	12 (70.58)	
MIBI scan				
Isoactive n (%)	76 (83.51)	9 (9.89)	6 (6.59)	-
Hyperactive n (%)	20 (54.05)	6 (16.21)	11 (29.72)	

SD: Standard deviation, TIRADS: Thyroid Imaging Reporting and Data System, MIBI: Methoxyisobutylisonitrile

of Tc-99m MIBI thyroid scintigraphy in detecting malignant nodules was calculated as 64.70%, and the positive predictive value was 29.72%. Additionally, the diagnostic accuracy of Tc-99m MIBI thyroid scintigraphy was found to be 67.96% (Table 3).

In the suspicious group (15 individuals), among the biopsied nodules, 6 (40%) were classified as isofunctional, and 9 (60%) were classified as hyperfunctional. Due to the inability to access subsequent biopsy results or postoperative biopsy results, the validity and reliability of scintigraphy in this group could not be calculated.

Figure 1 shows examples of true-positive, false-positive, true-negative, and false-negative patients in Tc-99m MIBI thyroid scintigraphy. The image of a primary thyroid lymphoma case, distinct from differentiated thyroid malignancies, is shown in Figure 2, where early and late images revealed radioactivity retention in a firm, fixed nodule covering the entire thyroid. Additionally, a metastatic right supraclavicular lymph node, confirmed histopathologically and showing Tc-99m MIBI retention in both early and late images, was identified.

Comparison of Telomere Lengths in Blood, Plasma, and Tissue

There was no statistically significant difference in the relative T/S ratio values of whole blood, plasma, and tissue among

Table 2. Thyroid biopsy results according to the Bethesda classification

Groups	Benign group	Suspicious group			Malignant group	Total
Biopsy results (Bethesda)	Benign	AUS FL-US	Follicular neoplasia or suspicion (including hurthle cell)	Suspicion of malignancy	Malignant	
Number	96	11	3	1	17	128
Percent	75.0	8.59	2.34	0.78	13.23	100%

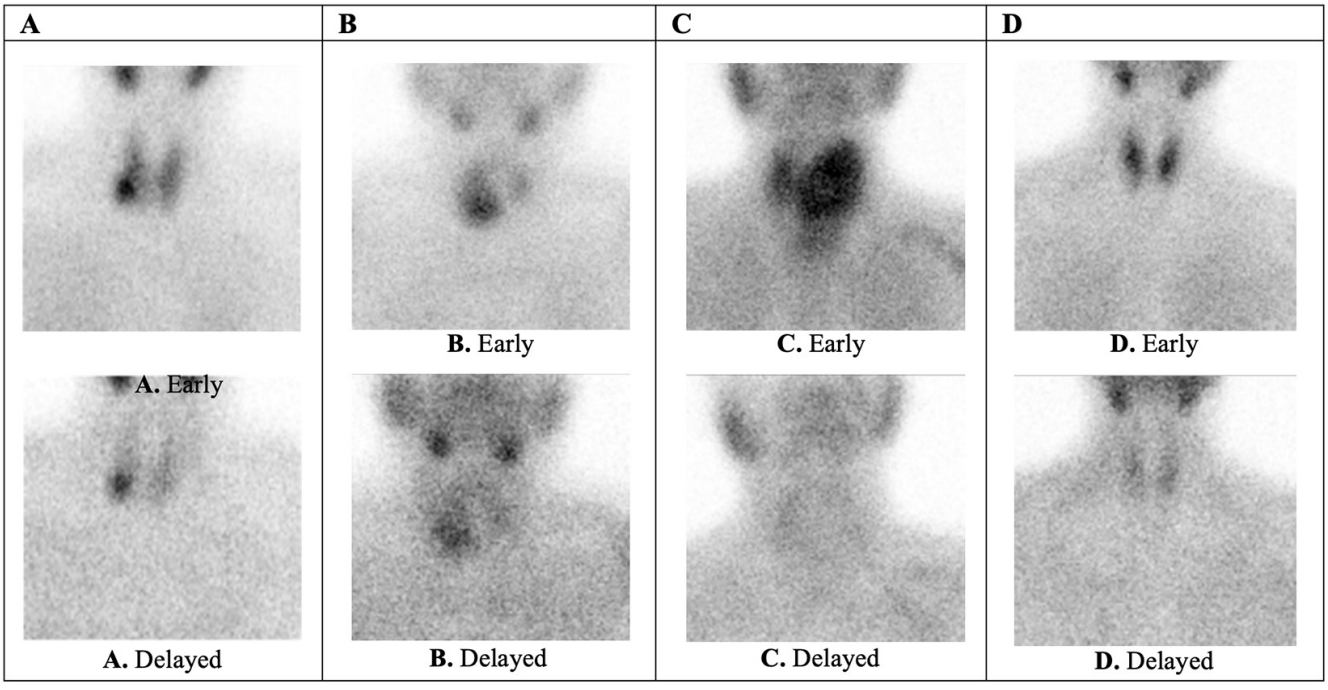

Figure 1. Tc-99m MIBI thyroid scintigraphy patient examples: A) A true positive patient example; the biopsy of the hyperactive nodule was reported as papillary thyroid carcinoma (22 mm nodule in the right lobe); B) A false positive patient example; the biopsy of the hyperactive nodule was reported as benign (35 mm nodule in the right lobe); C) A true negative patient example; the biopsy of the isoactive nodule was reported as benign (42 mm nodule in the right lobe); D) A false negative patient example; the biopsy of the isoactive nodule was reported as papillary thyroid carcinoma (17 mm nodule in the right lobe)
Tc-99m: Technetium-99m, MIBI: Methoxyisobutylisonitrile

the groups (Table 4). Although no statistical difference was found, it was observed that the relative T/S ratio values in whole blood for patients in the malignant group, were larger than those in the other groups. Conversely, for the plasma relative T/S ratio values, higher average values were obtained in the benign group compared to the suspicious and malignant groups. Additionally, the close similarity of the average tissue relative T/S ratios in the malignant and benign groups is noteworthy. When examining telomere lengths in all three groups, the order of telomere lengths was found to be "whole blood > plasma > tissue" in each group (Table 5).

On the other hand, in the ROC curve analyses, the area under the curve (AUC) for the whole blood relative T/S ratio was found to be 0.507 (Figure 3). For the plasma relative T/S ratio, AUC= 0.558 (Figure 4); and for the tissue relative T/S ratio, AUC=0.504 (Figure 5). These values indicate insufficient diagnostic accuracy (Tables 6,7,8).

Table 3. The sensitivity, specificity, positive predictive value, and negative predictive value ratios of Tc-99m MIBI scintigraphy in detecting malignant and benign nodules

Scintigraphy findings	Pathology results		
	Benign group n (%)	Suspicious group n (%)	Malignant group n (%)
Hyperactive nodule n=37	20 (20,83)	6 (40)	11 (64.70)
Isoactive nodule n=91	76 (79.17)	9 (60)	6 (35.30)
Total n=128	96 (100)	15 (100)	17 (100)

Sensitivity: 64.70%; Specificity: 79.16%; Positive predictive value: 29.72%; Negative predictive value: 83.51%; Diagnostic accuracy: 67.96% Tc-99m: Technetium-99m, MIBI: Methoxyisobutylisonitrile

Discussion

Due to the limitations of existing methods for detecting thyroid cancer, research on new non-invasive approaches is ongoing. In this study, we aimed to evaluate the role of scintigraphic imaging with Tc-99m MIBI and DNA telomere length measurement in distinguishing malignant from benign thyroid nodules.

Tc-99m MIBI scintigraphy, employed to evaluate malignancies like lung, breast, brain, lymphoma, bone, and soft tissue cancers, has also been investigated for predicting thyroid cancers. The studies reported show significant differences in diagnostic performance values, in addition to heterogeneity in inclusion criteria and methods used (15,16,17). Overall, Tc-99m MIBI scintigraphy appears to be a cost-effective method that contributes to the evaluation of tyroid nodules. However, current guidelines do not recommend the use of Tc-99m MIBI scintigraphy to predict the cancer risk of thyroid nodules (6,18,19).

In a meta-analysis by Treglia et al. (7), which included 21 studies, the pooled sensitivity and specificity of Tc-99m MIBI scintigraphy in detecting malignant thyroid nodules per lesion were 85.1% and 45.7%, respectively, regardless of previous technetium pertechnetate or iodine-123 scan results. When a limited sub-analysis was performed with data on hypofunctioning nodules from Tc-99m pertechnetate or iodine-123 scans, the pooled sensitivity and specificity were 82.1% and 62.8%, respectively. The researchers concluded that this imaging method could be helpful in patients with thyroid nodules suspected of malignancy based on conventional diagnostic techniques. They also noted that higher specificity could be achieved in hypofunctioning thyroid nodules (7,20). Based on the results of a prospective study, the researchers stated that

Table 4. The comparison of cfDNA telomere length values between groups

cfDNA groups	Study group (n=98)			
	Benign group (n=77)	Suspicious group (n=7)	Malignant group (n=14)	p-value
Blood relative T/S ratio				0.668
Mean ± SD	3.89±3.27	3.45±3.80	4.24±3.41	
(Min.-max.)	(0.03-11.47)	(0.04-9.51)	(0.59-11.74)	
Plasma relative T/S ratio				0.472
Mean ± SD	2.09±4.29	1.80±2.08	0.84±0.66	
(Min-max)	(0.008-23.75)	(0.11-6.14)	(0.07-2.20)	
Tissue relative T/S ratio				0.396
Mean ± SD	0.58±1.03	1.51±2.82	0.55±1.08	
(Min.-max.)	(0.005-6.86)	(0.07-7.83)	(0.01-4.08)	

cfDNA: Cell-free DNA, T/S: Telomere/single copy gene, SD: Standard deviation

Tc-99m MIBI scintigraphy was significantly more accurate than mutation analysis and that a negative Tc-99m MIBI scan could reliably rule out malignancy. Eighteen another study reported a strong negative relationship between Tc-99m MIBI uptake in thyroid lesions and MDR-associated protein-1 (21).

Although many studies have reported a high sensitivity, Tc-99m MIBI scintigraphy has low specificity and is not recommended as a first-line investigation. Instead, it is suggested as a second-line test to help reduce unnecessary surgeries (22,23).

In our study, we found the sensitivity, specificity, positive predictive value, negative predictive value, and accuracy of Tc-99m MIBI scintigraphy in distinguishing between malignant and benign thyroid nodules to be 64.7%, 79.16%, 29.72%, 83.51%, and 67.96%, respectively, in that order. Our results are generally consistent with those reported in the literature; however, the heterogeneity in patient selection and methods used in the studies make direct comparison difficult.

One liquid biopsy method measures the telomere lengths of cells, focusing on two primary telomere repair mechanisms: telomerase activation and the alternative lengthening of telomeres (ALT), pathway, which functions independently of telomerase. While 85-95%

Table 5. The pairwise comparison of telomere lengths across all groups

n=98	Benign group (n=77)	Suspicious group (n=7)	Malignant group (n=14)
Blood-plasma relative T/S			
Z	0.380	-0.107	0.354
p-value	0.001	0.819	0.215
Plasma-tissue relative T/S			
Z	0.306	0.714	0.240
p-value	0.007	0.071	0.409
Tissue-blood relative T/S			
Z	0.026	-0.321	0.169
p-value	0.822	0.482	0.563

T/S: Telomere/single copy gene

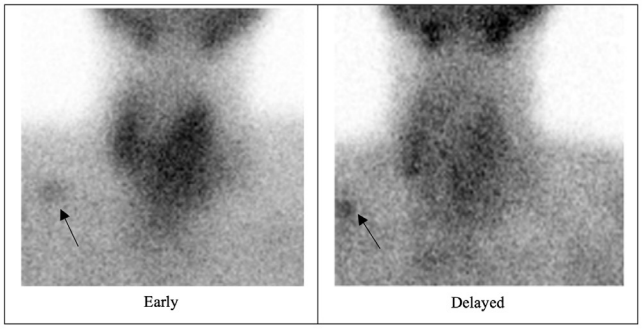

Figure 2. A Tc-99m MIBI thyroid scintigraphy example of a patient with primary thyroid lymphoma. The arrow indicates a metastatic right supraclavicular lymph node, confirmed histopathologically, showing Tc-99m MIBI retention in both early and late images
Tc-99m: Technetium-99m, MIBI: Methoxyisobutylisonitrile

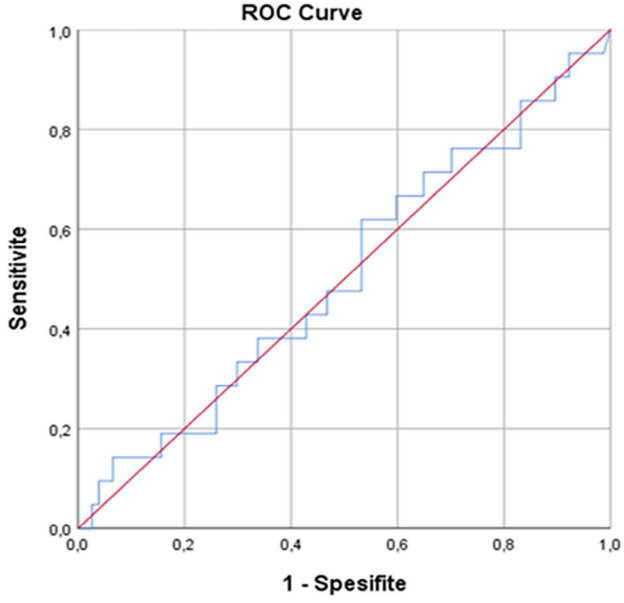

Figure 3. ROC curve analysis of blood relative T/S ratio
ROC: Receiver operating characteristic, T/S: Telomere/single copy gene

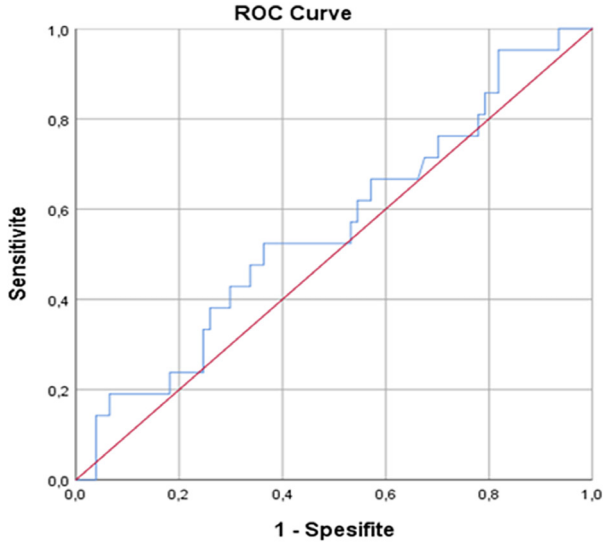

Figure 4. ROC curve analysis of plasma relative T/S ratio
ROC: Receiver operating characteristic, T/S: Telomere/single copy gene

of cancer cells express telomerase, 5-15% activate the ALT pathway (24,25). Telomerase is active in embryonic and stem cells and is upregulated in over 90% of cancers, including thyroid cancer, allowing indefinite replication of cancer cells. Telomerase comprises two subunits: telomerase RNA and telomerase reverse transcriptase (TERT) (26). TERT mutations occur in 11.3% of well-differentiated papillary thyroid cancers, 17.1% of follicular thyroid cancers, 32% of widely invasive Hurthle cell carcinomas, 43.2% of poorly differentiated thyroid cancers, and 40.1% of anaplastic thyroid cancers (27).

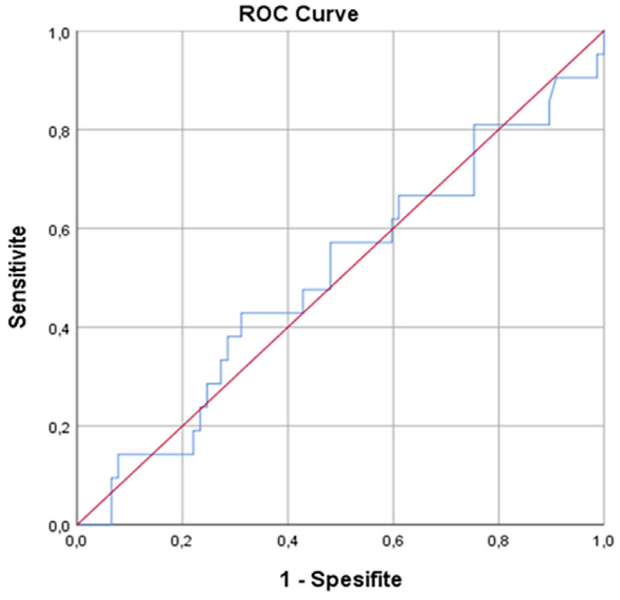

Figure 5. ROC curve analysis of thyroid biopsy tissue relative T/S ratio. ROC: Receiver operating characteristic, T/S: Telomere/single copy gene

Table 6. Blood relative T/S ratio ROC curve analysis result			
Area under the curve	**Standard deviation**	**p-value**	**95% confidence interval**
0.507	0.072	0.924	0.365-0.648
ROC: Receiver operating characteristic, T/S: Telomere/single copy gene			

Table 7. Plasma relative T/S ratio ROC curve analysis result			
Area under the curve	**Standard deviation**	**p-value**	**95% confidence interval**
0.558	0.071	0.416	0.418-0.698
ROC: Receiver operating characteristic, T/S: Telomere/single copy gene			

Table 8. Thyroid biopsy tissue relative T/S ratio ROC curve analysis result			
Area under the curve	**Standard deviation**	**p-value**	**95% confidence interval**
0.504	0.074	0.959	0.359-0.648
ROC: Receiver operating characteristic, T/S: Telomere/single copy gene			

In a meta-analysis by Ma et al. (28) (which included 21 studies), shorter telomeres were found to be significantly associated with cancer risk; particularly in smoking-related cancers like bladder and lung cancers; as well as digestive and urogenital system cancers. Telomerase activity was reported to increase and telomere length was reported to decrease in thyroid cancer tissues and follicular adenomas compared to normal peritumoral tissues. In a study by Capezzone et al. (29), the average relative telomere length of familial papillary thyroid carcinoma (PTC) patients was found to be short in neoplastic thyroid tissues (0.87±0.2), but no significant difference was observed compared to normal contralateral thyroid tissues (0.85±0.11) and extrathyroidal tissues (0.85±0.31). Conversely, in patients with sporadic PTC, the average relative telomere length was significantly shorter in neoplastic tissues (1.73±0.63) than in normal contralateral tissues (2.58±0.89) and extrathyroidal tissues (2.5±0.86) (29). Caria et al. (30) found that the relative telomere length was significantly shorter in familial PTC samples than in sporadic PTC samples (mean 0.93 vs. 1.9). In a study comparing telomere lengths among thyroid cancer subgroups, very short telomeres were detected in 12 out of 15 PTCs (80%), 1 out of 4 follicular carcinomas (25%), all 3 Hurthle cell carcinomas (100%), and 4 out of 12 follicular variant of papillary thyroid carcinomas (FVPTCs) (33%) when compared to adjacent normal thyroid tissue. In the same study, the average telomere lengths of thyroid tumors were statistically significant and shorter in the following order: PTC, flow cytometry/hydrocarbons, FVPTC, functional assessment/hemagglutinin, and hyperplastic nodules. Another study found that the *TINF2* gene was associated with melanoma and PTC, and in contrast to other studies, increased telomere length was observed in patients with these mutations (31).

In a prospective study measuring telomere length in leukocytes, a reduced average relative telomere length was found to be significantly associated with a higher risk of PTC (32). Another regression analysis investigating telomere length in leukocytes found that shorter relative telomere length was significantly associated with an increased risk of renal cell carcinoma (RCC), with an RTL of 3.18±1.50 in the RCC group compared to 4.39±1.99 in the control group (33). In a study measuring telomere length in hematological malignancies, patients had shorter average relative telomere lengths. This was observed in both familial and non-familial cases of hematological malignancies (34).

A study investigating the relationship between cfDNA levels and various biological and lifestyle factors found that acute exercise, pesticide exposure, and stress increased cfDNA. Smoking, body mass index, hypertension, circadian rhythm, gender, age, and chronic exercise caused inconsistent changes. Ionizing radiation decreased cfDNA, while alcohol consumption and menstruation did not cause any changes (35).

In studies on cfDNA telomere lengths during cancer development, shortened telomeres in serum samples were linked to increased gastric cancer risk and early breast cancer detection. Shorter telomeres were also observed in patients with ductal carcinoma in situ (34,35). In HBV patients, longer telomeres in baseline serum were associated with HCC risk. While shortened telomeres are known to promote cancer by inducing chromosomal instability, recent studies suggest that both shortened and abnormally elongated telomeres are linked to various cancers (36).

Unlike the reported studies, our research compared telomere lengths in leukocytes, plasma cfDNA, and tumor cells, and found no statistically significant difference between relative T/S values across these groups. Although not statistically significant, the relative leukocyte T/S value was found to be higher in the malignant group compared to other groups. The relative cfDNA T/S value was higher in the benign group than in the suspicious and malignant groups. Notably, the average relative T/S ratios in tissues was very close between the malignant and benign groups.

Study Limitations

In our study, the small total number of patients and subgroup sizes limited the ability to conduct reliable statistical analyses. Therefore, further prospective, case-controlled studies with larger sample sizes and standardization of methods are needed.

Conclusion

In this study, we investigated the validity and reliability of non-invasive methods, such as Tc-99m MIBI scintigraphy and DNA telomere length measurements, in predicting the presence of malignancy in thyroid nodules. The results indicate that Tc-99m MIBI scintigraphy has a reasonable diagnostic performance in predicting the risk of malignancy in thyroid nodules. With its high negative predictive value, a negative Tc-99m MIBI scan can reliably rule out malignancy. According to our findings, the relative telomere lengths in blood (leukocytes), plasma (cfDNA), and tissue samples did not provide statistically significant results in distinguishing between malignant and benign groups. This finding is inconsistent with the limited literature suggesting that relative telomeric length may be a valid method for predicting thyroid malignancy. In the evaluation of malignancy in thyroid nodules, Tc-99m MIBI scintigraphy appears to be a more accurate and cost-effective method compared to telomere length analysis.

Ethics

Ethics Committee Approval: This study received ethical approval from the Çanakkale Onsekiz Mart University Rectorate Clinical Research Ethics Committee (date: 12/03/2020, decision no: 2020-04).

Informed Consent: All participants were informed about the study prior to the collection of blood and biopsy samples, and they were included after obtaining signed consent forms.

Acknowledgement

This study supported by Scientific Research Coordination Unit of Çanakkale Onsekiz Mart University under the project number TTU-2020-3369.

Footnotes

Authorship Contributions

Concept: S.U.Ö., Design: F.K.Ö., S.U.Ö., Data Collection or Processing: F.K.Ö., S.U.Ö., E.K., F.S., Analysis or Interpretation: F.K.Ö., S.U.Ö., E.K., F.S., Literature Search: F.K.Ö., S.U.Ö., Writing: F.K.Ö., S.U.Ö.

Conflict of Interest: No conflict of interest was declared by the authors.

Financial Disclosure: This study supported by Scientific Research Coordination Unit of Çanakkale Onsekiz Mart University under the project number TTU-2020-3369.

References

1. Ospina NS, Papaleontiou M. Thyroid nodule evaluation and management in older adults: A review of practical considerations for clinical endocrinologists. Endocr Pract. 2021;27:261-268.
2. Alexander EK, Cibas ES. Diagnosis of thyroid nodules. Lancet Diabetes Endocrinol. 2022;10:533-539.
3. Xia M, Song F, Zhao Y, Xie Y, Wen Y, Zhou P. Ultrasonography-based radiomics and computer-aided diagnosis in thyroid nodule management: performance comparison and clinical strategy optimization. Front Endocrinol (Lausanne). 2023;14:1140816.
4. Burgos N, Ospina NS, Sipos JA. The future of thyroid nodule risk stratification. Endocrinol Metab Clin North Am. 2022;51:305-321.
5. Hamour AF, Yang W, Lee JJW, Wu V, Ziai H, Singh P, Eskander A, Sahovaler A, Higgins K, Witterick IJ, Vescan A, Freeman J, de Almeida JR, Goldstein D, Gilbert R, Chepeha D, Irish J, Enepekides D, Monteiro E. Association of the implementation of a standardized thyroid ultrasonography reporting program with documentation of nodule characteristics. JAMA Otolaryngol Head Neck Surg. 2021;147:343-349.
6. Giovanella L, Campenni A, Treglia G, Verburg FA, Trimboli P, Ceriani L, Bongiovanni M. Molecular imaging with (99m)Tc-MIBI and molecular testing for mutations in differentiating benign from malignant follicular

neoplasm: a prospective comparison. Eur J Nucl Med Mol Imaging. 2016;43:1018-1026.
7. Treglia G, Caldarella C, Saggiorato E, Ceriani L, Orlandi F, Salvatori M, Giovanella L. Diagnostic performance of (99m)Tc-MIBI scan in predicting the malignancy of thyroid nodules: a meta-analysis. Endocrine. 2013;44:70-78.
8. Mo H, Wang X, Ma F, Qian Z, Sun X, Yi Z, Guan X, Li L, Liu B, Xu B. Genome-wide chromosomal instability by cell-free DNA sequencing predicts survival in patients with metastatic breast cancer. Breast. 2020;53:111-118.
9. Adhit KK, Wanjari A, Menon S, K S. Liquid biopsy: An evolving paradigm for non-invasive disease diagnosis and monitoring in medicine. Cureus. 2023;15:e50176.
10. Lone SN, Nisar S, Masoodi T, Singh M, Rizwan A, Hashem S, El-Rifai W, Bedognetti D, Batra SK, Haris M, Bhat AA, Macha MA. Liquid biopsy: a step closer to transform diagnosis, prognosis and future of cancer treatments. Mol Cancer. 2022;21:79.
11. Fan HC, Chang FW, Tsai JD, Lin KM, Chen CM, Lin SZ, Liu CA, Harn HJ. Telomeres and cancer. Life (Basel). 2021;11:1405.
12. Okamoto K, Seimiya H. Revisiting telomere shortening in cancer. Cells. 2019;8:107.
13. Velez Torres JM, Vaickus LJ, Kerr DA. Thyroid fine-needle aspiration: the current and future landscape of cytopathology. Surg Pathol Clin. 2024;17:371-381.
14. Juhlin CC, Baloch ZW. Pitfalls in Thyroid fine-needle aspiration cytopathology: an approach to atypical findings. Acta Cytol. 2024;68:179-193.
15. Xu HB, Li L, Xu Q. Tc-99m sestamibi scintimammography for the diagnosis of breast cancer: meta-analysis and meta-regression. Nucl Med Commun. 2011;32:980-988.
16. Nosotti M, Santambrogio L, Gasparini M, Baisi A, Bellaviti N, Rosso L. Role of (99m)tc-hexakis-2-methoxy-isobutylisonitrile in the diagnosis and staging of lung cancer. Chest. 2002;122:1361-1364.
17. Giovanella L, Petranović Ovčariček P. Functional and molecular thyroid imaging. Q J Nucl Med Mol Imaging. 2022;66:86-92.
18. Giubbini R, Bertagna F. 99mTc-MIBI imaging in thyroid nodules: is it useful? Endocrine. 2014;46:1-2.
19. Verburg FA, Behrendt FF, Mottaghy FM, Heinzel A. Cost-effectiveness of (99m)Tc-MIBI in the evaluation of thyroid nodules for malignancy: A new lease of life for an old radiopharmaceutical? Eur J Nucl Med Mol Imaging. 2014;41:102-104.
20. Manevska N, Makazlieva T, Stoilovska Rizova B, Stojanoski S. The usefulness of [99mTc]MIBI scintigraphy in the diagnostic algorithm of ultrasonographical suspected thyroid nodules by using EU-TIRADS criteria. Nucl Med Rev Cent East Eur. 2023;26:29-33.
21. Saggiorato E, Angusti T, Rosas R, Martinese M, Finessi M, Arecco F, Trevisiol E, Bergero N, Puligheddu B, Volante M, Podio V, Papotti M, Orlandi F. 99mTc-MIBI imaging in the presurgical characterization of thyroid follicular neoplasms: relationship to multidrug resistance protein expression. J Nucl Med. 2009;50:1785-1793.
22. Campennì A, Giovanella L, Siracusa M, Alibrandi A, Pignata SA, Giovinazzo S, Trimarchi F, Ruggeri RM, Baldari S. (99m)Tc-methoxy-isobutyl-ısonitrile scintigraphy is a useful tool for assessing the risk of malignancy in thyroid nodules with indeterminate fine-needle cytology. Thyroid. 2016;26:1101-1109.
23. Wale A, Miles KA, Young B, Zammit C, Williams A, Quin J, Dizdarevic S. Combined (99m)Tc-methoxyisobutylisonitrile scintigraphy and fine-needle aspiration cytology offers an accurate and potentially cost-effective investigative strategy for the assessment of solitary or dominant thyroid nodules. Eur J Nucl Med Mol Imaging. 2014;41:105-115.
24. Sohn EJ, Goralsky JA, Shay JW, Min J. The molecular mechanisms and therapeutic prospects of alternative lengthening of telomeres (ALT). Cancers (Basel). 2023;15:1945.
25. Palm W, de Lange T. How shelterin protects mammalian telomeres. Annu Rev Genet. 2008; 42:301-334.
26. Shay JW, Wright WE. Role of telomeres and telomerase in cancer. Semin Cancer Biol. 2011;21:349-353.
27. Fumagalli M, Rossiello F, Clerici M, Barozzi S, Cittaro D, Kaplunov JM, Bucci G, Dobreva M, Matti V, Beausejour CM, Herbig U, Longhese MP, d'Adda di Fagagna F. Telomeric DNA damage is irreparable and causes persistent DNA-damage-response activation. Nat Cell Biol. 2012;14:355-365.
28. Ma H, Zhou Z, Wei S, Liu Z, Pooley KA, Dunning AM, Svenson U, Roos G, Hosgood HD 3rd, Shen M, Wei Q. Shortened telomere length is associated with increased risk of cancer: a meta-analysis. PLoS One. 2011;6:e20466.
29. Capezzone M, Marchisotta S, Cantara S, Pacini F. Telomeres and thyroid cancer. Curr Genomics. 2009;10:526-533.
30. Caria P, Cantara S, Frau DV, Pacini F, Vanni R, Dettori T. Genetic heterogeneity of HER2 amplification and telomere shortening in papillary thyroid carcinoma. Int J Mol Sci. 2016;17:1759.
31. He H, Li W, Comiskey DF, Liyanarachchi S, Nieminen TT, Wang Y, DeLap KE, Brock P, de la Chapelle A. A truncating germline mutation of TINF2 in individuals with thyroid cancer or melanoma results in longer telomeres. Thyroid. 2020;30:204-213.
32. Li J, An C, Zheng H, Lei T, Zhang N, Zheng Y, Yang M. Leukocyte telomere length and risk of papillary thyroid carcinoma. J Clin Endocrinol Metab. 2019;104:2712-2718.
33. Park JY, Luu HN, Park HY, Lin HY, Radlein S, Di Pietro G, Yeo CD, Kim SJ, Kang N, Antwi S, Sexton WJ, Spiess PE, Dickinson S, Parker A. Telomere length in peripheral blood leukocytes and risk of renal cell carcinoma. Transl Cancer Res. 2019;8(Suppl 4):S397-S403.
34. Blackburn NB, Charlesworth JC, Marthick JR, Tegg EM, Marsden KA, Srikanth V, Blangero J, Lowenthal RM, Foote SJ, Dickinson JL. A retrospective examination of mean relative telomere length in the tasmanian familial hematological malignancies study. Oncol Rep. 2015;33:25-32.
35. Medina JE, Dracopoli NC, Bach PB, Lau A, Scharpf RB, Meijer GA, Andersen CL, Velculescu VE. Cell-free DNA approaches for cancer early detection and interception. J Immunother Cancer. 2023;11:e006013.
36. Wan S, Hann HW, Ye Z, Hann RS, Lai Y, Wang C, Li L, Myers RE, Li B, Xing J, Yang H. Prospective and longitudinal evaluations of telomere length of circulating DNA as a risk predictor of hepatocellular carcinoma in HBV patients. Carcinogenesis. 2017;38:439-446.

Original Article

Mol Imaging Radionucl Ther 2025;34:107-113 *DOI:10.4274/mirt.galenos.2025.56514*

Physiological Distribution of ^{18}F-FDG in the Spinal Cord of Disease-Free Subjects

Hastalıksız Bireylerde Spinal Kordda Fizyolojik ^{18}F-FDG Dağılımı

Selin Kesim[1], Salih Özgüven[2]

[1]*University of Health Sciences Türkiye, Kartal Dr. Lutfi Kırdar City Hospital, Clinic of Nuclear Medicine, İstanbul, Türkiye*
[2]*Marmara University Pendik Training and Research Hospital, Clinic of Nuclear Medicine, İstanbul, Türkiye*

Abstract

Objectives: ^{18}Fluorine-fluorodeoxyglucose (^{18}F-FDG) uptake in the spinal cord is not unusual and may mimic metastatic disease. The physiological characterization and variability of spinal cord ^{18}F-FDG metabolism provide valuable information, especially in patients with suspected malignancies. We aimed to investigate the physiological ^{18}F-FDG uptake pattern within the spinal cord and its associations in a normal population.

Methods: We retrospectively analyzed ^{18}F-FDG positron emission tomography/computed tomography images of 140 adult patients who were confirmed to be disease-free over a one-year follow-up period. The maximal and mean standard uptake values (SUV_{max}, SUV_{mean}) were measured at each mid-vertebral level from C1 to L5, and normalized to liver and blood pool uptake. Correlations between ^{18}F-FDG uptake and patient demographics, clinical parameters, and environmental temperature were evaluated.

Results: ^{18}F-FDG uptake demonstrated a decreasing trend from the cervical to lumbar vertebrae, with a notable increase at the lower thoracic levels (T11-T12). There was a significant negative correlation between ^{18}F-FDG uptake and age ($p<0.001$), fasting glucose level ($p=0.016$), and diabetic status ($p=0.003$). No significant association was found between spinal cord ^{18}F-FDG uptake and gender, weight, height, body mass index, ^{18}F-FDG dose, or environmental temperature.

Conclusion: Normal distribution of ^{18}F-FDG in the spinal cord of disease-free individuals decreases from cervical to lumbar levels, although it notably increases at the lower thoracic and mid-lower cervical levels. Uptake significantly decreases with age, with a higher fasting blood glucose level, and in diabetic patients.

Keywords: Spinal cord, ^{18}Fluorine-fluorodeoxyglucose, positron emission tomography/computed tomography, physiological uptake

Öz

Amaç: Spinal kordda ^{18}Flor-florodeoksiglukoz (^{18}F-FDG) tutulumu nadir değildir ve metastatik hastalığı taklit edebilir. Spinal kord ^{18}F-FDG metabolizmasının fizyolojik karakterizasyonu ve değişkenliği, özellikle malignite şüphesi olan hastalarda değerli bilgiler sağlar. Bu çalışmada, normal popülasyonda spinal korddaki fizyolojik ^{18}F-FDG tutulum paternini ve ilişkilerini araştırmayı amaçladık.

Yöntem: Bir yıllık takip süresi boyunca hastalıksız olduğu teyit edilen 140 yetişkin hastanın ^{18}F-FDG pozitron emisyon tomografisi/bilgisayarlı tomografi görüntüleri retrospektif olarak incelendi. C1'den L5'e kadar her orta-vertebral seviyede spinal kanalın maksimum ve ortalama standart

Address for Correspondence: Selin Kesim, University of Health Sciences Türkiye, Kartal Dr. Lütfi Kırdar City Hospital, Clinic of Nuclear Medicine, İstanbul, Türkiye
E-mail: selinkesim@yandex.com **ORCID ID:** orcid.org/0000-0002-6164-9781
Received: 30.10.2024 **Accepted:** 12.01.2025 **Epub:** 15.05.2025 **Publication Date:** 03.05.2025

Cite this article as: Kesim S, Özgüven S. Physiological distribution of ^{18}F-FDG in the spinal cord of disease-free subjects. Mol Imaging Radionucl Ther. 2025;34:107-113.

tutulum değerleri (SUV_{maks}, SUV_{ort}) ölçüldü ve karaciğer ve kan havuzu tutulumu ile normalize edildi. ^{18}F-FDG tutulum yoğunluğu ile hastaların demografik özellikleri, klinik parametreleri ve çevre sıcaklığı arasındaki korelasyonlar araştırıldı.

Bulgular: Spinal korddaki ^{18}F-FDG tutulumu servikal vertebralardan lomber vertebralara doğru azalan bir patern göstermiş olup alt torasik (T11-T12) seviyelerde anlamlı bir artış izlenmiştir. ^{18}F-FDG tutulumu ile yaş (p<0,001), açlık glukoz düzeyi (p=0,016) ve diyabetik durum (p=0,003) arasında anlamlı bir negatif korelasyon bulunmuştur. Spinal kord ^{18}F-FDG tutulumu ile cinsiyet, kilo, boy, vücut kitle indeksi, ^{18}F-FDG dozu veya çevre sıcaklığı arasında ise anlamlı bir ilişki saptanmamıştır.

Sonuç: Hastalıksız bireylerde spinal kordda ^{18}F-FDG dağılımı servikalden lumbar seviyelere doğru azalmakta olup alt torasik ve orta-alt servikal seviyelerde belirgin artış göstermektedir. ^{18}F-FDG tutulumu artan yaşla, açlık kan şekeri seviyesinin yükselmesiyle ve diyabetik hastalarda önemli ölçüde azalmaktadır.

Anahtar kelimeler: Spinal kord, ^{18}Flor-florodeoksiglukoz, pozitron emisyon tomografisi/bilgisayarlı tomografi, fizyolojik tutulum

Introduction

^{18}Fluorine-fluorodeoxyglucose (^{18}F-FDG) positron emission tomography/computed tomography (PET/CT) imaging is increasingly being used in the initial diagnosis, staging, restaging, and monitoring therapy response in oncological patients. The physiological distribution of ^{18}F-FDG has been welldefined; it has high uptake in the heart, liver and brain, eliminates in urine, and concentrates in the gastrointestinal tract with varying degrees. ^{18}F-FDG uptake in the spinal cord is not unusual and may be either physiological or indicative of underlying diseases such as metastatic involvement, vascular, infectious, or inflammatory diseases (1). Spinal metastases constitute approximately 8.5% of all the central nervous system metastases, with lung and breast cancer being the most common primaries (2). Normal variants of physiological uptake in the spinal cord can cause misdiagnosis and unnecessary treatments in oncologic patients. Hence, it is crucial to understand the physiologic distribution of ^{18}F-FDG in the spinal cord for a correct interpretation of PET imaging.

Several studies examined the physiological distribution of ^{18}F-FDG within the spinal cord of adult cancer patients with non-central nervous system malignancies (1,3,4,5,6,7,8), while two studies evaluated the physiological metabolism of the spinal cord in oncologic pediatric patients (9,10). However, these studies have confounding factors such as chemotherapy, radiation therapy, or surgery, that might affect ^{18}F-FDG uptake in the spinal cord due to radiation myelopathy (11,12). To date, only two studies with small sample sizes (n=16, n=30) reported physiologic uptake of ^{18}F-FDG within the spinal cord in disease-free patients (13,14). The aim of this study is to evaluate the physiological ^{18}F-FDG distribution within the spinal cord in disease-free subjects, and assess the influence of gender, age, body weight, body mass index (BMI), diabetes and environmental temperature on spinal cord ^{18}F-FDG uptake in a larger cohort population.

Materials and Methods

Study Design and Patient Selection

We retrospectively evaluated ^{18}F-FDG PET/CT images of adult patients who were referred to our clinic for evaluating suspected malignancy, or characterization of solitary pulmonary nodules over a 24-month period from June 2021 to June 2023. Only 140 patients who were proven to be disease-free during a one-year follow-up were included in the study. Patients with abnormal ^{18}F-FDG PET/CT findings suggestive of malignant disease, a history of former malignancies, chemotherapy, inflammatory or degenerative vertebral diseases affecting spinal cord, and previous spinal operations were excluded from participating in the study. Additionally, patients whose fasting blood glucose levels were higher than 126 mg/dL were excluded, in accordance with the European Association of Nuclear Medicine procedural guidelines for research studies (15). Medical parameters including gender, age, weight, height, BMI, fasting glucose level, diabetes status, and ^{18}F-FDG dose were recorded. Daily local average temperature values were obtained from the national meteorology archives. This study was conducted in accordance with the ethical principles outlined in the Declaration of Helsinki. Approval was obtained from the Marmara University Faculty of Medicine Clinical Research Ethics Committee (number: 09.2021.1437, date: 03.12.2021) and informed consent was obtained from each participant.

^{18}F-FDG PET/CT Protocol

^{18}F-FDG PET/CT images were acquired after a 6-hour fast and approximately 1 hour after intravenous injection of ^{18}F-FDG using a dedicated combined scanner (GE Discovery ST; GE Healthcare, Milwaukee, WI). All patients had a blood sugar level of less than or equal to 126 mg/dL before ^{18}F-FDG injection. First, a multi-slice CT scan was performed with a 16-slice multidetector scanner (parameters: 80 mA; 140kV; table speed: 27 mm/rotation; and slice thickness: 3 mm) from the top of the head through the feet in the

supine position in a shallow breathing patient. A routine whole-body PET scan was conducted in 3D mode, with an acquisition time of 3 minutes per bed position, covering the same area as the CT scan. PET data were reconstructed using an iterative processing algorithm, and the acquisition data transferred to a workstation (Advantage Windows Server 4.5; GE Healthcare) for manual segmentation and interpretation.

Image Analysis

All ^{18}F-FDG PET/CT images were evaluated by two experienced nuclear medicine physicians.

The maximal and mean standard uptake values (SUV_{max}; SUV_{mean}) of the spinal cord at each mid-vertebral level from C1 to L5 were recorded with a standard region of interest (ROI) size. The ROIs for each spinal cord measurement were manually drawn while avoiding the margins of vertebrae (Figure 1). For internal normalization, a reference ROI was placed over the liver, on the 6th hepatic segment, and over the blood pool, particularly on the right atrium, to calculate the normalized SUV_{max} ($nSUV_{max}$) and the normalized SUV_{mean} ($nSUV_{mean}$) values.

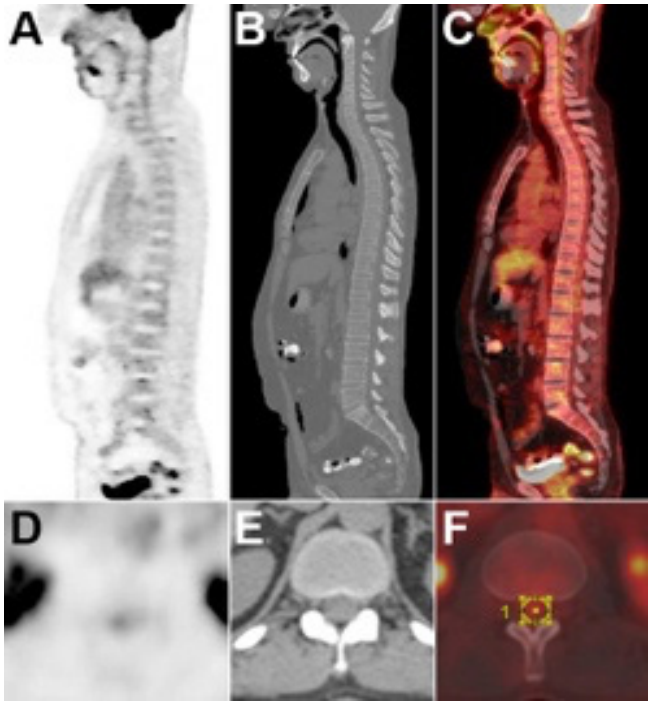

Figure 1. Example of region-of-interest (ROI) delineation for ^{18}F-FDG uptake in the spinal cord. ROIs were manually drawn on fused PET/CT images at the mid-height of each vertebral body level from C1 to L5, avoiding the vertebral margins. (A; sagittal PET image, B; CT image, C; fused PET/CT image, D-E; axial PET, CT, and fused PET/CT images)

PET/CT: Positron emission tomography/computed tomography, ^{18}F-FDG: ^{18}Fluorine-fluorodeoxyglucose

Statistical Analysis

Descriptive statistics were used to present the characteristics of the study population. Continuous data were reported as means ± standard deviations or median, (range), while categorical variables were expressed as frequencies (percentage). A preliminary Kolmogorov-Smirnov test was used to assess the normality of variables. Means were compared with Student's t-test. The correlations of SUV with age, weight, ^{18}F-FDG dose, and temperature were tested with Spearman's correlation analysis. Pearson's correlation analysis was used to determine the relationship between glucose level, height, BMI, and the ^{18}F-FDG uptake of each vertebral level. The pattern of physiological spinal cord, ^{18}F-FDG, distribution was determined by drawing a graph based on the mean $nSUV_{max}$/$nSUV_{mean}$ of each vertebral level. Data were analyzed using IBM SPSS® software version 29.0. Results with two-sided $p<0.05$ were considered statistically significant.

Results

Patient Characteristics

One hundred forty patients (72 men, 68 women) who met the inclusion criteria and were enrolled in the study. The mean age of the patients was 55±16 (men 54.9±16, women 55.2±16.2) years, while the median age was 53.5. Population characteristics are summarized in Table 1.

SUV Measurements

The highest SUV_{max} value was noted at the C1 level (range 1.3-3.1, mean 2.1), while the lowest SUV_{max} value was observed at the L5 level (range 0.5-2.4, mean 1.1). Physiologic ^{18}F-FDG uptake showed a decreasing pattern in the spinal cord from cervical to lumbar vertebrae with a significant increase at the lower thoracic (T11-T12) levels and a relatively insignificant increase at mid-cervical (C4) level. It is notable that the SUV_{max} and SUV_{mean} values, as well as $nSUV_{max}$ and $nSUV_{mean}$ values, were highly correlated ($p<0.000$). The mean SUV_{max} of the spinal cord at the C1 and T12 levellevels was 2.1 and 1.8, respectively. Normal distribution of maximal spinal cord SUV measurements is presented in Figure 2.

Factors affecting ^{18}F-FDG uptake in the spinal cord

There was a statistically significant association between spinal cord ^{18}F-FDG uptake intensity and the presence or absence of diabetes ($p=0.003$). Also, spinal cord ^{18}F-FDG uptake had a negative correlation with age and fasting glucose level ($r=-0.37$, $p<0.001$ and $r=-0.20$, $p=0.016$, respectively, Figure 3). However, no significant association was found between spinal cord ^{18}F-FDG uptake intensity and

Table 1. Patient characteristics			
	n (%)	**n (%)**	**p-value**
Gender	72 (51.4%) men	68 (48.6%) women	0.27[a]
Diabetic status	21 (15%) diabetic	119 (85%) non-diabetic	**0.003**[a]
	Mean	**Range**	
Age	55±16 y	18-88 y	**<0.001**[b]
Weight	73.4±14.6 kg	41-120 kg	0.29[b]
Height	166.6±8.9 cm	140-190 cm	0.51[c]
BMI	26.5±5.2	16.5-44	0.44[c]
Fasting blood glucose level	90±14 mg/dL	60-125 mg/dL	**0.016**[b]
F-18 FDG dose	6±0.5 mCi (222±18.5 MBq)	4.6-7.6 mCi (170-281 MBq)	0.70[b]
Environmental temperature	16±7 °C	0-28.7 °C	0.27[b]

[a]Student t-test, [b]Pearson correlation test, [c]Spearman correlation test, BMI: Body mass index, FDG: Fluorine-fluorodeoxyglucose

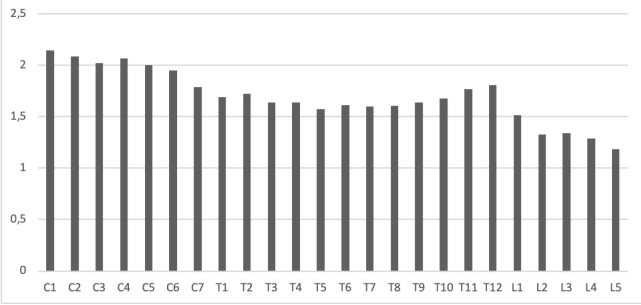

Figure 2. Distribution of ^{18}F-FDG uptake in the spinal cord at each mid-vertebral level

^{18}F-FDG: ^{18}Fluorine-fluorodeoxyglucose

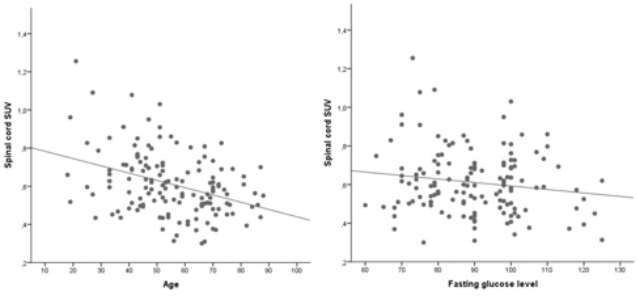

Figure 3. Correlation of mean spinal cord nSUV at the T12 level with age and fasting glucose levels

nSUV: Normalized standardized uptake value

gender (p=0.27), patient weight (p=0.29), height (p=0.51), BMI (p=0.44), ^{18}F-FDG dose (p=0.70), or environmental temperature (p=0.27). Figures 4 and 5 demonstrate that there is a decrease in ^{18}F-FDG uptake in the spinal cord in patients with diabetes and with increasing age, respectively.

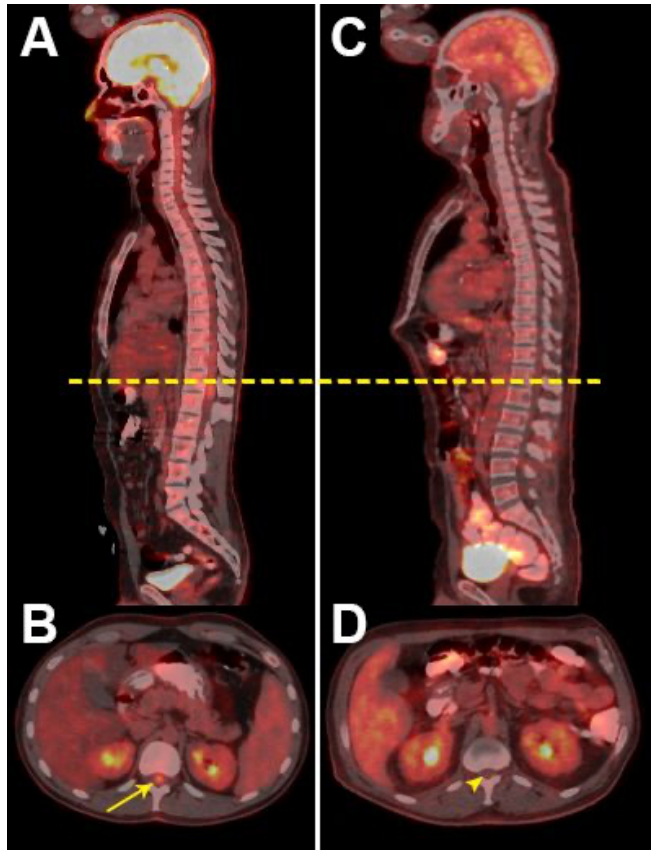

Figure 4. Demonstration of decreased ^{18}F-FDG uptake in diabetic patients. (A) Sagittal and (B) axial fused PET/CT images of a 41-year-old man, who does not have diabetes and and has a fasting glucose level of 79 mg/dL, showing higher spinal cord ^{18}F-FDG uptake (arrow) compared to (C) sagittal and (D) axial fused PET/CT images of a 50-year-old man, who has diabetes and a fasting glucose level of 125 mg/dL (arrowhead)

PET/CT: Positron emission tomography/computed tomography, ^{18}F-FDG: ^{18}Fluorine-fluorodeoxyglucose

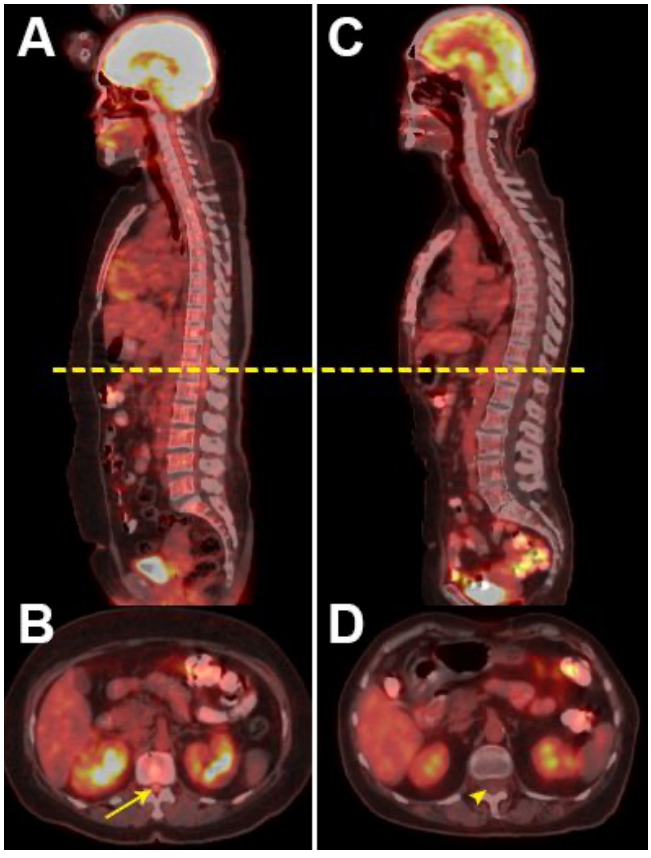

Figure 5. Demonstration of decreased ^{18}F-FDG uptake with age in non-diabetic patients. (A) Sagittal and (B) axial fused PET/CT images of a 31-year-old woman showing higher spinal cord ^{18}F-FDG uptake (arrow) compared to (C) sagittal and (D) axial fused PET/CT images of a 75-year-old woman (arrowhead)

PET/CT: Positron emission tomography/computed tomography, ^{18}F-FDG: ^{18}Fluorine-fluorodeoxyglucose

Discussion

Our results confirm that spinal cord ^{18}F-FDG uptake significantly correlates with patients' age, fasting blood glucose level and diabetic status. No significant association was found between SUV and gender, patient weight, height, BMI, ^{18}F-FDG dose, or environmental temperature. This study also shows the physiological distribution of ^{18}F-FDG uptake within the spinal cord, which is more evident in the cervical and lower thoracic levels. The main difference in our study lies in the study population, which is therapy-naive and proven to be disease-free with the largest sample size reported in the literature.

Several studies reported spinal cord ^{18}F-FDG distribution with a variety of investigation methods. Only two studies calculated SUV_{max} of all spinal segments and reported a decreasing pattern from cervical to lumbar levels with an increase at the lower thoracic and mid-lower cervical levels, which complies with our results (1,14). This pattern is attributed by the authors to cervical and lumbar enlargement and the increased amount of gray matter in children and adults (1,6,9). Another aspect of our study was to evaluate the consistency of SUV calculated within the spinal cord and those normalized to liver or blood pool. The physiological distribution of SUV_{max} and SUV_{mean} in the spinal cord correlated well with the distribution of $nSUV_{max}$ and $nSUV_{mean}$.

Most of the studies reported in the literature were carried out in patients with a history of cancer and radiation therapy. However, white matter necrosis, demyelination, and malacia are typical features of radiation damage to the spinal cord, which may result in decreased ^{18}F-FDG uptake (16). In addition, radiation myelopathy is associated with increased ^{18}F-FDG uptake in the irradiated spinal cord (11,12). Although some studies excluded patients who had previously received radiation therapy, the studies did not consider the impact of chemotherapy, which could also interrupt the blood-spinal cord barrier, resulting in edema, demyelination, and finally necrosis and atrophy of the spinal cord (17).

Two pediatric studies reported a significant increase in SUV within the spinal cord with increasing age (9,10). In adult patients, most studies did not find any correlation between spinal cord ^{18}F-FDG uptake and age (1,3,5,14,18). Contrary to these studies, Kamoto et al. (19) and Tan et al. (20) reported a negative association between metabolic activity of the spinal cord and age in oncologic patients. Our study is the first to determine a negative correlation between age and spinal cord metabolic activity in a healthy adult population. Although neural plasticity and volumetric growth of the spinal cord during childhood development could be responsible for the positive correlation between age and spinal cord activity, age-related decreases in SUV in adult patients may be a reflection of age-associated structural atrophy, reduced nerve conduction velocity, and reduced motor activity (21).

Greenspan et al. (7) reported a statistically significant association between distal spinal cord uptake and lower blood glucose levels; however, there was no significant association between patients' diabetic status and any other variable. In 2022, Tan et al. (20) reported that intense ^{18}F-FDG uptake in the distal spinal cord was more common in patients without diabetes and with lower blood glucose levels. Contrarily, the studies conducted by Nakamoto et al. (18) and Patel et al. (5) did not find a correlation between the plasma glucose level and the cervical spinal cord ^{18}F-FDG uptake. In our study, mean spinal cord SUV

and nSUV values were lower in diabetic patients, who also exhibited higher glucose levels. Previous studies reported lower cerebral ^{18}F-FDG uptake in patients with diabetes (22). Although the pathogenesis is not fully understood, insulin-induced upregulation of hepatic glucokinase results in hepatocellular glucose uptake and increased glucose flux to the central nervous system. While hyperglycemia is reported to have a greater impact on ^{18}F-FDG uptake in the central nervous system compared to the liver (23), the reduced SUV and nSUV in our study group may be explained by poorly controlled hyperglycemia in diabetes, leading to competitive inhibition of ^{18}F-FDG uptake in normal tissues.

In this study, no association was found between patients' weight, height, or BMI and spinal cord metabolism. A few studies reported a positive correlation between body weight and spinal cord ^{18}F-FDG uptake (6,10). Since ^{18}F-FDG distribution is very low in adipose tissue, higher SUV is expected in overweight patients. This vague result could be mitigated by applying SUV correction for lean body mass or body surface area.

With regard to seasonal variation, Amin et al. (3) reported increased cord ^{18}F-FDG uptake in winter, which is based on the hypothesis that activation of the sympathetico-adrenal system leads glucose flux to the central nervous system. However, similar to the results reported by other investigators, we did not find a relation between environmental temperature and spinal cord ^{18}F-FDG uptake (4,10,14).

An association between gender and cord uptake has been investigated by many authors. Greenspan et al. (7) and Taralli et al. (10) reported a positive correlation with female sex. This can be explained by the higher metabolism of the lumbosacral tract secondary to women's reproductive system innervation. However, sex difference was not reported in most other studies, which are similar to our results (3,5,14,18,20).

Study Limitations

The limitations of this study include its retrospective design. Also, the time interval between ^{18}F-FDG injection and imaging was not taken into account in correlation analyses. Nevertheless, the strong points of our study are the SUV measurement method, which includes each mid-vertebral spinal level, and the inclusion of a specific disease-free patient group.

Conclusion

In normal subjects, physiological ^{18}F-FDG uptake in the spinal cord decreases from cervical to lumbar levels, although there is an increase noted at the lower thoracic and mid-lower cervical regions. The present study provides evidence that spinal cord ^{18}F-FDG uptake significantly decreases with increasing age, blood glucose level, and diabetes status in patients. Even though our study included the largest number of normal adult participants to date, the conflicting results with other studies reported in the literature warrant further research with larger sample sizes to obtain more conclusive results.

Ethics

Ethics Committee Approval: Approval was obtained from the Marmara University Faculty of Medicine Clinical Research Ethics Committee (number: 09.2021.1437, date: 03.12.2021).

Informed Consent: Informed consent was obtained from each participant.

Footnotes

Authorship Contributions

Surgical and Medical Practices: S.K., S.Ö., Concept: S.Ö., Design: S.Ö., Data Collection or Processing: S.K., Analysis or Interpretation: S.K., Literature Search: S.K., Writing: S.K.

Conflict of Interest: No conflict of interest was declared by the authors.

Financial Disclosure: The authors declared that this study has received no financial support.

References

1. Do BH, Mari C, Tseng JR, Quon A, Rosenberg J, Biswal S. Pattern of 18F-FDG uptake in the spinal cord in patients with non-central nervous system malignancy. Spine. 2011; 36:1395-1401.
2. Kalayci M, Cağavi F, Gül S, Yenidünya S, Açikgöz B. Intramedullary spinal cord metastases: diagnosis and treatment - an illustrated review. Acta Neurochir. 2004; 146:1347-1354.
3. Amin A, Rosenbaum SJ, Bockisch A. Physiological ^{18}F-FDG uptake by the spinal cord: is it a point of consideration for cancer patients?. J Neurooncol. 2012; 107:609-615.
4. Guner LA, Unal K, Vardareli E, Kaya E, Temiz H, Dayioglu T. Physiological fluorodeoxyglucose uptake of spinal cord in adults. Nucl Med Commun. 2020; 41:659-665.
5. Patel NJ, Gupta V, Vibhute PG, Jain MK, Accurso JM. A large cohort study of 18F fluoro-deoxy-glucose uptake in normal spinal cord: quantitative assessment of the contamination from adjacent vertebral marrow uptake and validity of normalizing the cord uptake against the lumbar thecal sac. J Comput Assist Tomogr. 2017; 41:125-130.
6. Bhatt G, Li XF, Jain A, et al. The normal variant (18)F FDG uptake in the lower thoracic spinal cord segments in cancer patients without CNS malignancy. Am J Nucl Med Mol Imaging. 2013; 3:317-325.
7. Greenspan RL, Suprenant V, Atem F. Visualization of distal spinal cord on F-18 FDG PET/CT. Clin Nucl Med. 2012; 37:137-141.
8. Kiamanesh Z, Banezhad F, Nasiri Z, Emami F, Treglia G, Sadeghi R. Physiological distribution of 18F-FDG in the spinal cord: a systematic review. J Spinal Cord Med. 2021; 44:517-524.
9. McCarville MB, Monu N, Smeltzer MP, et al. PET-CT of the normal spinal cord in children. Acad Radiol. 2009; 16:881-885.

10. Taralli S, Leccisotti L, Mattoli MV, et al. Physiological activity of spinal cord in children: An 18F-FDG PET-CT study. Spine. 2015; 40:647-652.
11. Esik O, Lengyel Z, Sáfrány G, et al. A PET study on the characterization of partially reversible radiogenic lower motor neurone disease. Spinal Cord. 2002; 40:468-473.
12. Chamroonrat W, Posteraro A, El-Haddad G, Zhuang H, Alavi A. Radiation myelopathy visualized as increased FDG uptake on positron emission tomography. Clin Nucl Med. 2005; 30:560.
13. Uematsu H, Sadato N, Yonekura Y, et al. Coregistration of FDG PET and MRI of the head and neck using normal distribution of FDG. J Nucl Med. 1998; 39:2121-2127.
14. Chong A, Song HC, Byun BH, et al. Changes in (18)f-fluorodeoxyglucose uptake in the spinal cord in a healthy population on serial positron emission tomography/computed tomography. Chonnam Med J. 2013; 49:38-42.
15. Boellaard R, Delgado-Bolton R, Oyen WJ, et al. European Association of Nuclear Medicine (EANM). FDG PET/CT: EANM procedure guidelines for tumour imaging: version 2.0. Eur J Nucl Med Mol Imaging. 2015; 42:328-354.
16. Werner-Wasik M, Yu X, Marks LB, Schultheiss TE. Normal-tissue toxicities of thoracic radiation therapy: esophagus, lung, and spinal cord as organs at risk. Hematol Oncol Clin North Am. 2004;18:131-xi.
17. Newton HB. Neurological complications of chemotherapy to the central nervous system. Handb Clin Neurol. 2012; 105:903-916.
18. Nakamoto Y, Tatsumi M, Hammoud D, Cohade C, Osman MM, Wahl RL. Normal FDG distribution patterns in the head and neck: PET/CT evaluation. Radiology. 2005; 234:879-885.
19. Kamoto Y, Sadato N, Yonekura Y, et al. Visualization of the cervical spinal cord with FDG and high-resolution PET. J Comput Assist Tomogr. 1998; 22:487-491.
20. Tan X, Li D, Wu X, Yang Y, Hou Q, He L, Jiang L. Physiologically intense FDG uptake of distal spinal cord on total-body PET/CT. Ann Nucl Med. 2022; 36:643-650.
21. Nieto-Sampedro M, Nieto-Díaz M. Neural plasticity: changes with age. J Neural Transm. 2005; 112:3-27.
22. Eskian M, Alavi A, Khorasanizadeh M, et al. Effect of blood glucose level on standardized uptake value (SUV) in 18F- FDG PET-scan: a systematic review and meta-analysis of 20,807 individual SUV measurements. Eur J Nucl Med Mol Imaging. 2019; 46:224-237.
23. Sprinz C, Zanon M, Altmayer S, et al. Effects of blood glucose level on 18F fluorodeoxyglucose (18F-FDG) uptake for PET/CT in normal organs: an analysis on 5623 patients. Sci Rep. 2018; 8:2126.

Original Article

Mol Imaging Radionucl Ther 2025;34:114-121 *DOI:10.4274/mirt.galenos.2025.62134*

The Impact of ^{18}F-FDG PET/CT and Related Parameters on Staging, Disease Management and Prognosis in Patients with Cholangiocarcinoma

Kolanjiyokarsinomlu Hastalarda ^{18}F-FDG PET/BT ve İlgili Parametrelerin Evreleme, Hastalık Yönetimi ve Prognoz Üzerine Etkisi

Fatih Tamer, Khayala Mammadli, Ülkem Yararbaş

Ege University Faculty of Medicine, Department of Nuclear Medicine, İzmir, Türkiye

Abstract

Objectives: We aimed to evaluate the relationship of ^{18}Fluorine-fluorodeoxyglucose (^{18}F-FDG) positron emission tomography/computed tomography (PET/CT) parameters with diagnostic efficacy, disease management and prognosis in patients with cholangiocarcinoma (CCA). The prognostic value of the spleen/liver ^{18}F-FDG uptake ratio was also investigated.

Methods: The clinical and imaging findings of 39 patients who met the diagnostic criteria and underwent ^{18}F-FDG PET/CT imaging for staging between 2013 and 2023 were retrospectively analysed.

Results: The tumour was intrahepatic in 34 patients and extrahepatic in 5 patients. PET/CT detected nodal involvement in 21 patients (53.8%) and distant metastases in 35 patients (89.7%). Fourteen cases (35.9%) had regional-distant metastases detected by PET/CT but not by magnetic resonance imaging/CT, and the stage of the disease changed accordingly. SUV_{max}, SUV_{mean}, metabolic tumor volume, tumour lesion glycolysis, tumor-to-liver ratio (tumour/liver parenchyma SUV_{max}), tumor-to-background ratio (tumour/blood pool SUV_{max}), tumor-stroma ratio (tumour/spleen parenchyma SUV_{max}), and standardized liver ratio (SLR) (spleen/liver SUV_{max}) did not differ based on tumour location. Recurrence occurred in 14 patients (35.9%), and 2 patients survived. When the cut-off values for the parameters were determined by the Youden index, progression-free survival (PFS) was significantly shorter in patients with an SLR value of less than 0.94 compared to the others (p=0.04). Nodal involvement, metastatic location, and other PET/CT parameters had no significant effect on PFS and overall survival.

Conclusion: Our results highlight the efficacy of ^{18}F-FDG PET/CT in staging nodal and distant metastases, similar to several studies in patients with CCA. Although SLR was found to have significant efficacy in PFS among the parameters we analysed, it is appropriate to evaluate the prognostic significance of these parameters in larger patient groups.

Keywords: Cholangiocellular carcinoma, ^{18}Fluorine-fluorodeoxyglucose, positron emission tomography/computed tomography, positron emission tomography, survival

Address for Correspondence: Fatih Tamer MD, Ege University Faculty of Medicine, Department of Nuclear Medicine, İzmir, Türkiye
E-mail: drfatihtamer@gmail.com **ORCID ID:** orcid.org/0000-0002-5656-9955
Received: 06.11.2024 **Accepted:** 12.01.2025 **Epub:** 14.05.2025 **Publication Date:** 03.05.2025

Cite this article as: Tamer F, Mammadli K, Yararbaş Ü. The impact of ^{18}F-FDG PET/CT and related parameters on staging, disease management and prognosis in patients with cholangiocarcinoma. Mol Imaging Radionucl Ther. 2025;34:114-121.

Öz

Amaç: Bu çalışmada, ^{18}Flor-florodeoksiglukoz (^{18}F-FDG) pozitron emisyon tomografisi/bilgisayarlı tomografi (PET/BT) parametrelerinin kolanjiyokarsinom (CCK) hastalarında tanısal etkinlik, hastalık yönetimi ve prognoz ile ilişkisini değerlendirmeyi amaçladık. Ayrıca dalak/karaciğer ^{18}F-FDG tutulum oranının prognostik değerini de araştırdık.

Yöntem: 2013-2023 yılları arasında tanı kriterlerini karşılayan ve evreleme için ^{18}F-FDG PET/BT görüntülemesi yapılan 39 hastanın klinik ve görüntüleme bulguları retrospektif olarak analiz edildi.

Bulgular: Tümör 34 hastada intrahepatik, 5 hastada ise ekstrahepatikti. PET/BT ile 21 hastada (%53,8) nodal tutulum ve 35 hastada (%89,7) uzak metastaz tespit edildi. On dört olguda (%35,9) PET/BT ile bölgesel-uzak metastaz tespit edilirken manyetik rezonans görüntüleme/BT ile tespit edilemedi ve hastalığın evresi buna göre değişti. SUV_{maks}, SUV_{ort}, metabolik tümör volümü, tümör lezyon glikolizi, tümör/karaciğer oranı (tümör/karaciğer parankimi SUV_{maks}), tümör-arka plan oranı (tümör/kan havuzu SUV_{maks}), tümör-stroma oranı (tümör/dalak parankimi SUV_{maks}) ve standartlaştırılmış karaciğer oranı (SLR) (dalak/karaciğer SUV_{maks}) değerleri tümör yerleşimlerine göre farklılık göstermedi. Hastaların 14'ünde (%35,9) nüks gelişti ve 2 hastada sağkalım mevcuttu. Youden indeksi ile parametreler için cut-off değerleri belirlendiğinde, SLR değeri 0,94'ün altında olan hastalarda progresyonsuz sağkalım (PFS) diğerlerine kıyasla anlamlı olarak daha kısaydı (p=0,04). Nodal tutulum, metastatik yerleşim ve diğer PET/BT parametrelerinin PFS ve genel sağkalım üzerinde anlamlı bir etkisi yoktu.

Sonuç: Bulgularımız, ^{18}F-FDG PET/BT'nin nodal ve uzak metastaz evrelemesindeki etkinliğini vurgulamakta olup, CCK hastalarında yapılan birçok çalışmaya benzerdir. SLR, analiz ettiğimiz parametreler arasında PFS'de anlamlı etkinliğe sahip bulunsa da, bu parametrelerin prognostik öneminin daha büyük hasta gruplarında değerlendirilmesi uygun olacaktır.

Anahtar kelimeler: Kolanjiyoselüler karsinom, ^{18}Flor-florodeoksiglukoz, pozitron emisyon tomografisi/bilgisayarlı tomografi, pozitron emisyon tomografisi, sağkalım

Introduction

Cholangiocellular carcinoma is the second most common primary hepatobiliary tumour (5-30% of primary hepatobiliary tumours) and accounts for 3-5% of gastrointestinal cancers. It originates from the biliary epithelium and has an aggressive course and poor prognosis (1,2). Depending on the location of the tumour, cholangiocarcinoma (CCAs) are divided into 2 groups: intrahepatic CCA (iCCA) and extrahepatic CCA (eCCA) (Klatskin tumour and distal pancreatic duct tumours). It is predominantly eCCA, and in two-thirds of cases, the focus is at the bifurcation of the hepatic ducts. Although the incidence of CCA is higher in Asia than in Western countries, there has been an increase in both incidence and mortality rates, particularly for iCCA, CCA (3,4). While the majority of patients have no identifiable risk factors, there are a number of well-defined risk factors, including primary sclerosing cholangitis, cirrhosis, viral hepatitis, diabetes, and alcohol consumption (5). Nearly 90% of cases are adenocarcinomas, which may show varying degrees of differentiation. Clinical presentation is characterised by predominantly non-specific symptoms, until the advanced stage, making diagnosis difficult. This finding is supported by 2/3 recurrence of cases and 5-year survival rates of 20-40% (6,7). The only curative approach is radical surgical resection with a clear surgical margin. Therefore, tumour-related local features (tumour location, margin, relationship to surrounding structures/degree of invasion), regional lymph node (LN) involvement and distant metastatic status are important markers in this approach (8). This procedure cannot be used due to locally advanced disease, the presence of distant metastases, or insufficient liver capacity, which is observed in approximately 2/3 of cases at the time of diagnosis (9). However, in cases of aggressive or recurrent disease, multidisciplinary treatment modalities including systemic chemotherapy and/or radiotherapy are also used to improve survival (8,10). Imaging plays a pivotal role in the diagnosis of CCA, characterisation of the tumour, accurate staging, particularly in selecting patients for curative surgery, and detection of recurrence. Magnetic resonance imaging (MRI) (MRI, magnetic resonance cholangiopancreatography, contrast-enhanced and diffusion-weighted imaging) and contrast-enhanced computed tomography (CT) are two main non-invasive staging modalities that are routinely used. Although ^{18}Fluorine-fluorodeoxyglucose positron emission tomography/CT (^{18}F-FDG PET/CT), which combines anatomical and functional imaging, has made an important contribution to the assessment of nodal and distant metastatic disease status and the detection of recurrence, its routine clinical use remains controversial (8,11,12). While some studies have identified prognostic factors: LN involvement, distant metastasis, tumour diameter, tumour grade, vascular invasion, R0 resection, it is important to note that these factors primarily relate to postoperative outcomes (6,13). Determining the group of patients with poor prognosis or high risk of recurrence prior to treatment is another important factor that may be effective in selecting the correct staging and curative surgical option. in addition to its role in diagnosis and staging, the contributions of ^{18}F-FDG PET/CT in predicting the prognosis of the disease have been reported (14,15). In our study, we

aimed to evaluate the diagnostic efficacy of ^{18}F-FDG PET/CT parameters, and their relationship with prognostic data in patients with CCA. In addition investigated the prognostic value of the spleen/liver ^{18}F-FDG uptake ratio in patients with CCA, which has been reported in a few studies in the literature (16).

Materials and Methods

Patient Group

We studied 39 patients, who met the inclusion criteria, diagnosed with CCA by imaging or pathology, from a group of 161 patients who underwent staging ^{18}F-FDG PET/CT imaging between 2013 and 2023. Descriptive characteristics (sex, age at diagnosis, date of diagnosis, dates of treatment initiation and last follow-up), ^{18}F-FDG PET/CT staging findings, MRI, contrast-enhanced CT images, and survival characteristics were retrospectively recorded and analysed. Patients who had undergone local or systemic treatment and surgery prior to ^{18}F-FDG PET/CT imaging, patients whose archives did not contain sufficient information on the parameters to be used in the study, and patients with a metastatic second malignancy other than CCA were not included in the study. The definition of recurrence was the detection of local recurrence or distant metastatic lesions on MRI/CT and ^{18}F-FDG PET/CT imaging for restaging/therapy response if performed. Local recurrence was defined in the presence of the following findings: a) soft tissue with a tendency to enlarge in the primary tumour lesion on conventional imaging; causing disruption of the normal anatomical structure and/or obstruction/dilatation of the biliary tract, b) soft tissue with increased ^{18}F-FDG uptake on PET/CT that can be distinguished from an inflammatory lesion (especially in stented cases). Regional LN involvement was considered positive if it showed increased ^{18}F-FDG uptake or if its short axis was greater than 10 mm in the absence of increased metabolism. Again, metastatic involvement was defined as focal areas of ^{18}F-FDG uptake, even if normometabolic, not supported by physiological/inflammatory processes or accompanied by a suspicious morphological abnormality. Regional LN involvement was limited to the periduodenal, hilar, and peripancreatic regions, except for those defined as distant metastases. This retrospective study was conducted with the approval of the Ege University Medical Research Ethics Committee (decision no: 24-6T/48, date: 06.06.2024).

^{18}Fluorine-Fluorodeoxyglucose Positron Emission Tomography/Computed Tomography Imaging and Interpretation of Images

^{18}F-FDG PET/CT imaging was performed with a Siemens Biograph Truepoint-16 device. Images were interpreted as PET, CT, and fusion PET/CT across different slices (coronal, transverse, sagittal), utilizing visual and semiquantitative parameters. The standardised uptake value was calculated as follows: SUV= [tissue radioactivity concentration (Bq per mL)]/[injected radiopharmaceutical activity (Bq)/the body mass (g)]. Attenuation-corrected images were evaluated in two stages by two nuclear medicine specialists using the patients' archive data. The area of interest was drawn from the primary tumor site in cases detected by PET/CT, and from the area defined by conventional imaging and/or pathological sampling in cases not detected by PET/CT but diagnosed by other methods (CT or MRI). In addition to SUV_{max} (g/mL) and SUV_{mean} (g/mL) values, metabolic tumour volume (MTV) and tumour lesion glycolysis (TLG) values were determined by automated contouring, at 40% threshold. A 3 cm diameter area of interest was drawn from the right lobe of the liver and the spleen, and SUV_{max} values of the disease-free liver parenchyma/spleen parenchyma were measured. In addition, a 1 cm spherical region of interest was drawn through the descending aorta to measure blood pool SUV_{max}. The parameters tumour/liver SUV_{max} ratio [tumor-to-liver ratio (TLR)], tumour/blood pool SUV_{max} ratio [tumor-to-background ratio (TBR)], and tumour/spleen SUV_{max} ratio [tumor-stroma ratio (TSR)] were determined by comparing the SUV_{max} values of the primary tumour with the SUV_{max} values of the liver parenchyma, blood pool, and spleen. Date of diagnosis, date of last follow-up, and date of death for deceased patients were recorded. Progression-free survival (PFS) was defined as the time from first local-systemic treatment/curative surgery to relapse or death from any cause, while overall survival (OS) was defined as the time from diagnosis to death from any cause.

Statistical Analysis

The data in the study were analysed using SPSS version 25 (SPSS Inc., Chicago, IL). Normality was analysed using Shapiro-Wilk tests. The χ^2 and Fisher's exact tests (for categories with expected values <5) were used to analyze categorical variables, and independent two-sample t-test and Mann-Whitney U test were used to analyze the relationship between the dependent variable and numerical data. Numerical data are expressed as mean ± standard

deviation and median with 1st and 3rd quartiles (interquartile range), depending on whether they have a normal or skewed distribution. Categorical data are expressed as number and percentage. The Spearman correlation test was used to determine correlations between PET/CT parameters and serum carbohydrate antigen 19-9 (Ca19-9), carcinoembryonic antigen (CEA), and alpha-fetoprotein (AFP) levels. Receiver operating characteristic curves and Youden's index were used to calculate cut-off values of ^{18}F-FDG PET/CT-derived parameters for recurrence, and to categorise them. The Kaplan-Meier method was used for OS and PFS, and the log-rank test and Cox regression analysis were used to compare the incidence of events between patient groups.

The confidence interval for the tests was 95% and the statistical significance level (p) was 0.05.

Results

A total of 39 patients (19 women and 20 men) were included in the study. The diagnosis of CCA was confirmed pathologically in 28 patients, while 11 patients were diagnosed with CCA during follow-up with imaging studies. The clinical and imaging data of the patients are shown in the table (Table 1). The primary tumour was intrahepatic in 34 (87.2%) patients and extrahepatic in 5 (12.8%) cases. The primary lesion was detected by staging PET/CT in 37 patients (94.9%). Similarly, the primary lesion could not be detected by conventional imaging modalities in 2 cases only. Regional LN involvement or distant metastasis was detected by PET/CT in 35 (89.7%) patients, and in 14 (40%) of these, the metastatic focus could not be detected by conventional methods. The only metastatic site not detected by PET/CT but identified by MR/CT was the liver. In 14 (35.9%) patients, local recurrence and new/progressing metastases were detected during follow-up. Only 3 of these patients were still alive at the end of follow-up. No significant differences in PET/CT parameters (SUV_{max}, SUV_{mean}, MTV, TLG, spleen/liver ratio, TLR, TBR, TSR) were observed between patients with iCCA and eCCA (Table 2). No significant difference was observed between iCCA and eCCA cases with regard to the location of the metastatic focus (p=0.3) and regional LN involvement (p=0.424). No significant correlation was found between PET/CT parameters and Ca19-9 and CEA levels (p>0.05). Again, no significant difference in PET/CT parameters was observed between patients with AFP levels above and below the cut-off of 2.72 (p>0.05). Regional LN involvement, location of the metastatic focus, PET/CT parameters, serum CA19-9, CEA, and AFP levels did not have a significant effect on PFS and OS (Table 3). The cut-off values of PET/CT parameters associated with the development of relapse were determined. For each parameter, they were as follows: SUV_{max} 20.92 g/mL, SUV_{mean} 11.23 g/mL, MTV 24.54 mL, TLG 288.03 g, SLR 0.94, TLR 4.28, TBR 8.69, TSR 7.05. When comparing the groups, PFS was significantly shorter in patients with SLR values below 0.94 compared to the others (Table 4). Similarly, PFS was significantly shorter

Table 1. Clinical characteristics and descriptive findings of the patient group

Characteristics		**n**
Age		37-83 (mean:63)
Gender	Male	n=20 (51.3%)
	Female	n=19 (48.7%)
Tumor location	Intrahepatic	34 (87.2%)
	Extrahepatic	5 (12.8%)
PET/CT	Primary lesion +	37 (94.9%)
	Regional LN +	21 (53.8%)
	Distant metastasis +	35 (89.7%)
MRI/Contrast-enhanced CT	Primary lesion +	37 (94.9%)
	Regional LN-distant metastasis +	22 (56.4%)
Distant metastasis	LN	20 (51.3%)
	Liver	10 (25.6%)
	Peritoneal spread	6 (16.7%)
	Pulmonary	5 (12.8%)
	Bone	3 (7.7%)

LN: Lymph node, MRI: Magnetic resonance imaging, PET/CT: Positron emission tomography/computed tomography

Table 2. Analysis between clinical features, PET/CT parameters and tumor location			
	iCCA (n=34)	**eCCA (n=47)**	**p-value**
SUV_{max}	15.31±6.27	14.75±7.29	0.855
SUV_{mean}	8.48±3.89	8.54±4.89	0.976
MTV	55.12 (23.05-86.98)	8.9 (4.85-366.63)	0.120
TLG	436.86 (212.88-665.05)	75.87 (45.94-2987.01)	0.106
Splen/liver SUV_{max}	0.75±0.15	0.85±0.24	0.207
TLR	2.67 (1.92-3.93)	3.44 (1.95-3.65)	0.894
TBR	4.24 (3.09-6.13)	5.58 (3.29-6.56)	0.790
TSR	4.06 (2.48-5.44)	3.31 (2.55-4.65)	0.657

PET/CT-related parameters are shown as means ± SD or median (IQR). The units of the following parameters were as follows: SUV_{max} and SUV_{mean} are g/mL, MTV is mL, TLG is g.
PET/CT: Positron emission tomography/computed tomography, SD: Standard deviation, MTV: Metabolic tumour volume, TLG: Tumour lesion glycolysis, TLR: Tumor-to-liver ratio, TBR: Tumor-to-background ratio, TSR: Tumor-stroma ratio, iCCA: Intrahepatic cholangiocarcinoma , eCCA: Extrahepatic cholangiocarcinoma

Table 3. Univariate analysis of clinical features and PET/CT parameters regarding PFS and OS		
	PFS	**OS**
SUV_{max}	0.318	0.723
SUV_{mean}	0.283	0.594
MTV	0.932	0.249
TLG	0.633	0.238
Splen/liver SUV_{max}	0.798	0.297
TLR	0.170	0.711
TBR	0.161	0.705
TSR	0.176	0.584
Regional lymph node involvement	0.742	0.428
Distant metastatis (Liver-LN-peritonel spread/ visceral organ-bone)	0.371	0.095

PET/CT-related parameters are shown as means ± SD or median (IQR). The units of the following parameters were as follows; SUV_{max}'s and SUV_{mean}'s are g/mL, MTV's is mL, TLG's is gr.
LN: Lymph node, PET/CT: Positron emission tomography/computed tomography, SD: Standard deviation, MTV: Metabolic tumour volume, TLG: Tumour lesion glycolysis, TLR: Tumor-to-liver ratio, TBR: Tumor-to-background ratio, TSR: Tumor-stroma ratio, PFS: Progression-free survival, OS: Overall survival

Table 4. Univariate analysis of PET/CT parameters regarding PFS	
	PFS
SUV_{max} (<20.92 / ≥20.92)	0.155
SUV_{mean} (<11.23 / ≥11.23)	0.127
MTV (<24.54 / ≥24.54)	0.819
TLG (<288.03 / ≥288.03)	0.429
Splen/liver SUV_{max} (<0.94 / ≥0.94)	**0.040**
TLR (<4.28 / ≥4.28)	0.127
TBR (<8.69 / ≥8.69)	0.127
TSR (<7.05 / ≥7.05)	0.127
Regional lymph node involvement	0.742
Distant metastatis (Liver-LN-peritonel spread/visceral organ-bone)	0.371

PET/CT-related parameters are shown as means ± SD or median (IQR). The units of the following parameters were as follows; SUV_{max}'s and SUV_{mean}'s are g/mL, MTV's is mL, TLG's is gr.
LN: Lymph node, PET/CT: Positron emission tomography/computed tomography, SD: Standard deviation, MTV: Metabolic tumour volume, TLG: Tumour lesion glycolysis, TLR: Tumor-to-liver ratio, TBR: Tumor-to-background ratio, TSR: Tumor-stroma ratio, PFS: Progression-free survival

in patients with a spleen/liver SUV_{max} ratio below 0.94 compared to the other group (p=0.04) (Figure 1).

Discussion

CCA is the second most common primary hepatobiliary tumour and has a non-specific clinical presentation, an aggressive course, and a poor prognosis, particularly in advanced stages. The only curative treatment is surgery. Given the recurrence and advanced disease observed in 2/3 of cases, it is important to identify surgical candidates and possible prognostic criteria associated with recurrence. The contribution of ^{18}F-FDG PET/CT, the use of which is controversial for diagnosis/staging purposes other than MR-CT, is one of the issues still under evaluation. It can provide data related to recurrence/survival prior to treatment/surgery compared to prognostic factors defined by postoperative features (tumour diameter, tumour grade, vascular invasion, R0 resection, etc.). Our main aim was to evaluate the diagnostic efficacy, contribution to disease management, and prognostic efficacy of ^{18}F-FDG PET/CT staging parameters. We also investigated the prognostic value of the spleen/liver FDG uptake ratio in patients with CCA.

Table 5. Studies with multivariate analysis of clinical characteristics and PET/CT parameters		
	Prognostic	**Non-prognostic**
Yachi et al. (21)	SUV_{max}	-/NM
Pevner and Tanvetyanon (26)	SUV_{max}, Ca19-9	-/NM
Lin et al. (23)	SUV_{max}, TNR	-/NM
Sabaté-Llobera et al. (17)	CEA, TLR	SUV_{max}, Ca19-9
Lee et al. (18)	-	SUV_{max}, SUV_{mean}, MTV, TLG, SUV_{peak}
Lee et al. (24)	TLG	MTV, SUV_{max}
Harimoto et al. (25)	SUV_{max}, TLG	MTV, CEA, Ca19-9

NM: Non-mentioned, PET/CT: Positron emission tomography/computed tomography, MTV: Metabolic tumour volume, TLG: Tumour lesion glycolysis, TLR: Tumor-to-liver ratio, Ca19-9: Carbohydrate antigen 19-9, CEA: Carcinoembryonic antigen

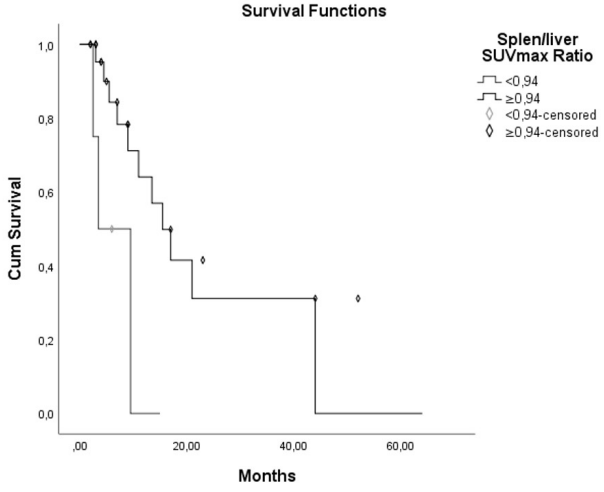

Figure 1. Survival table delineated by the splen/liver SUV_{max} ratio (p=0.04)

Differences and Relationships Between Clinical Findings and PET/CT Parameters

It is known that the incidence of eCCA is higher than that of iCCA in routine clinical practice. However, the different clinical presentation of both subtypes, including late-onset biliary obstruction and advanced stage of disease at diagnosis in iCCA-compared to hilar tumours- and tumour growth pattern, together with the retrospective nature of our study, may explain the predominance of iCCA in our cohort of patients referred with suspected metastases. Although the efficacy of PET/CT and conventional methods in detecting the primary lesion is similar, we believe that it would be more appropriate to test these data in prospective studies with this as the primary focus and a large patient population. In addition, we found that PET/CT was more effective than conventional methods in detecting regional nodal involvement and distant metastases and, consequently, in changing the modality/stage of the disease. Our findings in this regard were largely similar to those reported in the literature (11,14,17,18,19,20). In our study, we examined the SUV_{max} parameter, which is used in current practice, as well as the SUV_{mean} parameter and the MTV and TLG values based on volumetric assessment. In addition, the TLR value was used to minimise differences in the basal FDG uptake of the liver and bias in this area. TBR and TSR were additional parameters evaluated for similar purposes in our study. A further analysis was performed on the SLR parameter, which is known to be particularly effective for staging in the diagnosis of lymphoma, and has been evaluated in a small number of studies for patients with CCA (16). In the literature, it has been reported that both SUV_{max} and TLR were higher in patients with iCCA than in patients with eCCA (17,21). In our study, no significant difference was found in the PET/CT parameters we examined according to tumour location. It has been reported that possible factors such as patient selection (resectability, inclusion of non-CCA cancers such as gallbladder cancer in studies), tumour cell origin, and tumour growth pattern may be responsible for these differences observed between studies. Again, regional nodal involvement did not differ according to tumour location in our study, and this finding is consistent with the literature (17). Although not specific for the disease, serum tumour markers such as CA19-9, CEA, and AFP are used in the diagnosis and follow-up of patients with CCA and especially in the follow-up of recurrence. Sabaté-Llobera et al. (17) reported that SUV_{max} and TLR were significantly but weakly correlated with serum CA19-9 and CEA levels. In our data, no significant difference or correlation was found between these serum markers and PET/CT parameters.

Prognosis

As previously described in the literature for various types of cancer, prognostic parameters in CCA are predominantly associated with post-operative processes. However, it is important to identify poor prognostic markers in cases where curative surgery is not an option, and especially

in the early stages of the disease, before treatment or surgery. Accordingly, the prognostic efficacy of various clinical/imaging factors in patients with CCA has been described (Table 5) (11,14,17,18,21,22,23,24,25,26). In univariate analysis, regional LN involvement, metastatic location, PET/CT parameters, serum CA19-9, CEA, and AFP levels did not significantly affect PFS and OS. However, when the Youden index was used to determine cut-off values for SUV_{max}, SUV_{mean}, MTV, TLG, TLR, TSR, and SLR values, PFS was significantly shorter in patients with SLR values below 0.94 compared with the others. Although it provides a different perspective, we would like to point out that in our patient population, the survival analysis applied by setting cut-offs has limited power. This limitation is due to significant heterogeneity in the number of patients in the groups. Our study has several key findings. One was the evaluation of clinical and prognostic differences, as well as the effects on patients across a wide range of parameters. A contributing factor was the relatively high homogeneity of the patient group in our study in terms of tumour location (87.2% iCCA) and stage (94.9% stage IV), despite considering differences in prognosis between patients at different stages and at diagnosis of iCCA-eCCA patients.

Study Limitations

We emphasise that our study should be evaluated in light of several limitations. Most importantly, our study carries a foreseeable risk of selection bias due to its retrospective nature. Another disadvantage is the relatively small number of patients with eCCA in our cohort, which limits the evaluation of clinical and prognostic factors according to tumour location, although this was not the main aim of our study.

Conclusion

In conclusion, we consider that ^{18}F-FDG PET/CT is a useful imaging modality in cases of CCA, as it allows functional imaging in addition to anatomical imaging and allows whole-body imaging, especially when compared to MRI. In this regard, we would like to reiterate the necessity of PET/CT in cases of CCA, especially considering its greater effectiveness than conventional imaging in disease management and detection of regional/distant metastases. We note that the SLR parameter, which has been evaluated in a few studies, especially in the hepatobiliary cancer group, may be an effective factor in the development of recurrence in cases with CCA. We speculate that the conflicting findings in prognostic factors observed in our study and in the literature may be secondary to the composition of the patient group (iCCA-eCCA, additional diagnoses such as gallbladder cancer that cause heterogeneity) and other disease-related factors (differences in patient stage). In this context, we would like to emphasise again the need for prospective studies evaluating large series of patients.

Ethics

Ethics Committee Approval: This retrospective study was conducted with the approval of the Ege University Medical Research Ethics Committee (decision no: 24-6T/48, date: 06.06.2024).

Informed Consent: Retrospective study.

Footnotes

Authorship Contributions

Surgical and Medical Practices: F.T., Concept: F.T., Design: F.T., Data Collection or Processing: F.T., K.M., Analysis or Interpretation: F.T., K.M., Literature Search: F.T., Writing: F.T.,Ü.Y.

Conflict of Interest: No conflict of interest was declared by the authors.

Financial Disclosure: The authors declared that this study received no financial support.

References

1. Qurashi M, Vithayathil M, Khan SA. Epidemiology of cholangiocarcinoma. Eur J Surg Oncol. 2025;51:107064.
2. Valle JW, Kelley RK, Nervi B, Oh DY, Zhu AX. Biliary tract cancer. Lancet. 2021;397:428-444.
3. Vithayathil M, Khan SA. Current epidemiology of cholangiocarcinoma in Western countries. J Hepatol. 2022;77:1690-1698.
4. Banales JM, Cardinale V, Carpino G, Marzioni M, Andersen JB, Invernizzi P, Lind GE, Folseraas T, Forbes SJ, Fouassier L, Geier A, Calvisi DF, Mertens JC, Trauner M, Benedetti A, Maroni L, Vaquero J, Macias RI, Raggi C, Perugorria MJ, Gaudio E, Boberg KM, Marin JJ, Alvaro D. Expert consensus document: Cholangiocarcinoma: current knowledge and future perspectives consensus statement from the European Network for the Study of Cholangiocarcinoma (ENS-CCA). Nat Rev Gastroenterol Hepatol. 2016;13:261-280.
5. Palmer WC, Patel T. Are common factors involved in the pathogenesis of primary liver cancers? A meta-analysis of risk factors for intrahepatic cholangiocarcinoma. J Hepatol. 2012;57:69-76.
6. Yoh T, Hatano E, Nishio T, Seo S, Taura K, Yasuchika K, Okajima H, Kaido T, Uemoto S. Significant improvement in outcomes of patients with intrahepatic cholangiocarcinoma after surgery. World J Surg. 2016;40:2229-2236.
7. Bridgewater J, Galle PR, Khan SA, Llovet JM, Park JW, Patel T, Pawlik TM, Gores GJ. Guidelines for the diagnosis and management of intrahepatic cholangiocarcinoma. J Hepatol. 2014;60:1268-1289.
8. Benson AB, D'Angelica MI, Abrams T, Abbott DE, Ahmed A, Anaya DA, Anders R, Are C, Bachini M, Binder D, Borad M, Bowlus C, Brown D, Burgoyne A, Castellanos J, Chahal P, Cloyd J, Covey AM, Glazer ES, Hawkins WG, Iyer R, Jacob R, Jennings L, Kelley RK, Kim R, Levine M, Palta M, Park JO, Raman S, Reddy S, Ronnekleiv-Kelly S, Sahai V, Singh G, Stein S, Turk A, Vauthey JN, Venook AP, Yopp A, McMillian N, Schonfeld R, Hochstetler C. NCCN Guidelines® Insights: Biliary Tract Cancers, Version 2.2023. J Natl Compr Canc Netw. 2023;21:694-704.

9. Mazzaferro V, Gorgen A, Roayaie S, Droz Dit Busset M, Sapisochin G. Liver resection and transplantation for intrahepatic cholangiocarcinoma. J Hepatol. 2020;72:364-377.
10. Valle JW, Borbath I, Khan SA, Huguet F, Gruenberger T, Arnold D; ESMO Guidelines Committee. Biliary cancer: ESMO Clinical Practice Guidelines for diagnosis, treatment and follow-up. Ann Oncol. 2016;27(suppl 5):v28-v37.
11. Ma KW, Cheung TT, She WH, Chok KSH, Chan ACY, Dai WC, Chiu WH, Lo CM. Diagnostic and Prognostic Role of 18-FDG PET/CT in the Management of Resectable Biliary Tract Cancer. World J Surg. 2018;42:823-834.
12. Elias Y, Mariano AT Jr, Lu Y. Detection of primary malignancy and metastases with FDG PET/CT in patients with cholangiocarcinomas: lesion-based comparison with contrast enhanced CT. World J Nucl Med. 2016;15:161-166.
13. Izquierdo-Sanchez L, Lamarca A, La Casta A, Buettner S, Utpatel K, Klümpen HJ, Adeva J, Vogel A, Lleo A, Fabris L, Ponz-Sarvise M, Brustia R, Cardinale V, Braconi C, Vidili G, Jamieson NB, Macias RI, Jonas JP, Marzioni M, Hołówko W, Folseraas T, Kupčinskas J, Sparchez Z, Krawczyk M, Krupa Ł, Scripcariu V, Grazi GL, Landa-Magdalena A, Ijzermans JN, Evert K, Erdmann JI, López-López F, Saborowski A, Scheiter A, Santos-Laso A, Carpino G, Andersen JB, Marin JJ, Alvaro D, Bujanda L, Forner A, Valle JW, Koerkamp BG, Banales JM. Cholangiocarcinoma landscape in Europe: diagnostic, prognostic and therapeutic insights from the ENSCCA Registry. J Hepatol. 2022;76:1109-1121.
14. Kim NH, Lee SR, Kim YH, Kim HJ. Diagnostic performance and prognostic relevance of FDG positron emission tomography/computed tomography for patients with extrahepatic cholangiocarcinoma. Korean J Radiol. 2020;21:1355-1366.
15. Cho KM, Oh DY, Kim TY, Lee KH, Han SW, Im SA, Kim TY, Bang YJ. Metabolic characteristics of advanced biliary tract cancer using 18F-fluorodeoxyglucose positron emission tomography and their clinical implications. Oncologist. 2015;20:926-933.
16. Pak K, Kim SJ, Kim IJ, Kim DU, Kim K, Kim H, Kim SJ. Splenic FDG uptake predicts poor prognosis in patients with unresectable cholangiocarcinoma. Nuklearmedizin. 2014;53:26-31.
17. Sabaté-Llobera A, Gràcia-Sánchez L, Reynés-Llompart G, Ramos E, Lladó L, Robles J, Serrano T, Mestres-Martí J, Gámez-Cenzano C. Differences on metabolic behavior between intra and extrahepatic cholangiocarcinomas at ^{18}F-FDG-PET/CT: prognostic implication of metabolic parameters and tumor markers. Clin Transl Oncol. 2019;21:324-333.
18. Lee Y, Yoo IR, Boo SH, Kim H, Park HL, Hyun O J.The role of F-18 FDG PET/CT in intrahepatic cholangiocarcinoma. Nucl Med Mol Imaging. 2017;51:69-78.
19. Nishioka E, Tsurusaki M, Kozuki R, Im SW, Kono A, Kitajima K, Murakami T, Ishii K. Comparison of conventional imaging and 18F-fluorodeoxyglucose positron emission tomography/computed tomography in the diagnostic accuracy of staging in patients with intrahepatic cholangiocarcinoma. Diagnostics (Basel). 2022;12:2889.
20. Huang X, Yang J, Li J, Xiong Y. Comparison of magnetic resonance imaging and 18-fludeoxyglucose positron emission tomography/computed tomography in the diagnostic accuracy of staging in patients with cholangiocarcinoma: a meta-analysis. Medicine (Baltimore). 2020;99:e20932.
21. Yachi T, Yoshizawa T, Kimura N, Seino H, Morohashi S, Goto S, Ishido K, Kijima H, Hakamada K. ^{18}F-fluorodeoxyglucose positron emission tomography predicts recurrence and histological grade of extrahepatic bile duct cancer. Oncol Lett. 2023;25:125.
22. Yoh T, Seo S, Morino K, Fuji H, Ikeno Y, Ishii T, Taura K, Nakamoto Y, Higashi T, Kaido T, Uemoto S. Reappraisal of Prognostic Impact of Tumor SUVmax by ^{18}F-FDG-PET/CT in Intrahepatic Cholangiocarcinoma. World J Surg. 2019;43:1323-1331.
23. Lin Y, Chong H, Song G, Zhang C, Dong L, Aye L, Liang F, Yang S, Zeng M, Ding G, Zhang S, Shi J, Ke A, Wang X, Zhou J, Fan J, Gao Q. The influence of ^{18}F-fluorodeoxyglucose positron emission tomography/computed tomography on the N- and M-staging and subsequent clinical management of intrahepatic cholangiocarcinoma. Hepatobiliary Surg Nutr. 2022;11:684-695.
24. Lee EJ, Chang SH, Lee TY, Yoon SY, Cheon YK, Shim CS, So Y, Chung HW. Prognostic value of FDG-PET/CT total lesion glycolysis for patients with resectable distal bile duct adenocarcinoma. Anticancer Res. 2015;35:6985-6991.
25. Harimoto N, Hoshino K, Muranushi R, Hagiwara K, Yamanaka T, Ishii N, Tsukagoshi M, Igarashi T, Tanaka H, Watanabe A, Kubo N, Araki K, Tomonaga H, Higuchi T, Tsushima Y, Shirabe K. Impact of metabolic parameters of ^{18}F-fluorodeoxyglucose positron-emission tomography after hepatic resection in patients with intrahepatic cholangiocarcinoma. Anticancer Res. 2019;39:971-977.
26. Pevner JL, Tanvetyanon T. Prognostic value of positron emission tomography in advanced cholangiocarcinoma: a single-institution study and literature review. Cureus. 2022;14:e31026.

Original Article

Mol Imaging Radionucl Ther 2025;34:122-128 *DOI:10.4274/mirt.galenos.2025.15932*

Role of Lymphoscintigraphy in Repeat Sentinel Lymph Node Biopsy for cN0 Ipsilateral Breast Cancer Recurrence

cN0 İpsilateral Meme Tümör Nüksünde Tekrar Sentinel Lenf Nodu Biyopsisinde Lenfosintigrafinin Rolü

Burak Dinçer[1], Duygu Has Şimşek[2], Selman Emiroğlu[3], Mustafa Tükenmez[3], Mahmut Müslümanoğlu[3], Neslihan Cabıoğlu[3]

[1]University of Health Sciences Türkiye, Dr. Abdurrahman Yurtaslan Ankara Oncology Training and Research Hospital, Clinic of Surgical Oncology, Ankara, Türkiye

[2]İstanbul University, İstanbul Faculty of Medicine, Clinic of Nuclear Medicine, İstanbul, Türkiye

[3]İstanbul University, İstanbul Faculty of Medicine, Clinic of General Surgery, İstanbul, Türkiye

Abstract

Objectives: In patients with ipsilateral breast tumor recurrence (IBTR), lymphatic drainage may be altered due to factors such as prior axillary surgery and radiotherapy, thereby increasing the likelihood of sentinel lymph nodes (SLNs) in atypical locations. This study aimed to evaluate patients who underwent surgery for IBTR with lymphoscintigraphy for repeat SLN biopsy (re-SLNB), and to investigate the role of lymphoscintigraphy in re-SLNB in this patient group.

Methods: Patients diagnosed with IBTR who were evaluated using preoperative lymphoscintigraphy and subsequently underwent surgery were included in the study. Patients with systemic or nodal metastases, as well as those who did not undergo lymphoscintigraphy, were excluded. Demographic, clinical, and pathological data of the included patients were analyzed.

Results: A total of 16 patients were evaluated, with a median age of 56 years (range 30-73), all of whom were female. Lymphoscintigraphy successfully localized the SLN in 81.3% of the patients. In eight patients, the SLN was located in the ipsilateral axilla, while in five patients, it was found in the contralateral axilla. Axillary lymph node dissection (ALND) was performed in three patients (all in the contralateral axilla) due to metastatic involvement in the SLN. ALND during first surgery was associated with an increased likelihood of SLN detection in the contralateral axilla or Re-SLNB failure (p=0.043).

Conclusion: In patients undergoing surgery for IBTR, the likelihood of the SLN being in atypical locations is high. Lymphoscintigraphy may enhance the success of Re–SLNB in this patient group.

Keywords: Breast cancer, ipsilateral breast tumor recurrence, lymphoscintigraphy, sentinel lymph node biopsy

Address for Correspondence: Burak Dinçer MD, University of Health Sciences Türkiye, Dr. Abdurrahman Yurtaslan Ankara Oncology Training and Research Hospital, Clinic of Surgical Oncology, Ankara, Türkiye

E-mail: burak-dincer@hotmail.com **ORCID ID:** orcid.org/0000-0002-3133-9627

Received: 10.12.2024 **Accepted:** 18.04.2025 **Epub:** 23.05.2025 **Publication Date:** 03.05.2025

Cite this article as: Dinçer B, Has Şimşek D, Emiroğlu S, Tükenmez M, Müslümanoğlu M, Cabıoğlu N. Role of lymphoscintigraphy in repeat sentinel lymph node biopsy for cN0 ipsilateral breast cancer recurrence. Mol Imaging Radionucl Ther. 2025;34:122-128.

Öz

Amaç: İpsilateral meme tümörü rekürrensi (IMTR) olan hastalarda, geçirilmiş aksiller cerrahi ve radyoterapi gibi faktörler nedeniyle lenfatik drenaj değişebilmekte, buna bağlı olarak da atipik yerleşimlerde sentinel lenf nodları (SLN) olasılığı artmaktadır. Bu çalışmada, IMTR nedeniyle ameliyat edilen hastalarda tekrar SLN biyopsisi (re-SLNB) için lenfosintigrafi kullanımının değerlendirilmesi ve bu hasta grubunda lenfosintigrafinin re-SLNB'de rolünün incelenmesi amaçlanmıştır.

Yöntem: Çalışmaya, preoperatif lenfosintigrafi ile değerlendirilerek ameliyata alınan IBTR tanısı almış hastalar dahil edildi. Sistemik veya lenf nodu metastazları olan hastalar ve lenfosintigrafi yapılmayan hastalar dışlandı. Hastalar demografik, klinik ve patolojik verilerine göre analiz edildi.

Bulgular: Toplam 16 hasta değerlendirildi. Ortalama yaş 56 yıl (aralığı 30-73) ve hastaların hepsi kadındı. Lenfosintigrafi, SLN'yi hastaların %81,3'ünde başarıyla lokalize etti. Sekiz hastada SLN ipsilateral aksillada yer alırken, 5 hastada kontralateral aksillada bulundu. SLN'deki metastatik tutulum nedeniyle üç hastaya (tümü kontralateral aksillada) aksiller lenf nodu diseksiyonu (ALND) yapıldı. İlk ameliyat sırasında ALND, kontralateral aksillada SLN tespiti veya Re-SLNB başarısızlığı olasılığının artmasıyla ilişkiliydi (p=0,043).

Sonuç: IBTR için ameliyat edilen hastalarda SLN'nin atipik yerleşimlerde olma olasılığı yüksektir. Lenfosintigrafi bu hasta grubunda re-SLNB'nin başarısını artırabilir.

Anahtar kelimeler: Meme kanseri, ipsilateral meme tümörü rekürrensi, lenfosintigrafi, sentinel lenf nodu biyopsisi

Introduction

Breast cancer is the most common cancer and the leading cause of cancer-related deaths in women (1). One of the most critical factors in determining the prognosis of breast cancer is the status of the axillary lymph nodes. In early-stage breast cancer, axillary staging is typically performed using sentinel lymph node biopsy (SLNB) (2). However, in patients who have previously undergone breast-conserving surgery (BCS) and develop ipsilateral breast tumor recurrence (IBTR), repeat SLNB (Re-SLNB) becomes challenging. In these cases, lymphatic drainage is often impaired due to previous axillary surgery and treatments such as radiotherapy, increasing the likelihood of a SLN in atypical locations (3,4). The optimal approach to lymphatic staging in this patient group remains controversial in the literature (5). In our study, we aimed to evaluate the outcomes of re-SLNB in patients undergoing surgery for IBTR who were assessed preoperatively with lymphoscintigraphy.

Materials and Methods

Patients over the age of 18 who were diagnosed with IBTR between 2020 and 2023, and underwent surgery after SLN localization using preoperative lymphoscintigraphy, were included in our study. Patients who did not undergo lymphoscintigraphy, had systemic metastases, or were diagnosed with preoperative lymph node metastases, were excluded. Data were evaluated based on age, gender, menopausal status, SLN localization as determined by lymphoscintigraphy, types of breast and axillary surgeries performed for both first and recurrent tumor, histopathological diagnosis, molecular subtype, pathology results, locoregional and systemic recurrences as the third event, and survival. This study was approved by the İstanbul University İstanbul Medical Faculty Clinical Research Ethics committee (decision no: 23, date: 29.11.2024).

Lymphoscintigraphy and Surgical Technique

Lymphoscintigraphy for axillary staging was performed by administering two superficial (periareolar) and one deep (intratumoral) injection of approximately 50 MBq Tc99m-nanocolloid (Senti-Scint, Medicheck). After injection, preoperative imaging was conducted using a dual-head gamma camera (GE Discovery NM 670 SPECT/CT, USA) (Figure 1). If the SLN is localized from these images, its skin projection is marked. Intraoperatively, the SLN is located using a gamma probe and excised. The excised SLN is subsequently re-evaluated with a gamma probe for confirmation. Following SLNB, the axilla is explored again with a gamma probe for the presence of remaining lymph nodes exhibiting radionuclide uptake. If no further involvement is detected, the procedure is concluded. The SLN is evaluated intraoperatively with a frozen section, and if deemed necessary by the surgeon, lymph node dissection is performed.

Outcome Measures

The primary outcome was the effectiveness of lymphoscintigraphy in identifying the SLN in cases of IBTR. The secondary outcome was the localization of the SLN in patients with IBTR.

Statistical Analysis

Statistical analysis was performed using SPSS® version 25.0 (IBM Corp., Armonk, NY, USA). Descriptive statistics, including numbers, percentages, medians, were used to summarize the study data. The sample size was small, so the data are expressed as median and interquartile range

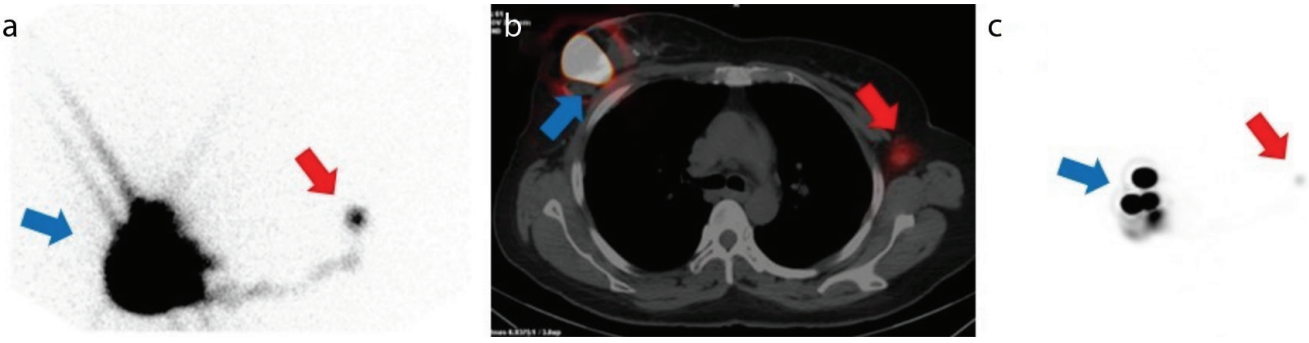

Figure 1. Anterior planar (A), SPECT/CT (B), and maximum intensity projection (C) images of lymphoscintigraphy demonstrate one contralateral axillary sentinel node indicated by the red arrows. The blue arrows indicate the injection site

SPECT: Single photon emission computed tomography, CT: Computed tomography

Table 1. Demographic and clinical features of study participants

Variables	All patients (n=16)
Age (years, median, range)	56 (30-73)
Menopausal status (n, %)	
Premenopausal	6 (37.5%)
Postmenopausal	10 (62.5%)
First breast surgery (n, %)	
BCS	11 (68.7%)
NSM	5 (31.3%)
First axillary surgery (n, %)	
SLNB	12 (75%)
ALND	4 (25%)
Interval time to IBTR (months, median, IQR)	50 (29-58)
Type of breast surgery for IBTR (n, %)	
BCS	4 (25%)
Mastectomy	10 (62.5%)
NSM	2 (12.5%)
Type of axillary surgery for IBTR (n, %)	
No surgery	3 (18.8%)
Re-SLNB	10 (62.5%)
ALND	3 (18.8%)
Localisation of re-SLN (n, %)	
Ipsilateral axilla	8 (50%)
Contralateral axilla	5 (31.3%)
Not found	3 (18.8%)

ALND: Axillary lymph node dissection, BCS: Breast conserving surgery, IBTR: Ipsilateral breast tumor recurrence, IQR: Interquartile range, NSM: Nipple sparing mastectomy, SLN: Sentinel lymph node, SLNB: Sentinel lymph node biopsy, Re-SLNB: Repeat sentinel lymph node biopsy

(IQR), and non-parametric tests were used. Categorical data were compared using Chi-square tests (Pearson Chi-square, continuity correction, Fisher's exact test), and numerical data were compared using the Mann-Whitney U test. Survival analyses included calculating locoregional disease-free survival (LDFS), systemic disease-free survival (SDFS), and overall survival (OS) from the diagnosis of cancer to the first locoregional recurrence, systemic recurrence, last follow-up visit, or death, respectively. Survival curves were generated using the Kaplan-Meier method, and the log-rank test was used to assess the effects of prognostic factors on LDFS, SDFS, and OS. Results were considered significant at $p<0.05$, with a confidence interval of 95%.

Results

Sixteen patients who underwent surgery for IBTR between 2020 and 2023 were included in this single-center retrospective study. The median age was 56 years (range 30-73), and all patients were female. Ten patients (62.5%) were postmenopausal. As the first surgeries for breast cancer, 11 patients (68.7%) underwent BCS, and 12 patients (75%) underwent SLNB. The median interval between the initial surgery and the diagnosis of IBTR was 50 months (IQR 29-58). For IBTR surgery, mastectomy was performed in 10 patients (62.5%). SLN localization via lymphoscintigraphy was achieved in 13 patients (81.3%). In eight patients, the SLN was located in the ipsilateral axilla, while in five patients, it was in the contralateral axilla. Axillary lymph node dissection (ALND) was performed in 3 of the 13 patients, in whom metastatic lymph nodes were detected via SLNB, all in the contralateral axilla (Table 1).

The median pathological diameter of the initial tumors was 21 mm (IQR 17-29), while the median diameter of IBTR was 17 mm (IQR 12-22). Fifteen patients were diagnosed with invasive ductal carcinoma, and one patient was

diagnosed with mucinous carcinoma. Molecular subtyping revealed that 8 patients were classified as luminal B, and 5 as triple-negative. Notably, 76.9% of the patients had grade 3 tumors. Among the 13 patients who underwent Re-SLNB, metastases were detected in 5 (Table 2).

When the factors affecting re-SLN localization were evaluated, no significant relationship was found between the initial tumor diameter, IBTR diameter, and the type of initial breast surgery and re-SLN localization (p=0.365, p=0.320, and p=0.137, respectively). However, it was observed that both the rate of SLN detection in the contralateral axilla and the failure to localize SLNs were significantly higher in patients who underwent ALND during the initial surgery compared to those who underwent SLNB (p=0.043) (Table 3).

During follow-up after surgery for IBTR, a third event (re-recurrence) was observed in four patients. All of these patients experienced locoregional recurrence, with two also having concomitant systemic metastases. Except for one patient who developed systemic metastases, all were alive at the last follow-up. No significant differences were found between patients who experienced a third event and those who did not in terms of menopausal status, type of breast and axillary surgery for IBTR, re-SLN localization, IBTR diameter, IBTR molecular subtype, or re-SLN pathological findings (Table 4).

The median follow-up period for the entire cohort was 27 months. At the end of the follow-up, the median LDFS, SDFS, and OS were not reached for the entire series. LDFS, SDFS, and OS were analyzed based on re-SLN localization and SLN status. No significant differences in survival times were observed according to re-SLN localization (p=0.472, p=0.375, and p=0.223). Among the 13 patients who underwent re-SLNB, LDFS was significantly shorter in those with metastatic SLNs (p=0.037). However, SDFS did not differ significantly between SLN-positive and SLN-negative patients (p=0.429). As all patients in both groups with evaluated SLNs were alive, OS was not compared using Kaplan-Meier analysis (Figures 2 and 3).

Table 2. Histopathological features of study participants

Variables	All patients (n=16)
Tumor diameter in first surgery (mm, median, IQR)	21 (17-29)
IBTR diameter (mm, median, IQR)	17 (12-22)
Histopathologic diagnosis of IBTR (n, %)	
Invasive ductal carcinoma	15 (93.7%)
Mucinous carcinoma	1 (6.3%)
Molecular subtypes of IBTR (n, %)	
Luminal B	8 (50%)
HR+ HER2+	1 (6.3%)
HR- HER2+	2 (12.5%)
Triple negative	5 (31.3%)
Tumor grade for IBTR (n, %)	
G1	0 (0%)
G2	5 (15.4%)
G3	11 (76.9%)
Re-SLN status (n=13, %)	
Negative	8 (61.5%)
Positive	5 (38.5%)

HER2+: Human epidermal growth factor receptor 2 positive, HR+: Hormon receptor positive, IBTR: Ipsilateral breast tumor recurrence, IQR: Interquartile range, SLN: Sentinel lymph node, Re-SLNB: Repeat sentinel lymph node biopsy

Table 3. Factors affecting on re-SLN localisation in IBTR cases

Variables	All patients (n=16)	Ipsilateral axilla (n=8)	Contralateral axilla (n=5)	Not found (n=3)	p-value
Tumor diameter in first surgery (mm, median, IQR)	21 (17-29)	23 (20-29)	16 (14-20)	21 (19-29)	0.365[a]
IBTR diameter (mm, median, IQR)	17 (12-22)	16 (13-19)	10 (10-22)	20 (19-25)	0.320[a]
First breast surgery (n, %)					
BCS	11 (68.7%)	4 (25%)	5 (31.3%)	2 (12.5%)	0.137[b]
NSM	5 (31.3%)	4 (25%)	0 (0%)	1 (6.3%)	
First axillary surgery (n, %)					
SLNB	12 (75%)	8 (50%)	3 (18.8%)	1 (6.3%)	**0.043[b]**
ALND	4 (25%)	0 (0%)	2 (12.5%)	2 (12.5%)	

All p-values less than 0.05 was bold
[a]Kruskal-Wallis Test, [b]Fisher's exact test, ALND: Axillary lymph node dissection, BCS: Breast conserving surgery, IBTR: Ipsilateral breast tumor recurrence, IQR: Interquartile range, NSM: Nipple sparing mastectomy, SLN: Sentinel lymph node, SLNB: Sentinel lymph node biopsy, Re-SLNB: Repeat sentinel lymph node biopsy

Discussion

Currently, conservative methods such as BCS and SLNB are prominent in the treatment of breast cancer, demonstrating survival rates comparable to more invasive procedures, such as mastectomy and ALND, which typically entail higher morbidity (6,7). While local recurrence rates following surgical treatment of breast cancer are generally low, IBTR occurs at a higher rate after BCS compared to mastectomy (7). The optimal treatment approach for cases with IBTR remains controversial in the literature; however, mastectomy and ALND are the most commonly employed surgical interventions (8). Nevertheless, several studies have reported successful outcomes with re-SLNB in this patient population (3,4,5). Re-SLNs were successfully localized in 81.3% of our patients, aligning with the existing literature.

Atypical SLN localizations may occur more frequently in cases of IBTR due to factors that can alter axillary drainage pathways, such as previous ALND and radiotherapy (9). In our study, Re-SLN localization was achieved in 13 out of 16 patients, with 5 of these patients having contralateral axillary Re-SLNs. It was observed that the identification of Re-SLNs in the contralateral axilla or the failure to locate Re-SLNs was significantly more frequent in patients who underwent ALND. Given the high frequency of atypical SLN localizations, preoperative identification of SLN location using techniques such as lymphoscintigraphy may enhance the success of re-SLNB in this patient group.

There is a limited number of studies comparing the applications of re-SLNB and ALND in axillary staging for cases of IBTR. In a retrospective study conducted by Lu et al. (10), it was reported that re-SLNB and ALND yielded similar survival rates in patients with IBTR. In our study, only 3 of the 16 patients underwent ALND. At the last follow-up, 15 patients were alive, and 12 of them were recurrence-free, suggesting that our findings align with the existing literature.

Survival rates after IBTR are reported to be worse than in patients without recurrence (11). However, data on the risk of developing a third event following IBTR remain scarce. While our study did not yield significant findings regarding third-event risk, this may be attributable to the small sample size. Further investigation in larger series is needed to address this gap in the literature.

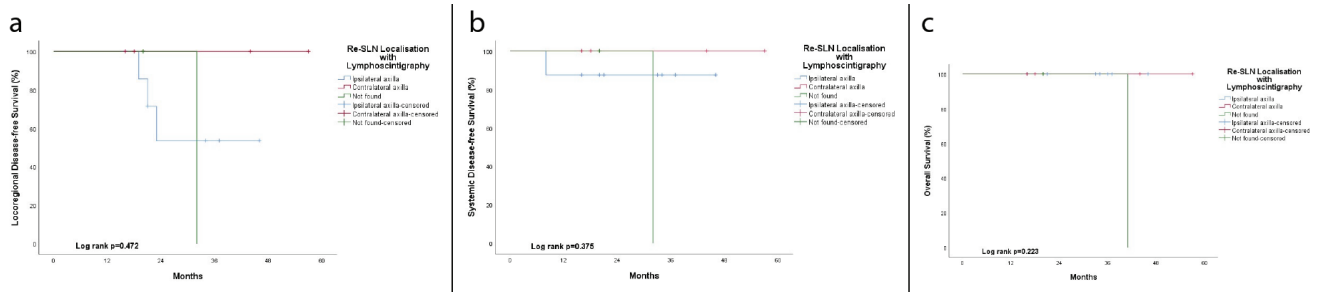

Figure 2. Kaplan-Meier curves illustrating the relationship between Re-SLN localization and survival for: a) LDFS, b) SDFS, and c) OS

Re-SLNB: Repeat sentinel lymph node biopsy, LDFS: Locoregional disease-free survival, SDFS: Systemic disease-free survival, OS: Overall survival

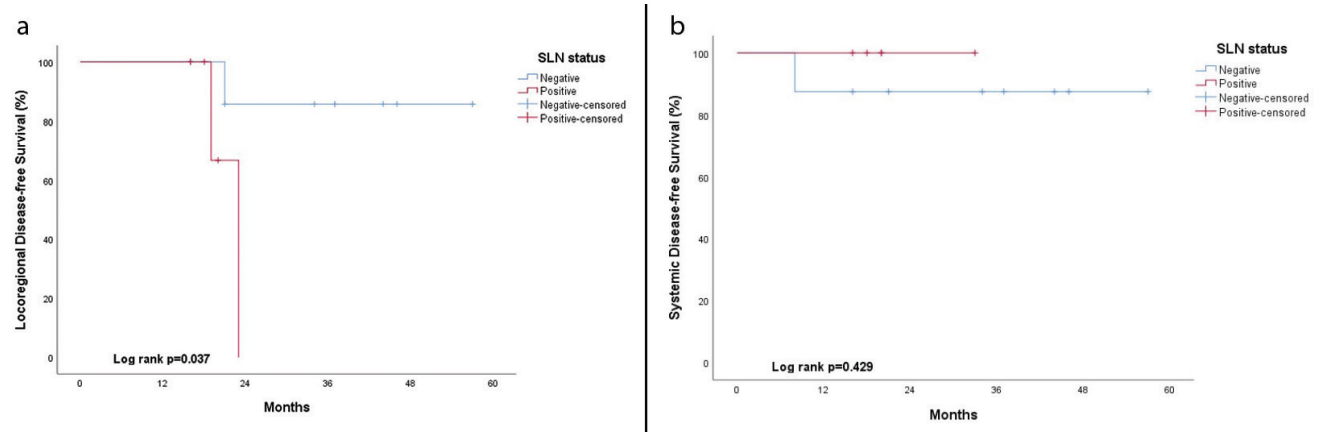

Figure 3. Kaplan-Meier curves illustrating the relationship between SLN status and survival for: a) LDFS, b) SDFS

SLN: Sentinel lymph node biopsy, LDFS: Locoregional disease-free survival, SDFS: Systemic disease-free survival

Table 4. Factors affecting risk of third event				
Variables	**All patients (n=16)**	**No event (n=12)**	**Third event (n=4)**	**p-value**
Menopausal status (n, %)				
Premenopausal	6 (37.5%)	4 (25%)	2 (12.5%)	0.604[a]
Postmenopausal	10 (62.5%)	8 (50%)	2 (12.5%)	
Type of breast surgery for IBTR (n, %)				
BCS	4 (25%)	3 (18.8%)	1 (6.3%)	0.736[a]
Mastectomy	10 (62.5%)	8 (50%)	2 (12.5%)	
NSM	2 (12.5%)	1 (6.3%)	1 (6.3%)	
Type of axillary surgery for IBTR (n, %)				
No surgery	3 (18.8%)	2 (12.5%)	1 (6.3%)	1.000[a]
Re-SLNB	11 (68.8%)	8 (50%)	3 (18.8%)	
ALND	2 (12.5%)	2 (12.5%)	0 (0%)	
Localisation of re-SLN (n, %)				
Ipsilateral axilla	8 (50%)	5 (31.3%)	3 (18.8%)	0.330[a]
Contralateral axilla	5 (31.3%)	5 (31.3%)	0 (0%)	
Not found	3 (18.8%)	2 (12.5%)	1 (6.3%)	
IBTR diameter (mm, median, IQR)	17 (12-22)	17 (12-21)	22 (12-31)	0.627[b]
Molecular subtypes of IBTR (n, %)				
Luminal B	8 (50%)	6 (37.5%)	2 (12.5%)	1.000[a]
HR+ HER2+	1 (6.3%)	1 (6.3%)	0 (0%)	
HR- HER2+	2 (12.5%)	2 (12.5%)	0 (0%)	
Triple negative	5 (31.3%)	3 (18.8%)	2 (12.5%)	
SLN status (n=13, %)				
Negative	8 (61.5%)	7 (53.8%)	1 (7.7%)	0.510[a]
Positive	5 (38.5%)	3 (23.1%)	2 (15.4%)	

[a]Fisher's exact test, [b]Mann-Whitney U test, ALND: Axillary lymph node dissection, BCS: Breast conserving surgery, HER2+: Human epidermal growth factor receptor 2 positive, HR+: Hormon receptor positive, IBTR: Ipsilateral breast tumor recurrence, IQR: Interquartile range, NSM: Nipple sparing mastectomy, SLN: Sentinel lymph node, SLNB: Sentinel lymph node biopsy, Re-SLNB: Repeat sentinel lymph node biopsy

Study Limitations

The main limitations of our study are its retrospective design and the small sample size. Larger studies and prospective trials will aid in determining the optimal approach for the treatment of IBTR.

Conclusion

In cases of IBTR, re-SLNB can be successfully performed, albeit at a lower success rate compared to primary cases. Additionally, lymphoscintigraphy may enhance the success rates of re-SLNB in this patient population by identifying atypical SLN localizations.

Ethics

Ethics Committee Approval: This study was approved by the İstanbul University İstanbul Medical Faculty Clinical Research Ethics committee (decision no: 23, date: 29.11.2024).

Informed Consent: Written informed consent was obtained from participants.

Footnotes

Authorship Contributions

Surgical and Medical Practices: B.D., D.H.Ş., S.E., M.T., M.M., N.C., Concept: B.D., D.H.Ş., N.C., Design: B.D., D.H.Ş., N.C., Data Collection or Processing: B.D., D.H.Ş., S.E., M.T., M.M., N.C., Analysis or Interpretation: B.D., D.H.Ş., N.C., Literature Search: B.D., N.C., Writing: B.D., D.H.Ş., S.E., M.T., M.M., N.C.

Conflict of Interest: No conflict of interest was declared by the authors.

Financial Disclosure: The authors declared that this study has received no financial support.

References

1. Bray F, Laversanne M, Sung H, Ferlay J, Siegel RL, Soerjomataram I, Jemal A. Global cancer statistics 2022: GLOBOCAN estimates of incidence and mortality worldwide for 36 cancers in 185 countries. CA Cancer J Clin. 2024;74:229-263.
2. Magnoni F, Galimberti V, Corso G, Intra M, Sacchini V, Veronesi P. Axillary surgery in breast cancer: An updated historical perspective. Semin Oncol. 2020;47:341-352.
3. Sávolt Á, Cserni G, Lázár G, Maráz R, Kelemen P, Kovács E, Győrffy B, Udvarhelyi N, Vörös A, Ormándi K, Mátrai Z. Sentinel lymph node biopsy following previous axillary surgery in recurrent breast cancer. Eur J Surg Oncol. 2019;45:1835-1838.
4. Folli S, Falco G, Mingozzi M, Buggi F, Curcio A, Ferrari G, Taffurelli M, Regolo L, Nanni O. Repeat sentinel lymph node biopsy in patients with ipsilateral recurrent breast cancer after breast-conserving therapy and negative sentinel lymph node biopsy: a prospective study. Minerva Chir. 2016;71:73-79.
5. Park WK, Kim HJ, Ryu JM, Chae BJ, Yu J, Kim SW, Nam SJ, Lee JE. Evaluating the feasibility of repeat sentinel lymph node biopsy in ipsilateral breast tumor recurrence: Technical considerations and oncologic outcomes. Eur J Surg Oncol. 2024;50:108644.
6. Veronesi U, Paganelli G, Viale G, Luini A, Zurrida S, Galimberti V, Intra M, Veronesi P, Maisonneuve P, Gatti G, Mazzarol G, De Cicco C, Manfredi G, Fernández JR. Sentinel-lymph-node biopsy as a staging procedure in breast cancer: update of a randomised controlled study. Lancet Oncol. 2006;7:983-990.
7. Veronesi U, Cascinelli N, Mariani L, Greco M, Saccozzi R, Luini A, Aguilar M, Marubini E. Twenty-year follow-up of a randomized study comparing breast-conserving surgery with radical mastectomy for early breast cancer. N Engl J Med. 2002;347:1227-1232.
8. Wadasadawala T, Vadgaonkar R, Bajpai J. Management of isolated locoregional recurrences in breast cancer: a review of local and systemic modalities. Clin Breast Cancer. 2017;17:493-502.
9. Sato A, Sakai T, Iwase T, Kano F, Kimura K, Ogiya A, Koizumi M, Tanabe M, Horii R, Akiyama F, Ueno T, Ohno S. Altered lymphatic drainage patterns in re-operative sentinel lymph node biopsy for ipsilateral breast tumor recurrence. Radiat Oncol. 2019;14:159.
10. Lu X, He M, Yu L, Gou Z. Is repeat sentinel lymph node biopsy possible for surgical axillary staging among patients with ipsilateral breast tumor recurrence? Cancer. 2023;129:1492-1501.
11. Wapnir IL, Anderson SJ, Mamounas EP, Geyer CE Jr, Jeong JH, Tan-Chiu E, Fisher B, Wolmark N. Prognosis after ipsilateral breast tumor recurrence and locoregional recurrences in five National Surgical Adjuvant Breast and Bowel Project node-positive adjuvant breast cancer trials. J Clin Oncol. 2006;24:2028-2037.

Interesting Image

Mol Imaging Radionucl Ther 2025;34:129-131 *DOI:10.4274/mirt.galenos.2024.93270*

Comparison of ^{68}Ga-FAPI-04 and ^{68}Ga-PSMA in a Case of Interstitial Lung Disease

İnterstisyel Akciğer Hastalığı Olgusunda ^{68}Ga-FAPI-04 ve ^{68}Ga-PSMA'nın Karşılaştırılması

Hasan Önner[1], Abidin Kılınçer[2]

[1]*Selçuk University Institute of Social Sciences, Faculty of Medicine, Department of Nuclear Medicine, Konya, Türkiye*
[2]*Selçuk University Institute of Social Sciences, Department of Radiology, Konya, Türkiye*

Abstract

We present the ^{68}Ga-prostate-specific membrane antigen (PSMA) and ^{68}Ga-fibroblast activation protein inhibitor (FAPI)-04 positron emission tomography/computed tomography (PET/CT) findings comparatively of a 76-year-old man with a history of progressive dyspnea and evidence of interstitial lung disease (ILD) abnormalities on high-resolution CT. Moderate PSMA uptake was observed in areas with ILD abnormalities on ^{68}Ga-PSMA PET/CT. ^{68}Ga-FAPI-04 PET/CT showed relatively higher FAPI-04 uptake in these regions. These findings offer the potential to assess disease activity at the cellular and molecular levels. This approach may provide valuable insight into the pathophysiology of ILD beyond the structural changes captured by traditional imaging methods.

Keywords: Fibroblast activation protein inhibitor, interstitial lung disease, PSMA, PET

Öz

İlerleyen dispne öyküsü ve yüksek çözünürlüklü bilgisayarlı tomografide (BT) interstisyel akciğer hastalığı (İAH) bulgusu bulunan 76 yaşındaki erkek hastanın ^{68}Ga-prostat spesifik membran antijeni (PSMA) ve ^{68}Ga-fibroblast aktivasyon protein inhibitörü (FAPİ)-04 pozitron emisyon tomografisi (PET)/BT bulgularını karşılaştırmalı olarak sunmaktayız. ^{68}Ga-PSMA PET/BT'de İAH anormallikleri olan bölgelerde orta düzeyde ^{68}Ga-PSMA tutulumu gözlendi. ^{68}Ga-FAPİ-04 PET/BT'de, bu bölgelerde ^{68}Ga-PSMA PET/BT'ye göre nispeten daha yüksek ^{68}Ga-FAPİ-04 tutulumu gözlenmektedir. Bu bulgu, hastalık aktivitesini hücresel ve moleküler düzeyde değerlendirme potansiyeli sunarak, geleneksel görüntüleme yöntemleriyle yakalanan yapısal değişikliklerin ötesinde İAH'nın patofizyolojisi hakkında değerli bilgiler sağlayabilir.

Anahtar kelimeler: Fibroblast aktivasyon protein inhibitörü, interstisyel akciğer hastalığı, PSMA, PET

Address for Correspondence: Hasan Önner, Selçuk University Institute of Social Sciences, Faculty of Medicine, Department of Nuclear Medicine, Konya, Türkiye
E-mail: hasanonner_1988@hotmail.com **ORCID ID:** orcid.org/0000-0003-1002-2097
Received: 26.04.2024 **Accepted:** 04.08.2024 **Publication Date:** 03.05.2025

Cite this article as: Önner H, Kılınçer A. Comparison of ^{68}Ga-FAPI-04 and ^{68}Ga-PSMA in a case of interstitial lung disease. Mol Imaging Radionucl Ther. 2025;34:129-131.

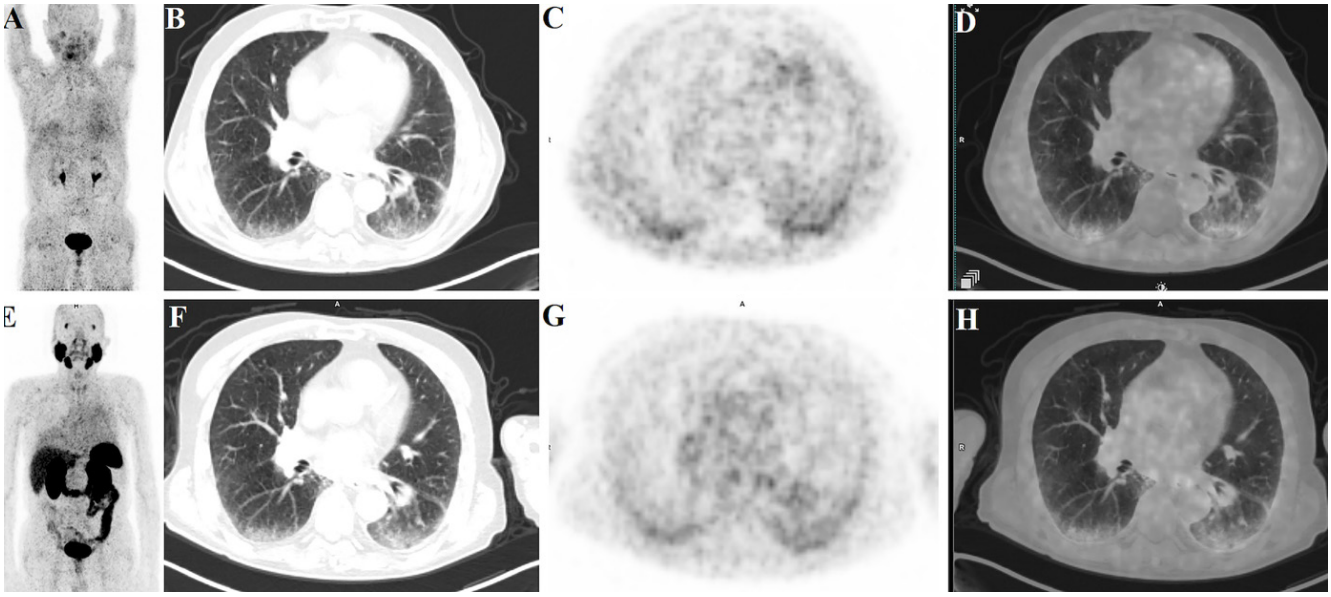

Figure 1. A 76-year-old man diagnosed with interstitial lung disease (ILD) presented with newly diagnosed prostate carcinoma with a Gleason score of 4+3. ^{68}Ga-prostate specific membrane antigen (PSMA) positron emission tomography/computed tomography (PET/CT) was performed for staging. Dependent atelectasis, subpleural reticular density increase, and traction bronchiectasis were observed in the lower lobes of both lungs, showing moderate PSMA uptake in both lungs (E, PSMA PET MIP; F, axial CT image; G, axial PET image, and H axial PET/CT fusion image). There was no evidence of prostate cancer residue or metastasis. Subsequently, the patient underwent a ^{68}Ga-fibroblast activation protein inhibitor (FAPI)-04 PET/CT scan as part of the prospective research conducted at our clinic. The patient provided written informed consent. In ILD findings where PSMA uptake (SUV_{max}: 4.8) was observed, FAPI-04 uptake (SUV_{max}: 6.4) was at a relatively higher uptake to PSMA on ^{68}Ga-FAPI-04 PET/CT (A, FAPI-04 PET MIP; B, axial CT image; C, axial PET image, and D axial PET/CT fusion image). ILD is a heterogeneous group of parenchymal lung disorders characterized by inflammation and fibrosis (1). High-resolution computed tomography has been the cornerstone of imaging in ILD, providing detailed anatomical information and aiding disease classification (2). However, the quest for more precise and comprehensive imaging techniques has led to exploring molecular imaging modalities such as PET using novel radiotracers. PSMA has garnered interest in non-prostatic diseases due to its increased expression in neoangiogenesis associated with inflammation and fibrosis (3). Similarly, FAPI, targeting fibroblast activation, has shown promise in visualizing and monitoring fibrotic lung diseases (4,5,6,7,8,9). These emerging PET tracers have the potential to assess disease activity at the cellular and molecular level, providing valuable insights into the pathophysiology of ILD beyond structural changes captured by conventional imaging modalities. This report underscores the potential of PET imaging with novel radiotracers as useful adjuncts to traditional diagnostic modalities, which may offer a deeper understanding of disease pathogenesis and pave the way for targeted therapies in patients with ILD.

Ethics

Informed Consent: The patient provided written informed consent.

Footnotes

Authorship Contributions

Surgical and Medical Practices: H.Ö., A.K., Concept: H.Ö., A.K., Design: H.Ö., A.K., Data Collection or Processing: H.Ö., A.K., Analysis or Interpretation: H.Ö., A.K., Literature Search: H.Ö., A.K., Writing: H.Ö., A.K.

Conflict of Interest: No conflicts of interest were declared by the authors.

Financial Disclosure: The authors declare that this study has received no financial support.

References

1. Mendes RG, Castello-Simões V, Trimer R, Garcia-Araújo AS, Gonçalves Da Silva AL, Dixit S, Di Lorenzo VAP, Archiza B, Borghi-Silva A. Exercise-Based Pulmonary Rehabilitation for Interstitial Lung Diseases: A Review of Components, Prescription, Efficacy, and Safety. Front Rehabil Sci. 2021;2:744102.
2. Rodriguez K, Ashby CL, Varela VR, Sharma A. High-Resolution Computed Tomography of Fibrotic Interstitial Lung Disease. Semin Respir Crit Care Med. 2022;43:764-779.
3. de Galiza Barbosa F, Queiroz MA, Nunes RF, Costa LB, Zaniboni EC, Marin JFG, Cerri GG, Buchpiguel CA. Nonprostatic diseases on PSMA PET imaging: a spectrum of benign and malignant findings. Cancer Imaging. 2020;20:23.
4. Rosenkrans ZT, Massey CF, Bernau K, Ferreira CA, Jeffery JJ, Schulte JJ, Moore M, Valla F, Batterton JM, Drake CR, McMillan AB, Sandbo N, Pirasteh A, Hernandez R. [(68) Ga]Ga-FAPI-46 PET for non-invasive detection of pulmonary fibrosis disease activity. Eur J Nucl Med Mol Imaging. 2022;49:3705-3716.
5. Dendl K, Koerber SA, Kratochwil C, Cardinale J, Finck R, Dabir M, Novruzov E, Watabe T, Kramer V, Choyke PL, Haberkorn U, Giesel FL. FAP

and FAPI-PET/CT in Malignant and Non-Malignant Diseases: A Perfect Symbiosis? Cancers (Basel). 2021;13:4946.

6. Yang P, Luo Q, Wang X, Fang Q, Fu Z, Li J, Lai Y, Chen X, Xu X, Peng X, Hu K, Nie X, Liu S, Zhang J, Li J, Shen C, Gu Y, Liu J, Chen J, Zhong N, Su J. Comprehensive Analysis of Fibroblast Activation Protein Expression in Interstitial Lung Diseases. Am J Respir Crit Care Med. 2023;207:160-172.
7. Sviridenko A, di Santo G, Virgolini I. Imaging Fibrosis. PET Clin. 2023;18:381-388.
8. Mori Y, Kramer V, Novruzov E, Mamlins E, Röhrich M, Fernández R, Amaral H, Soza-Ried C, Monje B, Sabbagh E, Florenzano M, Giesel FL, Undurraga Á. Initial results with [(18)F]FAPI-74 PET/CT in idiopathic pulmonary fibrosis. Eur J Nucl Med Mol Imaging. 2024;51:1605-1611.
9. Röhrich M, Leitz D, Glatting FM, Wefers AK, Weinheimer O, Flechsig P, Kahn N, Mall MA, Giesel FL, Kratochwil C, Huber PE, Deimling AV, Heußel CP, Kauczor HU, Kreuter M, Haberkorn U. Fibroblast Activation Protein-Specific PET/CT Imaging in Fibrotic Interstitial Lung Diseases and Lung Cancer: A Translational Exploratory Study. J Nucl Med. 2022;63:127-133.

Interesting Image

Mol Imaging Radionucl Ther 2025;34:132-134 *DOI:10.4274/mirt.galenos.2024.87004*

Pancreatic Involvement in Follicular Lymphoma Detected on ^{18}FDG-PET/CT

^{18}FDG-PET/BT'de Tespit Edilen Foliküler Lenfomada Pankreas Tutulumu

Yassir Benameur, Salah Oueriagli Nabih, Omar Ait Sahel, Abderrahim Doudouh

Department of Nuclear Medicine, Mohammed V Military Teaching Hospital, Rabat, Morocco

Abstract

Follicular lymphoma (FL) is clinically classified as a common type of indolent non-Hodgkin's lymphoma. FL is generally indolent and has good prognosis, it can involve a variety of extranodal sites, including the gastrointestinal tract, bone marrow, spleen, liver, skin, and other organs. Secondary involvement of pancreas in FL is rare. We report the case of a patient with FL whose initial fluorodeoxyglucose-positron emission tomography/computed tomography (FDG-PET/CT) revealed subdiaphragmatic involvement with isolated diffuse pancreatic hypermetabolism. Uncovering such rare site highlights the role of FDG-PET/CT in staging of lymphomas.

Keywords: FDG, PET/CT, pancreas involvement, lymphoma

Öz

Foliküler lenfoma (FL), klinik olarak yaygın bir indolent non-Hodgkin lenfoma türü olarak sınıflandırılır. FL genellikle indolenttir ve iyi bir prognoza sahiptir, gastrointestinal sistem, kemik iliği, dalak, karaciğer, cilt ve diğer organlar dahil olmak üzere çeşitli ekstranodal bölgeleri tutabilir. FL'de pankreasın sekonder tutulumu nadirdir. Bu olgu sunumunda hastaya yapılan ilk florodeoksiglukoz-pozitron emisyon tomografisi/bilgisayarlı tomografide (FDG-PET/BT) izole diffüz pankreas hipermetabolizması ile subdiyafragmatik tutulum saptanan FL'li bir hasta bildiriyoruz. Bu kadar nadir bir bölgenin ortaya çıkarılması, lenfomaların evrelendirmesinde FDG-PET/BT'nin rolünü vurgulamaktadır.

Anahtar kelimeler: FDG, PET/BT, pankreas tutulumu, lenfoma

Address for Correspondence: Yassir Benameur, Department of Nuclear Medicine, Mohammed V Military Teaching Hospital, Rabat, Morocco
E-mail: benameur.yassir@gmail.com **ORCID ID:** orcid.org/0000-0003-4611-1753
Received: 07.05.2023 **Accepted:** 04.08.2024 **Publication Date:** 03.05.2025

Cite this article as: Benameur Y, Nabih SO, Sahel OA, Doudouh A. Pancreatic involvement in follicular lymphoma detected on ^{18}FDG-PET/CT. Mol Imaging Radionucl Ther. 2025;34:132-134.

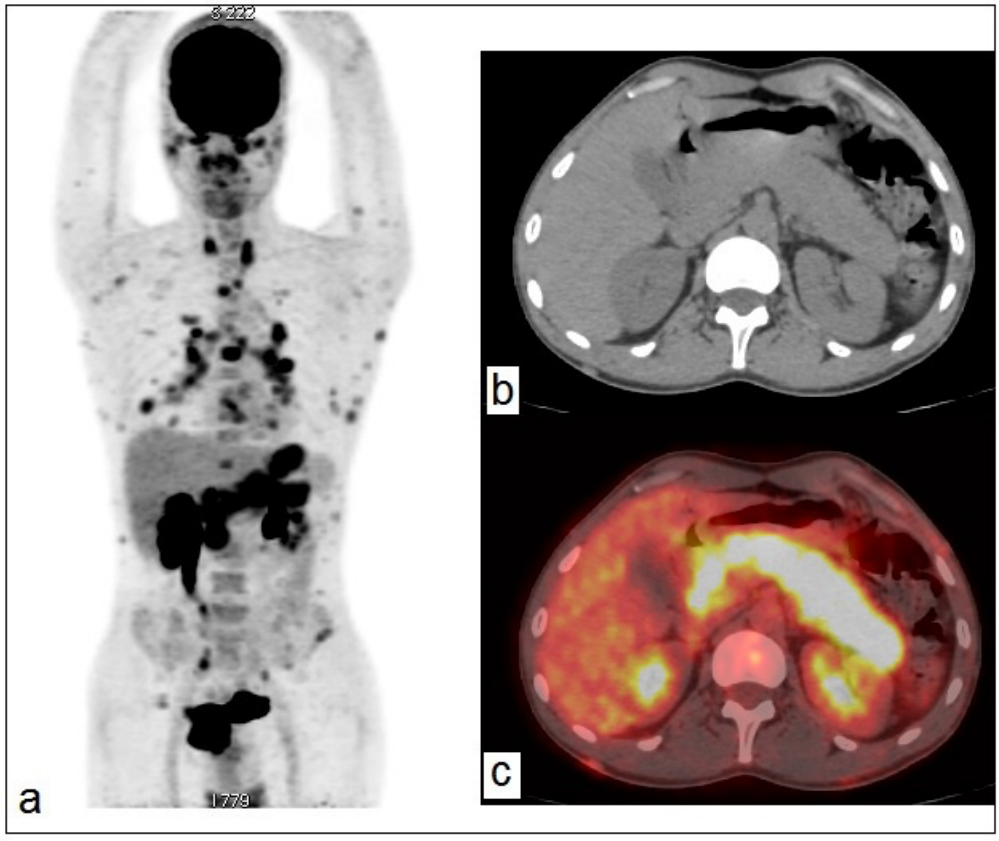

Figure 1. Fluorodeoxyglucose-positron emission tomography/computed tomography (FDG-PET/CT) maximum intensity projection (a), transaxial CT image (b) and transaxial FDG-PET/CT image (c) showed enlarged pancreas and increased FDG uptake in head and body of the pancreas, and disseminated cutaneous, nodal, and solid organ FDG-uptake.

A 38-year-old man, without past medical history, diagnosed with follicular lymphoma by biopsy of a right inguinal lymph node. Positron emission tomography/computed tomography (PET/CT) performed as initial assessment of disease extension and showed fluorodeoxyglucose (FDG)-avid lymphadenopathy in multiple locations above the diaphragm, as well as a focal lung, bone and cutaneous FDG uptake. An uncommon isolated subdiaphragmatic involvement with diffuse and intense FDG uptake was seen in the head, the body and the tail of the pancreas. Pancreatic enzymes were normal, allowing us to rule out acute pancreatitis, which has a similar appearance on PET-CT.

The present report describes a unique case of follicular lymphoma with secondary pancreatic involvement. Pancreas involvement in non-Hodgkin lymphoma (NHL) is rare and only few case reports have been reported, secondary pancreatic involvement has been reported in only 0.2-2% of patients with NHL (1). Currently, FDG-PET/CT is the approach of choice for evaluation of extranodal involvement by lymphoma (2). The FDG uptake patterns in pancreatic NHL lesions have been rarely reported and are non-spesific and can be seen in many pancreatic entities (3). Dong et al. (4) described four FDG uptake patterns in pancreatic NHL lesions including solitary, diffuse, multiple, and segmental, with solitary being the most common. In our case, the intensity of the diffuse involvement of the whole pancreas on FDG-PET/CT and the diffusely enlarged pancreas on the CT scan in context of disseminated lymphomatous disease, made it possible to dispense with the pancreatic biopsy and to consider the pancreatic involvement as being secondary. FDG-PET/CT allowed us to accurate staging, risk stratification and treatment planning.

The detection of pancreatic involvement in follicular lymphoma may impact the overall staging of the disease and influence treatment decisions.

Informed Consent: An informed consent was obtained from the patient.

Authorship Contributions

Surgical and Medical Practices: Y.B., A.D., Concept: Y.B., A.D., Design: Y.B., A.D., Data Collection or Processing: Y.B., S.N.O., O.A.S., Analysis or Interpretation: Y.B., S.N.O., O.A.S., Literature Search: Y.B., Writing: Y.B.

Conflict of Interest: No conflicts of interest were declared by the authors.

Financial Disclosure: The authors declare that this study has received no financial support.

References

1. Saif MW, Khubchandani S, Walczak M. Secondary pancreatic involvement by a diffuse large B-cell lymphoma presenting as acute pancreatitis. World J Gastroenterol 2007;13:4909-11.
2. Kwee TC, Kwee RM, Nievelstein RA (2008) Imaging in staging of malignant lymphoma: a systematic review. Blood 111:504–516
3. Dong A, Dong H, Zhang L, Zuo C (2013) Hypermetabolic lesions of the pancreas on FDG PET/CT. Clin Nucl Med 38:e354–e366.
4. Dong A, Cui Y, Gao L, Wang Y, Zuo C, Yang J. Patterns of FDG uptake in pancreatic non-Hodgkin's lymphoma lesions. Abdom Imaging. 2014 Feb;39(1):175-86. doi: 10.1007/s00261-013-0041-5. PMID: 24136586.

Interesting Image

Mol Imaging Radionucl Ther 2025;34:135-138 *DOI:10.4274/mirt.galenos.2024.80388*

^{18}F-FDG PET/CT of a Multicentric Castleman Disease with Lymph Node and Skin Involvement

^{18}F-FDG PET/BT'de Lenf Nodu ve Deri Tutulumları Olan Multisentrik Castleman Hastalığı

Merve Yücel[1], Tarık Şengöz[1], Nilay Şen Türk[2]

[1]*Pamukkale University Faculty of Medicine, Department of Nuclear Medicine, Denizli, Türkiye*
[2]*Pamukkale University Faculty of Medicine, Department of Pathology, Denizli, Türkiye*

Abstract

Herein, we describe a rare case of multicentric Castleman disease with multiple lymph node and skin involvement. Ultrasonography of a 38-year-old patient with weakness and fever revealed multiple lymphadenopathies in both inguinal regions. Diagnosed via lymph node biopsy was Castleman's disease, a plasma cell variant. He was diagnosed with prurigo nodularis, lymphocytic vasculitis, and stasis dermatitis in the biopsies of skin lesions located in different regions. ^{18}F-fluorodeoxyglucose positron emission tomography/computed tomography showed multiple hypermetabolic lymph nodes in the axilla, abdomen, pelvis, and both popliteal areas, multiple hypermetabolic skin thickenings, and skin lesions in both arms, legs, and feet.

Keywords: ^{18}F-FDG PET/CT, multicentric Castleman disease, skin involvement

Öz

Multipl lenf nodu ve deri tutulumu ile seyreden nadir bir multisentrik Castleman hastalığı olgusunu tanımlıyoruz. Halsizlik ve ateş yakınması olan 38 yaşındaki hastaya yapılan ultrasonografide her iki inguinal bölgede çok sayıda lenfadenopati saptandı. Lenf nodu biyopsisi ile Castleman hastalığı, plazma hücre varyantı tanısı kondu. Farklı bölgelerdeki deri lezyonlarından yapılan biyopsilerde prurigo nodülaris, lenfositik vaskülit ve staz dermatit tanısı almış olup, ^{18}F-florodeoksiglukoz pozitron emisyon tomografisi/bilgisayarlı tomografide aksilla, abdomen, pelvis ve her iki popliteal bölgede çok sayıda hipermetabolik lenf nodu, her iki kolda, her iki bacakta ve ayakta multipl hipermetabolik deri kalınlaşması ve deri lezyonları görüldü.

Anahtar kelimeler: ^{18}F-FDG PET/BT, multisentrik Castleman hastalığı, deri tutulumu

Address for Correspondence: Merve Yücel, Asst. Pamukkale University Faculty of Medicine, Department of Nuclear Medicine, Denizli, Türkiye
E-mail: myycell96@gmail.com **ORCID ID:** orcid.org/0009-0008-1651-6083
Received: 15.02.2024 **Accepted:** 08.08.2024 **Epub:** 25.05.2025 **Publication Date:** 03.05.2025

Cite this article as: Yücel M, Şengöz T, Şen Türk N. ^{18}F-FDG PET/CT of a multicentric Castleman Disease with lymph node and skin involvement. Mol Imaging Radionucl Ther. 2025;34:135-138.

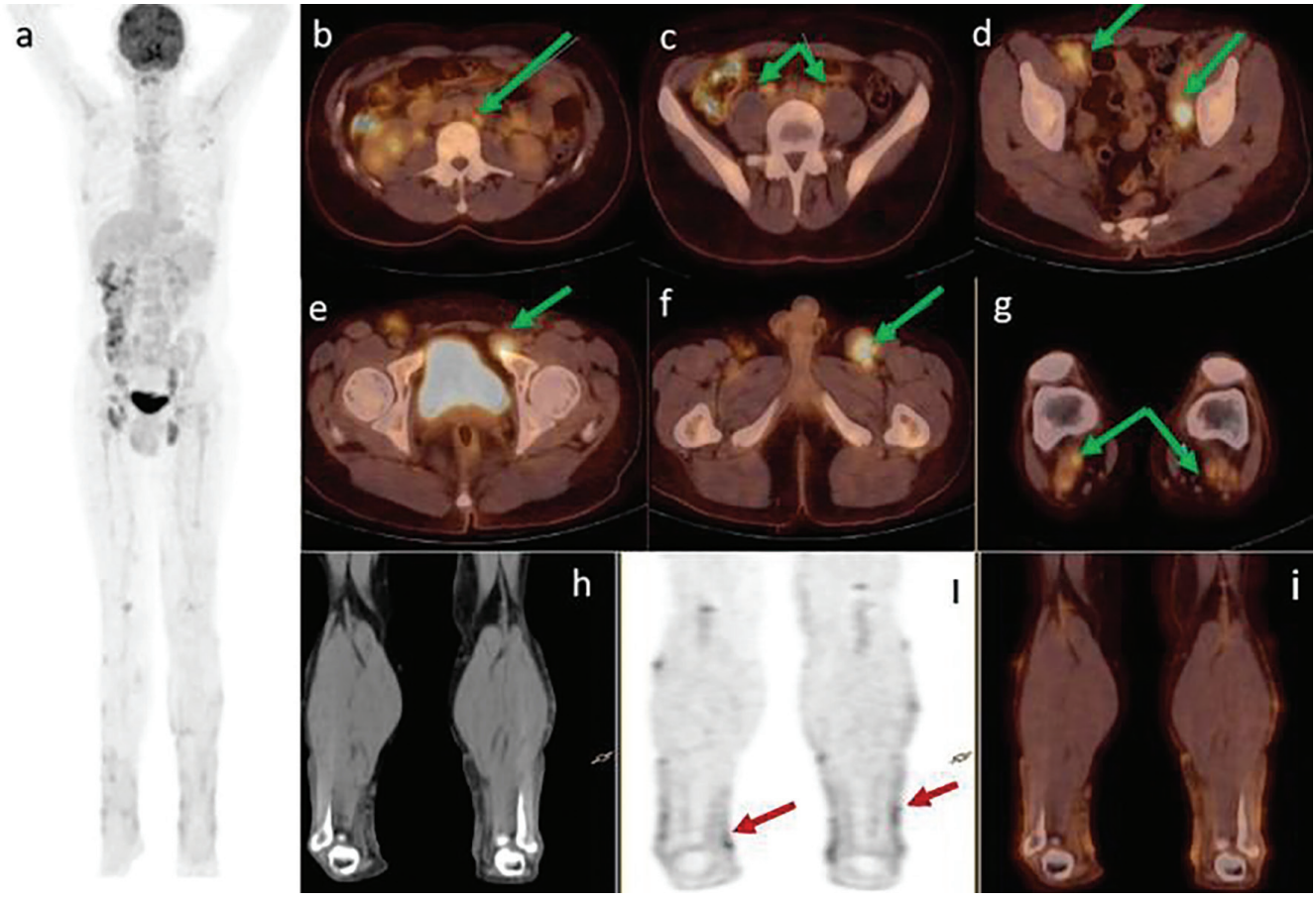

Figure 1. A 38-year-old male patient with weakness and fever. He had itchy skin lesions for 10 years and has been treated for dermatitis, but the lesions persisted despite treatment. Ultrasonography revealed multiple lymphadenopathies in both inguinal regions. In routine blood tests, C-reactive protein, white blood cells, sedimentation, urea, and blood urea nitrogen levels are high. Acute renal failure. Serum protein electrophoresis revealed hypoalbuminemia and hypergammaglobinemia. Human herpes virus 8 (HHV8) was negative. On physical examination, extensive erythematous excoriated plaques were observed on the trunk and extremities and purplish hyperkeratotic plaques with atrophic ulcerated areas in the middle were observed. Whole-body ^{18}F-fluorodeoxyglucose positron emission tomography/computed tomography (^{18}F-FDG PET/CT) maximum intensity projection images (a) and transaxial fusion PET/CT images revealed bilateral paraaortic (b), bilateral parailiac (c) (arrowhead; SUV_{max}: 3.5), bilateral external-internal iliac (d), left inguinal and femoral (e, f) (arrowhead; SUV_{max}: 6.3), bilateral popliteal (g) (arrowhead; SUV_{max}: 4.2) hypermetabolic lymph nodes (green arrows). Multiple hypermetabolic skin lesions are seen on transaxial CT (h), PET (ı; red arrows) and fusion PET/CT images (i).

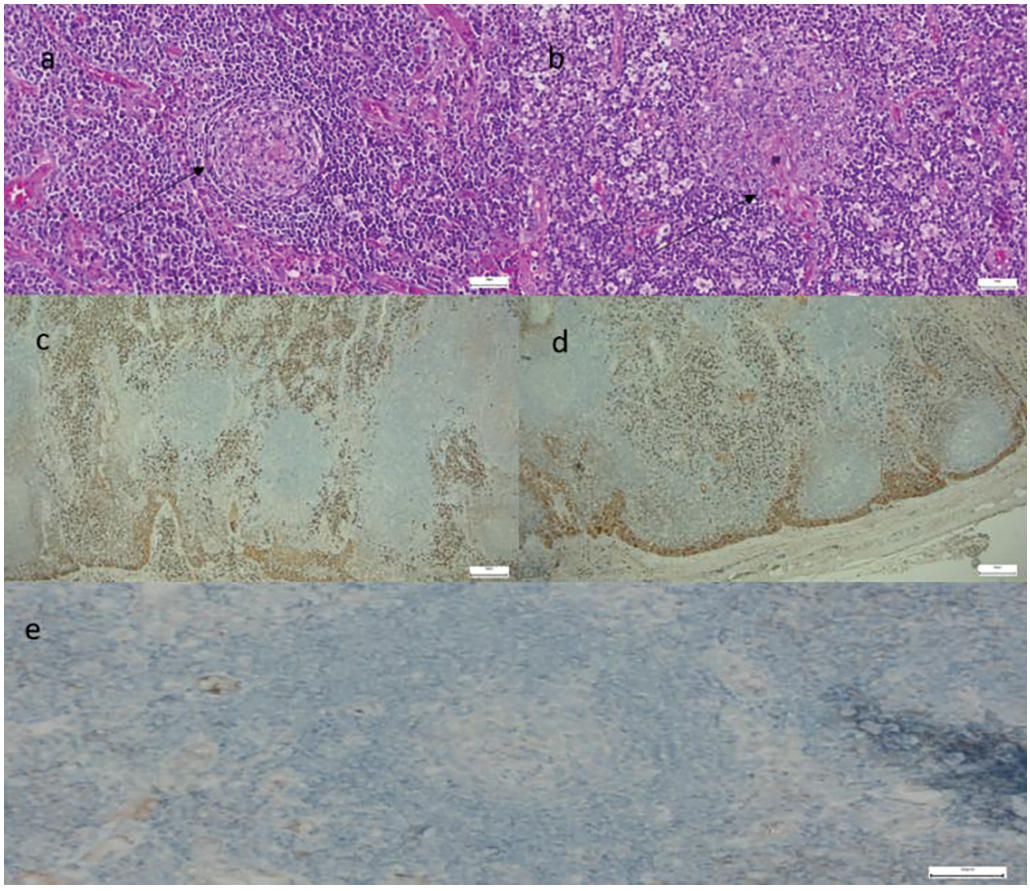

Figure 2. Biopsy of the left inguinal lymph node was performed. In microscopic examination, hyperplastic follicles were observed in the lymph nodes (a) (black arrow). In the hyperplastic follicles, the hyalinized vascular structures extended to the germinal center (b) (black arrow). Polyclonal staining was observed in plasma cells stained with kappa and lambda light chains (c, d). HHV8 was negative (e). Hodkin and non-Hodkin lymphoma were ruled out with Castleman's disease 3 (CD) 3, CD 20, paxillin antigen expression in synovial tissue (PAXS), optical coherence tomography-2, B-cell lymphoma (Bcl)-2, Bcl-6, cyclin D1, CD4, CD8, CD30, epithelial membrane antigen, anaplastic lymphoma kinase, CD21, CD68, kappa, lambda, and Ki-67 antibodies. The pathological diagnosis was made as "CD, Plasma Cell Variant" with morphological and immunohistochemical findings. He was diagnosed with prurigo nodularis, lymphocytic vasculitis, and stasis dermatitis based on biopsies of skin lesions located in different regions. CD is a rare chronic lymphoproliferative disorder characterized by unexplained enlarged lymph nodes that was first described by Castleman et al. (1) in 1956. There are two clinical types of CD: unicentric CD and multicentric Castleman's disease (MCD). MCD is a systemic disease characterized by multiple lymph nodes, in addition to symptoms such as fever, night sweats, and weight loss (2,3). Although rare, renal involvement can complicate the disease. Nephrotic syndrome, acute renal failure, interstitial nephritis, thrombotic microangiopathy, renal lymphoma, and renal amyloidosis have been reported (4). Skin involvement is very rare in CD. In the literature, skin lesions such as paraneoplastic pemphigus, lichenoid-nodular and maculopapular eruptions, Kaposi's sarcoma, polyneuropathy, organomegaly, endocrinopathy, monoclonal gammopathy, skin changes syndrome, autoimmune bleeding disorders, cutaneous necrotizing vasculitis, and xanthogranuloma have been reported (5). A few case reports and one original article were found regarding the use of ^{18}F-FDG-PET/CT in CD (5,6,7). In the study of Lee et al. (7), 4 of 12 patients with CD were unicentric, whereas 8 were multicentric. All lesions had moderate to high ^{18}F-FDG uptake. There are no studies in the literature on ^{18}F-FDG PET/CT in patients with MCD and skin lesions. Our case was clinically considered to be one of the skin diseases seen in CD patients. ^{18}F-FDG draws attention as a case of acute renal failure with skin and multiple lymph node involvement on PET/CT. Studies on ^{18}F-FDG PET/CT in MCD patients have been published. In a study by Jiang et al. (8), multiple lymphadenopathies as well as thickened skin with increased activity in the hip area were observed in a patient on ^{18}F-FDG PET/CT images (SUV_{max}: 10.9). Skin biopsy revealed infection.

Ethics

Informed Consent: Patient consent was obtained.

Footnotes

Authorship Contributions

Surgical and Medical Practices: M.Y., T.Ş., Concept: T.Ş., Design: M.Y., T.Ş., N.Ş.T., Data Collection or Processing: N.Ş.T., Analysis or Interpretation: T.Ş., Literature Search: M.Y., Writing: M.Y.

Conflict of Interest: No conflicts of interest were declared by the authors.

Financial Disclosure: The authors declare that this study has received no financial support.

References

1. Castleman B, Iverson L, Menendez VP. Localized mediastinal lymphnode hyperplasia resembling thymoma. Cancer. 1956;9:822-830.
2. Cervantes CE, Correa R. Castleman disease: a rare condition with endocrine manifestations. Cureus. 2015;7:e380.
3. Kessler E. Multicentric giant lymph node hyperplasia. A report of seven cases. Cancer. 1985;56:2446-2451.
4. Uthup S, Balachandran K, Ammal VA, Abdul Salam R, George J, Nair GM, Leela M. Renal involvement in multicentric Castleman disease with glomeruloid hemangioma of skin and plasmacytoma. Am J Kidney Dis. 2006;48:e17-24.
5. Kim HJ, Han JH, Bang CH, Park KS, Cho SG, Yoo DS, Kim KM, Park HJ, Park YM, Lee JY, Lee JH. Cutaneous disorders associated with Castleman's disease. Acta Derm Venereol. 2019;99:984-989.
6. Hwang JP, Kim J, Park JM. Human immunodeficiency virus negative multicentric Castleman's disease coexistent with Kaposi's sarcomaon 18F FDG PET/CT: A case report. Mol Clin Oncol 2019;10:318-320.
7. Lee ES, Paeng JC, Park CM. Metabolic characteristics of castleman disease on 18F-FDG PET in relation to clinical Implication. Clin Nucl Med 2013;38:339-342.
8. Jiang Y, Hou G, Zhu Z, Huo L, Li F, Cheng W. 18F-FDG PET/CT imaging features of patients with multicentric Castleman disease. Nucl Med Commun. 2021;42:833-838.

Interesting Image

Mol Imaging Radionucl Ther 2025;34:139-142 *DOI:10.4274/mirt.galenos.2024.48403*

^{68}Ga-PSMA-Avid Sinonasal Intestinal-Type Adenocarcinoma

^{68}Ga-PSMA-Tutulumu Gösteren Barsak Tipi Sinonazal Adenokarsinomu

Hasan Önner[1], Halil Özer[2], Muhammet Fatih Gökmen[3], Orhan Önder Eren[4]

[1]Selçuk University Faculty of Medicine, Department of Nuclear Medicine, Konya, Türkiye
[2]Selçuk University, Faculty of Medicine, Department of Radiology, Konya, Türkiye
[3]Selçuk University, Faculty of Medicine, Department of Ear, Nose and Throat Diseases, Konya, Türkiye
[4]Selçuk University, Faculty of Medicine, Department of Medical Oncology, Konya, Türkiye

Abstract

A rare tumor, intestinal-type adenocarcinoma (ITAC), accounts for 8-25% of all sinonasal malignancies. The tumor's histological resemblance to gastrointestinal tract adenocarcinoma is implied by its name. ITAC develops in the ethmoid sinus and upper nasal cavity. Herein, we present sinonasal ITAC with increased prostate-specific membrane antigen expression and fluorodeoxyglucose uptake.

Keywords: ^{68}Ga-PSMA, sinonasal intestinal-type adenocarcinoma, fluorodeoxyglucose

Öz

Nadir bir tümör olan barsak tipi adenokarsinomu (ITAC), tüm sinonazal malignitelerin %8 ila 25'ini oluşturur. Tümörün histolojik olarak gastrointestinal sistem adenokarsinomlarına benzerliği, adından da anlaşılmaktadır. ITAC, etmoid sinüste ve üst burun boşluğunda gelişir. Bu olgu sunumu ile artmış prostat spesifik membran antijeni ekspresyonu ve artmış florodeoksiglikoz tutulumu gösteren sinonazal ITAC kitlesini bildiriyoruz.

Anahtar kelimeler: ^{68}Ga-PSMA, sinonazal barsak tipi adenokarsinom, florodeoksiglikoz

Address for Correspondence: Hasan Önner, MD, Selçuk University, Faculty of Medicine, Department of Nuclear Medicine, Konya, Türkiye
E-mail: hasanonner_1988@hotmail.com **ORCID ID:** orcid.org/0000-0003-1002-2097
Received: 02.02.2024 **Accepted:** 18.08.2024 **Publication Date:** 03.05.2025

Cite this article as: Önner H, Özer H, Gökmen MF, Eren OÖ. ^{68}Ga-PSMA-avid sinonasal intestinal-type adenocarcinoma. Mol Imaging Radionucl Ther. 2025;34:139-142.

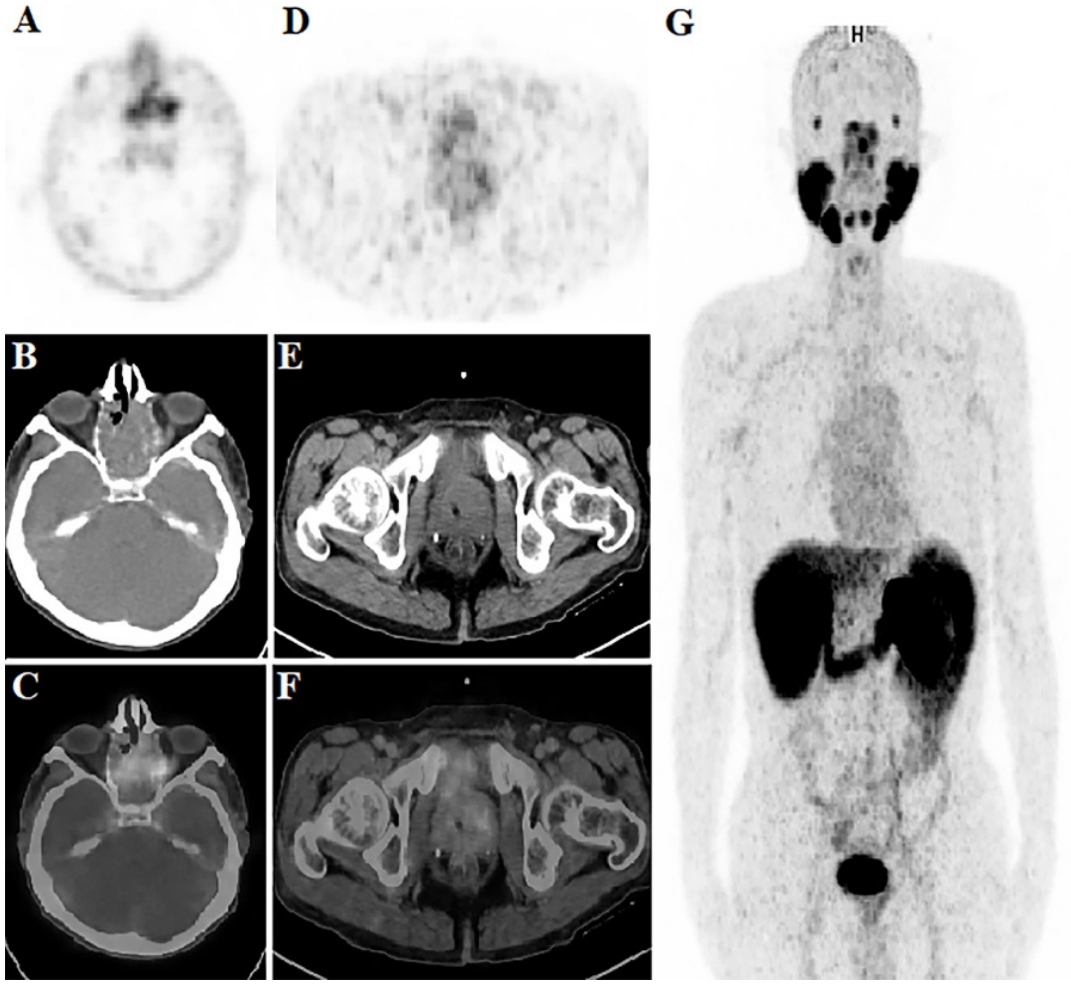

Figure 1. A systematic biopsy was conducted on the prostate gland of a 64-year-old man who previously underwent right radical nephrectomy for renal cell cancer due to the presence of high PSA (9.67 ng/mL). Biopsy revealed an International Society of Urological Pathology grade 3 prostate cancer with a Gleason score of 3+4. ^{68}Ga-prostate-specific membrane antigen (^{68}Ga-PSMA) positron emission tomography/computerized tomography (PET/CT) scan was conducted to assess the extent of metastatic disease. ^{68}Ga-PSMA-avid sinonasal mass and heterogeneous ^{68}Ga-PSMA uptake in the prostate gland were observed on the ^{68}Ga-PSMA PET maximum intensity projection image (A). Axial ^{68}Ga-PSMA PET (B), computed tomography (C), and fused ^{68}Ga-PSMA PET/CT (D) images showing ^{68}Ga-PSMA–avid mass involving the left maxillary sinus, left half of the nasal cavity, and both posterior ethmoid sinuses (SUV_{max}: 12.33). Axial ^{68}Ga PSMA PET (E), CT (F), and fused ^{68}Ga-PSMA PET/CT (G) images showed heterogeneous slightly increased uptake of ^{68}Ga-PSMA in the large prostate glands (SUV_{max}: 7.33). The histomorphology of the biopsy from the sinonasal mass revealed stratified papillary structures consisting of atypical cells. It was observed that these cells were immunohistochemically stained with CK7, CK20, SATB-2, and Ki-67 (high), but not with PSA and NKX3.1, and these findings were evaluated as compatible with sinonasal intestinal-type adenocarcinoma (ITAC).

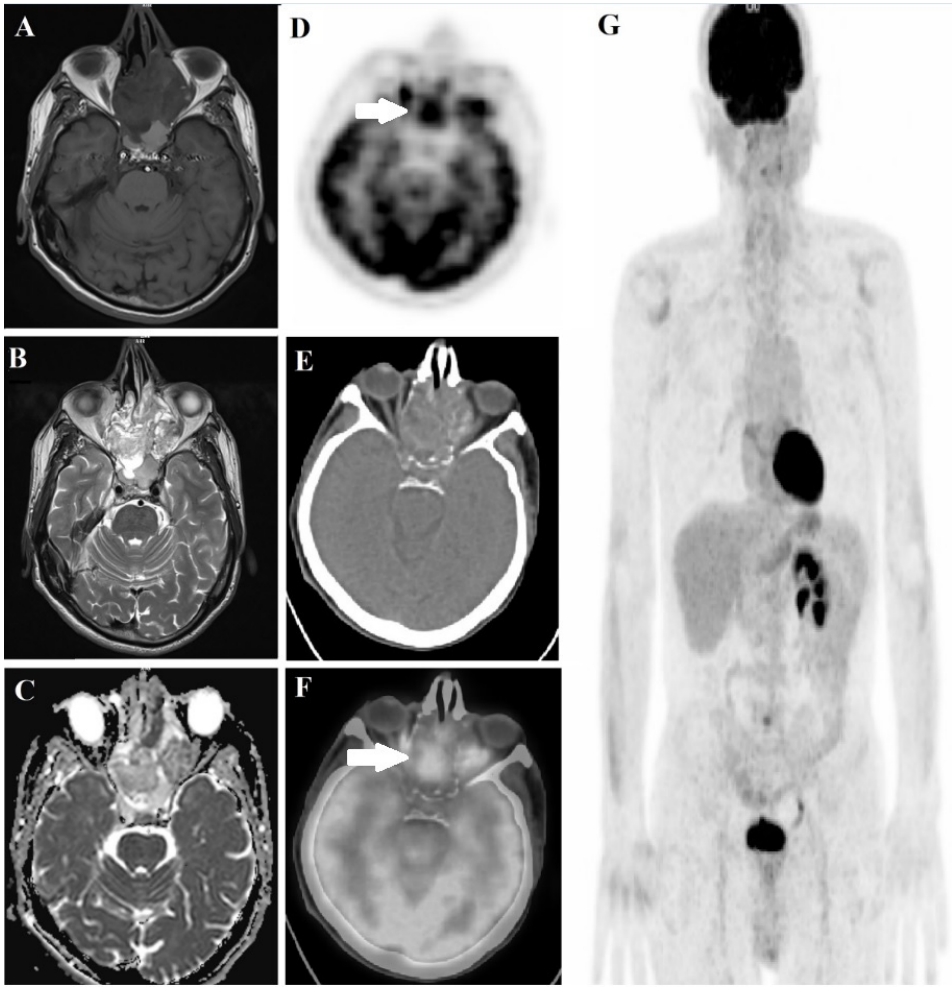

Figure 2. To rule out the risk of metastasis from other adenocarcinomas, ^{18}F- fluorodeoxyglucose (FDG) PET/CT was performed. Only the sinonasal mass was found to have ^{18}F- FDG avidity. Axial ^{18}F-FDG) PET (E), CT (F), and fused ^{18}F-FDG) PET/CT (G) images showing marked hypermetabolism (SUV_{max}: 12.18) in the primary tumor. There was no lymph node involvement in the cervical region, evidence of another primary adenocarcinoma, or distant metastasis. In addition, the right kidney was not observed after the operation. Magnetic resonance imaging shows lesions with low signal on T1-weighted images (A), high signal on T2-weighted images (B), and diffusion-weighted images (C). The upper nasal cavity and ethmoid sinus are the primary origin sites of ITACs (1,2,3). The most common symptoms include unilateral, non-spesific unilateral nasal blockage, epistaxis, and rhinorrhea (4). Colonic ITAC is the most common subtype, with papillary, mucinous, solid, and mixed types (5). It is difficult to distinguish between primary ITAC and nasal cavity metastases of adenocarcinomas due to the similarity of microscopic characteristics and immunohistochemistry (6,7). Therefore, diagnosing primary ITAC in the sinonasal region is only possible after excluding all other adenocarcinomas. This case hints at the value of ^{18}F-FDG PET/CT in the diagnosis of primary ITAC in the nasal cavity and demonstrates the ^{68}Ga-PSMA avidity of ITAC. In general, for non-prostatic solid tumors associated with neovascularity, endothelial PSMA expression has been shown (8). Therefore, PSMA expression in non-prostatic solid tumors on PET imaging requires readers to consider the histology, imaging, and clinical details of tumor neovascularization. Although demonstrating PSMA expression in non-prostatic diseases is disadvantageous, PSMA has paved the way for PET imaging to be applied as an additional theranostic tool for this malignancy (9).

Footnote

Informed Consent: Patient consent was obtained.

Authorship Contributions

Surgical and Medical Practices: H.Ö., H.Öz., M.F.G., O.Ö.E., Concept: H.Ö., H.Öz., M.F.G., O.Ö.E., Design: H.Ö., H.Öz., M.F.G., O.Ö.E., Data Collection or Processing: H.Ö., H.Öz., M.F.G., O.Ö.E., Analysis or Interpretation: H.Ö., H.Öz., M.F.G., O.Ö.E., Literature Search: H.Ö., H.Öz., M.F.G., O.Ö.E., Writing: H.Ö., H.Öz., M.F.G., O.Ö.E.

Conflict of Interest: No conflicts of interest were declared by the authors.

Financial Disclosure: The authors declare that this study has received no financial support.

References

1. Kılıç S, Samarrai R, Kılıç SS, Mikhael M, Baredes S, Eloy JA. Incidence and survival of sinonasal adenocarcinoma by site and histologic subtype. Acta Otolaryngol. 2018;138:415-421.
2. Abecasis J, Viana G, Pissarra C, Pereira T, Fonseca I, Soares J. Adenocarcinomas of the nasal cavity and paranasal sinuses: a clinicopathological and immunohistochemical study of 14 cases. Histopathology. 2004;45:254-259.
3. Hoeben A, van de Winkel L, Hoebers F, Kross K, Driessen C, Slootweg P, Tjan-Heijnen VC, van Herpen C. Intestinal-type sinonasal adenocarcinomas: The road to molecular diagnosis and personalized treatment. Head Neck. 2016;38:1564-1570.
4. Choussy O, Ferron C, Védrine PO, Toussaint B, Liétin B, Marandas P, Babin E, De Raucourt D, Reyt E, Cosmidis A, Makeiff M, Dehesdin D; GETTEC Study Group. Adenocarcinoma of Ethmoid: a GETTEC retrospective multicenter study of 418 cases. Laryngoscope. 2008;118:437-443.
5. Vivanco B, Llorente JL, Perez-Escuredo J, Alvarez Marcos C, Fresno MF, Hermsen MA. Benign lesions in mucosa adjacent to intestinal-type sinonasal adenocarcinoma. Patholog Res Int. Patholog Res Int. 2011;2011:230147.
6. Projetti F, Durand K, Chaunavel A, Léobon S, Lacorre S, Caire F, Bessède JP, Moreau JJ, Coulibaly B, Labrousse F. Epidermal growth factor receptor expression and KRAS and BRAF mutations: study of 39 sinonasal intestinal-type adenocarcinomas. Hum Pathol. 2013;44:2116-2125.
7. Fu Z, Zhang J, Liu M, Li Z, Li Q. Diagnosis of Primary Intestinal-Type Adenocarcinoma in the Nasal Cavity by 18F-FDG PET/CT. Clin Nucl Med. 2016;41:888-889.
8. Backhaus P, Noto B, Avramovic N, Grubert LS, Huss S, Bögemann M, Stegger L, Weckesser M, Schäfers M, Rahbar K. Targeting PSMA by radioligands in non-prostate disease-current status and future perspectives. Eur J Nucl Med Mol Imaging. 2018;45:860-877.
9. An S, Huang G, Liu J, Wei W. PSMA-targeted theranostics of solid tumors: applications beyond prostate cancers. Eur J Nucl Med Mol Imaging. 2022;49:3973-3976.

Interesting Image

Mol Imaging Radionucl Ther 2025;34:143-145 *DOI:10.4274/mirt.galenos.2024.60320*

Cancer Integrin Imaging with [^{68}Ga]Ga-Trivehexin PET/CT for a Patient with Breast Cancer and Neuroendocrine Neoplasm: A Case of Both (^{18}F)FDG PET/CT and [^{68}Ga]Ga-DOTATATE Positive but Integrin αvβ6 Negative Lesion on [^{68}Ga]Ga-Trivehexin PET

Meme Kanseri ve Nöroendokrin Neoplazmlı Hastada İntegrin PET Görüntülemesi: [^{18}F] FDG PET/BT ve [^{68}Ga]Ga-DOTATATE Pozitif, ancak [^{68}Ga]Ga-Trivehexin PET/BT'de İntegrin αvβ6 Negatif Lezyon

Gamze Beydağı[1], Nalan Alan Selçuk[1], Kaan Akçay[1], Onur Yaprak[2], Murat Kalaycı[3], Levent Kabasakal[4]

[1]*Yeditepe University Hospital, Clinic of Nuclear Medicine, İstanbul, Türkiye*
[2]*Medipol University Hospital, Clinic of General Surgery, İstanbul, Türkiye*
[3]*Yeditepe University Hospital, Clinic of General Surgery, İstanbul, Türkiye*
[4]*İstanbul University-Cerrahpaşa, Cerrahpaşa Faculty of Medicine, İstanbul, Department of Nuclear Medicine, İstanbul, Türkiye*

Abstract

Integrins play crucial roles in the migration of tumor cells during angiogenesis and metastasis. Consequently, αvβ6-integrin-targeted positron emission tomography (PET) radiopharmaceuticals have been developed and tested in humans, with clinical trials highlighting their applications in idiopathic pulmonary fibrosis and carcinomas. However, data on integrins are limited, and the role of [^{68}Ga]Ga-Trivehexin tomography/computed tomography (CT) PET/CT is not well-established. Some studies have suggested that [^{68}Ga]Ga-Trivehexin PET/CT is more specific than ^{18}F-fluorodeoxyglucose (^{18}F-FDG) PET/CT, which can yield false-positive results. It has been shown to be more efficient in evaluating pancreatic lesions and head and neck tumors. The role of [^{68}Ga]Ga Trivehexin PET/CT in neuroendocrine tumors is not yet clearly defined. In our case, integrin was negative in the pancreatic neuroendocrine tumor but positive in the breast lobular tumor. Additionally, we observed that the lobular carcinoma lesion in the right breast is somatostatin receptor+positive on [^{68}Ga]Ga-DOTATATE PET/CT.

Keywords: Neuroendocrine tumor, integrin positron emission tomography, [^{68}Ga]Ga-Trivehexin positron emission tomography/computed tomography

Öz

İntegrinler, anjiyogenez ve metastaz sırasında tümör hücrelerinin göçünde önemli bir rol oynar. Bu nedenle, αvβ-6integrin hedefli pozitron emisyon tomografisi (PET) radyofarmasötikleri geliştirilmiştir ve klinik çalışmalar bu ajanların idiyopatik pulmoner fibrozis ve karsinomlarda etkinliğini vurgulamaktadır. Ancak, integrinler hakkındaki veriler hala sınırlıdır ve [^{68}Ga]Ga-Triveheksin PET/bilgisayarlı tomografi (BT)'nin rolü iyi tanımlanmamıştır. Bazı çalışmalar, [^{68}Ga]Ga-Triveheksin PET/BT'nin, yanlış pozitif sonuçlar verebilen (^{18}F)FDG PET/BT'ye göre daha spesifik olduğunu öne sürmektedir. Pankreas lezyonları ve baş-boyun tümörlerini değerlendirmede başarılı olduğunu gösterilmiştir. Ancak [^{68}Ga]Ga-

Address for Correspondence: Nalan Alan Selçuk Prof., Yeditepe University Hospital, Department of Nuclear Medicine, İstanbul, Türkiye
E-mail: nalanselcuk@yeditepe.edu.tr **ORCID ID:** orcid.org/0000-0001-7187-7203
Received: 29.05.2024 **Accepted:** 25.08.2024 **Epub:** 23.05.2025 **Publication Date:** 03.05.2025

Cite this article as: Beydağı G, Alan Selçuk N, Akçay K, Yaprak O, Kalaycı M, Kabasakal L. Cancer integrin imaging with [^{68}Ga]Ga-Trivehexin PET/CT for a patient with breast cancer and neuroendocrine neoplasm: A case of both (^{18}F)FDG PET/CT and [^{68}Ga]Ga-DOTATATE positive but integrin avβ6 negative lesion on [^{68}Ga]Ga-Trivehexin PET. Mol Imaging Radionucl Ther. 2025;34:143-145.

Triveheksin PET/BT'nin nöroendokrin tümörlerdeki rolü henüz net olarak tanımlanmamıştır. Bizim olgumuzda, pankreatik nöroendokrin tümörde integrin negatif, ancak meme lobuler tümöründe pozitif bulunmuştur. Ayrıca, sağ memedeki lobüler karsinom lezyonunun [68Ga]Ga-DOTATATE PET/BT'de somatostatin reseptörü+pozitif olduğunu gözlemledik.

Anahtar kelimeler: Nöroendokrin tümör, integrin pozitron emisyon tomografisi, [68Ga]Ga-Triveheksin pozitron emisyon tomografisi/bilgisayarlı tomografi

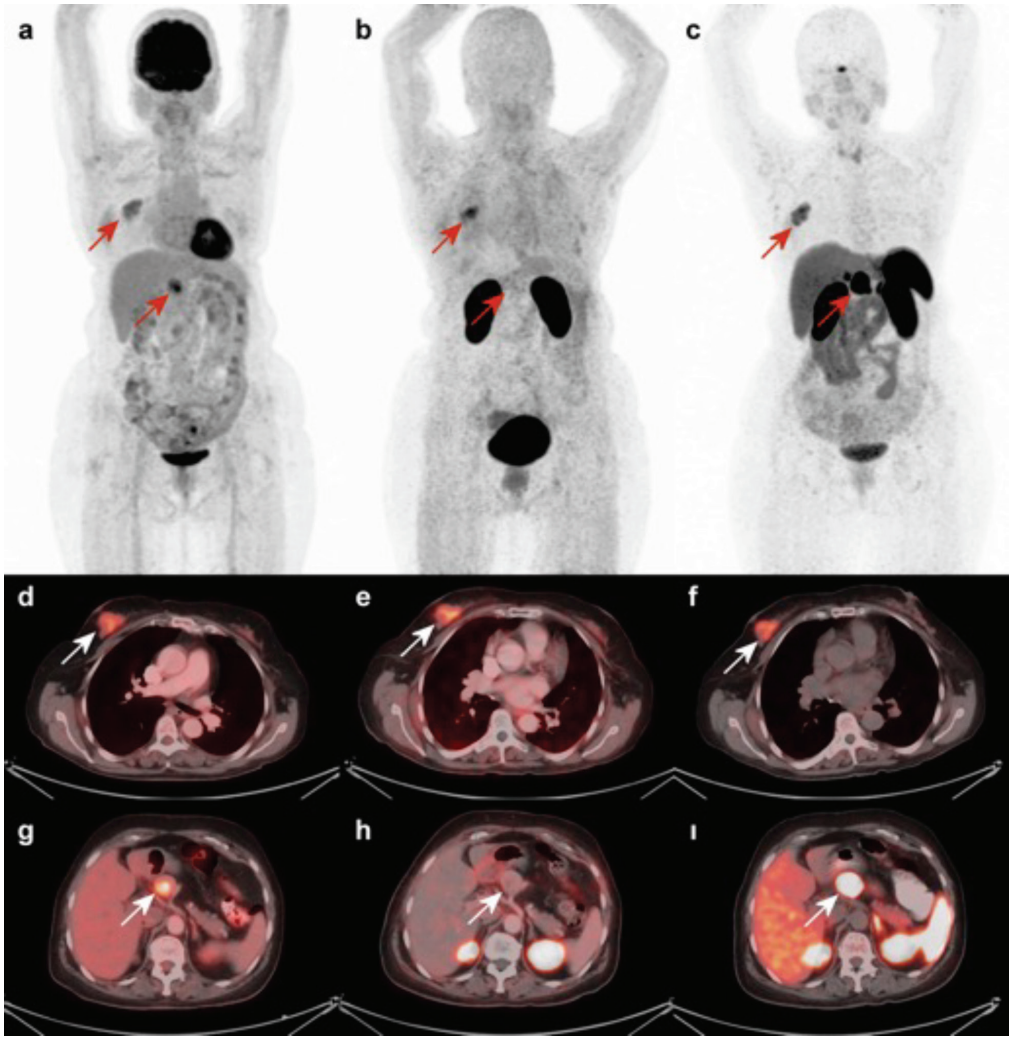

Figure 1. A 71-year-old woman presented with breast lobular carcinoma for evaluation staging with ^{18}F-fluorodeoxyglucose (^{18}F-FDG) positron emission tomography/computed tomography (PET/CT) (a). In the ^{18}F-FDG PET/CT scan, a hypermetabolic mass consistent with the known primary malignancy was observed in the retroareolar region of the right breast (d). Additionally, in the head-body of the pancreas, a well-defined hypermetabolic lesion was identified (g). Given the possibility of ^{18}F-FDG PET/CT false positivity in the pancreatic head mass, a [^{68}Ga]Ga-Trivehexin PET/CT (b) scan was conducted. The [^{68}Ga]Ga-Trivehexin PET/CT showed increased activity uptake in a portion of the right breast mass (e), and no activity uptake was observed in the pancreatic head mass (h). Based on these findings, a biopsy was performed to further investigate the pancreatic mass, which revealed a grade 2 neuroendocrine tumor. Additionally, a [^{68}Ga]Ga DOTATATE PET/CT (c) was performed, which demonstrated intense somatostatin receptor expression in the right breast mass (f) and pancreatic head lesion (ı). Integrins, particularly αvβ6-integrin, are involved in tumor cell migration, angiogenesis, and metastasis. Recently, αvβ6-integrin-targeted PET radiopharmaceuticals like [^{68}Ga]Ga-Trivehexin have shown promise in imaging certain cancers and fibrotic diseases (1,2). Comparative studies suggest that [^{68}Ga]Ga-Trivehexin may offer advantages over conventional ^{18}F-FDG PET/CT by reducing false-positive findings. Despite promising results in pancreatic, head and neck lesions, its diagnostic performance in NETs is not yet clearly defined (3,4,5). This study presents a case in which a pancreatic neuroendocrine tumor was integrin-negative, whereas a concurrent lobular carcinoma of the breast showed integrin positivity, also demonstrating somatostatin receptor on [^{68}Ga]Ga-DOTATATE PET/CT.

Ethics

Informed Consent: Patient consent was obtained for this study.

Footnotes

Authorship Contributions

Surgical and Medical Practices: O.Y., M.K., Concept: G.B., N.A.S., K.A., L.K., Design: N.A.S., L.K., Data Collection or Processing: G.B., Analysis or Interpretation: G.B., N.A.S., L.K., Literature Search: N.A.S., K.A., Writing: G.B., N.A.S., K.A.

Conflict of Interest: No conflicts of interest were declared by the authors.

Financial Disclosure: The authors declare that they have received financial support for this study from Nukleon Nuclear Technology Research Ind. Trade Ltd. Co.

References

1. Urso L, Napolitano R, Speltri G, Tuncel M, Badrane I, Uccelli L, Porto F, Martini P, Niorettini A, Cittanti C, Bartolomei M, Boschi A. Ga-trivehexin: current status of αvβ6-integrin imaging and perspectives. Cancers. 2025;17:1504.
2. Maher TM, Simpson JK, Porter JC, Wilson FJ, Chan R, Eames R, Cui Y, Siederer S, Parry S, Kenny J, Slack RJ, Sahota J, Paul L, Saunders P, Molyneaux PL, Lukey PT, Rizzo G, Searle GE, Marshall RP, Saleem A, Kang'ombe AR, Fairman D, Fahy WA, Vahdati-Bolouri M. A positron emission tomography imaging study to confirm target engagement in the lungs of patients with idiopathic pulmonary fibrosis following a single dose of a novel inhaled αvβ6 integrin inhibitor. Respir Res. 2020;21:75.
3. Strobel O, Büchler MW. Pancreatic cancer: FDG-PET is not useful in early pancreatic cancer diagnosis. Nat Rev Gastroenterol Hepatol. 2013;10:203-205.
4. Quigley NG, Steiger K, Hoberück S, Czech N, Zierke MA, Kossatz S, Pretze M, Richter F, Weichert W, Pox C, Kotzerke J, Notni J. PET/CT imaging of head-and-neck and pancreatic cancer in humans by targeting the "Cancer Integrin" αvβ6 with Ga-68-Trivehexin. Eur J Nucl Med Mol Imaging. 2022;49:1136-1147.
5. Alan Selçuk N, Akçay K, Beydağı G, Sönmez Ö, Çelik S, Öven BB, Kabasakal L. Revision of the histopathological examination following 68Ga-DOTA-FAPI-04 PET/CT of a breast tumor diagnosed as invasive ductal carcinomatosis. Mol Imaging Radionucl Ther. 2024;33:134-137.

Interesting Image

Mol Imaging Radionucl Ther 2025;34:146-148 *DOI:10.4274/mirt.galenos.2024.75547*

Combined ^{68}Ga-PSMA PET/CT and mpMRI Findings Improve Tumor Localization and Biopsy Guidance in the Initial Diagnosis of Prostate Cancer

Kombine ^{68}Ga-PSMA PET/BT ve mpMRI Bulgularının Prostat Kanserinin ilk Tanısında Tümör Lokalizasyonunu ve Biyopsi Rehberliğini Desteklemesi

Yavor Gramatikov[1], Petia Nikolova[1], Mihaela Ilcheva[1], Valentin Yotovski[2], Nikolay Halachev[3], Valeria Hadzhiyska[1]

[1]*University Hospital Alexandrovska, Clinic of Nuclear Medicine, Sofia, Bulgaria*
[2]*University Hospital Alexandrovska, Clinic of Urology, Sofia, Bulgaria*
[3]*Medical Institute of the Ministry of Interior, Clinic of Urology, Sofia, Bulgaria*

Abstract

Gallium-68 (^{68}Ga)-prostate-specific membrane antigen (PSMA) positron emission tomography/computed tomography (PET/CT) is a relatively new imaging modality that has already proved its role in the initial staging of prostate cancer and in biochemical recurrence following definitive primary therapy. Furthermore, emerging data several ongoing studies demonstrate its potential role in the primary diagnosis of this malignancy. We present a 67-year-old male patient with increasing clinical suspicion of prostate cancer despite a previous negative prostate gland biopsy. He was referred to our nuclear medicine department for a ^{68}Ga-PSMA PET/CT with the aim of improving tumor localization and assisting in the guidance of repeat prostate biopsy. One month before presentation of elevated prostate-specific antigen levels, he underwent multiparametric magnetic resonance imaging (mpMRI), which revealed a prostate imaging reporting and data system 4 lesion in the right lobe of the prostate gland. The MRI lesion completely matched a PRIMARY score 5 lesion registered by PET/CT. Furthermore, we detected another suspicious finding in the left lobe (PRIMARY score 4). The patient underwent PSMA PET/CT-guided MRI/ultrasonography fusion transperineal biopsy of both lesions. The latter were histologically confirmed as prostate carcinoma with a Gleason score of 3+4 =7.

Keywords: ^{68}Ga-PSMA PET/CT, mpMRI, initial diagnosis of prostate cancer

Öz

^{68}Ga-prostat-spesifik membran antijeni (PSMA) pozitron emisyon tomografisi/bilgisayarlı tomografi (PET/BT), prostat kanserinin ilk evrelemesinde ve birincil tedaviyi takiben biyokimyasal nükste rolünü kanıtlamış nispeten yeni bir görüntüleme yöntemidir. Ayrıca, devam eden birkaç çalışmadan elde edilen yeni veriler, bu malignitenin birincil tanısında potansiyel rolünü göstermektedir. Daha önce negatif prostat bezi biyopsisine rağmen artan prostat kanseri klinik şüphesi olan 67 yaşında erkek hastayı sunuyoruz. Hasta tümör lokalizasyonunu iyileştirmek ve tekrar prostat biyopsisinin rehberliğine yardımcı olmak amacıyla ^{68}Ga-PSMA PET/BT için nükleer tıp bölümümüze sevk edildi. Bir ay önce yüksek prostat spesifik antijen seviyeleri nedeniyle multiparametrik manyetik rezonans görüntüleme (mpMRG) uygulanan hastada prostat bezinin sağ lobunda prostat görüntüleme raporlama ve veri sistemi 4 lezyon saptandı. MRG lezyonu PET/BT ile kaydedilen PRİMARY skor 5 lezyonla tamamen uyuşuyordu. Ayrıca sol lobda PRİMARY skor 4 olan bir şüpheli lezyon daha tespit ettik. Hastanın her iki lezyonundan PSMA PET/BT kılavuzluğunda MRI/ultrasonografi füzyon transperineal biyopsi alındı ve histolojik olarak Gleason skoru 3+4=7 olan prostat karsinomu doğrulandı.

Anahtar kelimeler: ^{68}Ga-PSMA PET/BT, mpMRG, prostat kanserinin ilk tanısı

Address for Correspondence: Yavor Gramatikov, MD, University Hospital Alexandrovska, Clinic of Nuclear Medicine, Sofia, Bulgaria
E-mail: yavorgramatikov@abv.bg **ORCID ID:** orcid.org/0009-0001-2901-2940
Received: 16.07.2024 **Accepted:** 08.09.2024 **Publication Date:** 03.05.2025

Cite this article as: Gramatikov Y, Nikolova P, Ilcheva M, Yotovski V, Halachev N, Hadzhiyska V. Combined ^{68}Ga-PSMA PET/CT and mpMRI findings improve tumor localization and biopsy guidance in the initial diagnosis of prostate cancer. Mol Imaging Radionucl Ther. 2025;34:146-148.

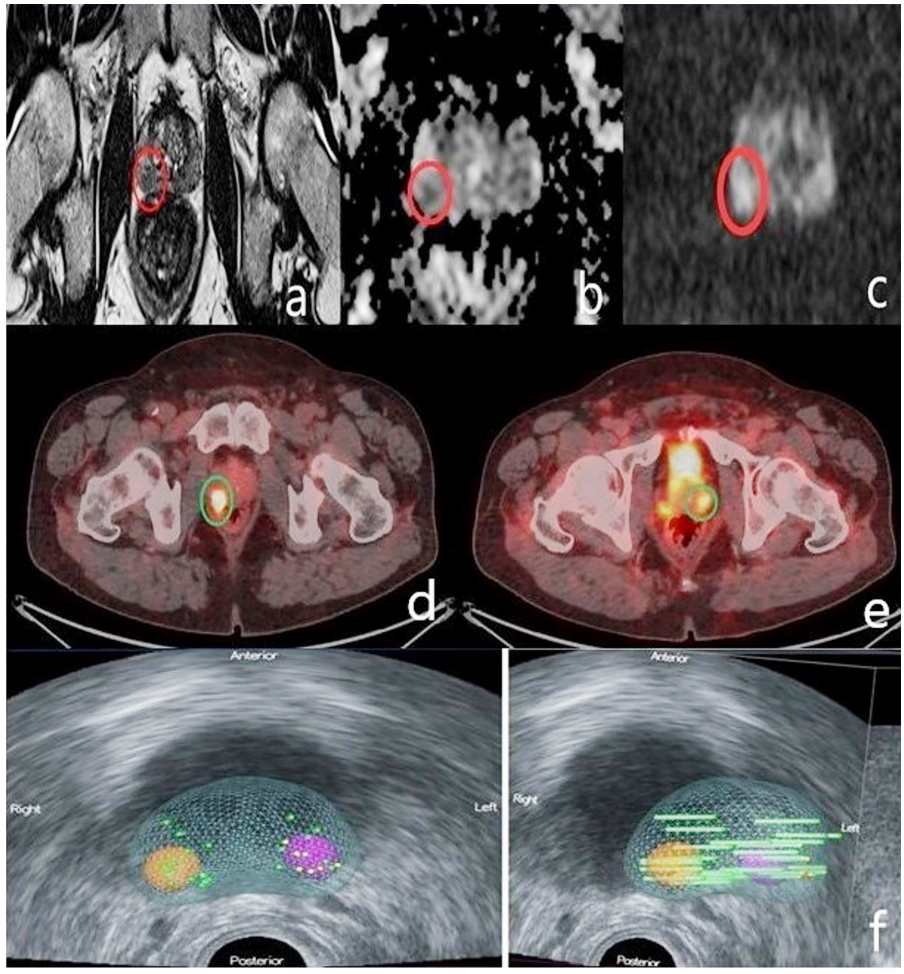

Figure 1. A 67-year-old male patient with increasing clinical suspicion of prostate cancer (PCa) based on a consistent increase in prostate-specific antigen (PSA) levels despite a previous negative 12-core systematic prostate gland biopsy. He was referred to our nuclear medicine department for a ^{68}Ga-PS membrane antigen (PSMA) positron emission tomography/computed tomography (PET/CT) with the aim of improving tumor localization and assisting in the guidance of repeat prostate biopsy. One month before presentation of elevated PSA levels (4.1 ng/mL) and intermediate-to-high PSA density risk (0.16 ng/mL^2) he underwent multiparametric magnetic resonance imaging (mpMRI). Axial T2-weighted (Figure 1a) and diffusion-weighted (Figure 1b and Figure 1c) images show a hypointense nodule with restricted diffusion (red circles) in the right peripheral prostate zone, corresponding to a prostate imaging reporting and data system (PI-RADS) 4 lesion. The MRI lesion completely matched a primary score 5 lesion registered by ^{68}Ga-PSMA PET/CT with a maximum standardized uptake value (SUV_{max}) 13.4 (Figure 1d-green circle). Furthermore, this relatively new hybrid imaging technique revealed one more suspicious finding, located in the left peripheral zone of the prostate base, classified as primary score 4 (Figure 1e-green circle). The patient underwent PSMA PET/CT-guided MRI/ultrasonography fusion transperineal biopsy of both lesions. A patient-specific 3D prostate map (Figure 1f) shows 7 cores taken from the lesion in the right lobe (PI-RADS 4/primary score 5 - orange sphere), 11 cores from the lesion in the left lobe (primary score 4 - purple sphere) and 9 cores from the systematic biopsy of both lobes. Both of the targeted lesions, including the additional lesion in the left lobe detected only on the ^{68}Ga-PSMA PET/CT, were histologically confirmed as clinically significant PCa with a Gleason score of 3+4=7. ^{68}Ga-PSMA PET/CT has already proven its role in the initial staging of PCa and in biochemical recurrence following definitive primary therapy. Furthermore, emerging data several ongoing studies demonstrate its potential role in the primary diagnosis of this malignancy. In March 2022, Emmett L. et al. (1) published the largest prospective multicenter study to date in 291 biopsy-naive men with suspected PCa and studied the additive role of ^{68}Ga-PSMA PET/CT combined with mpMRI in the diagnosis of clinically significant PCa. The results indicated that the combination of the two imaging methods had higher negative predictive value and sensitivity for clinically significant PCa than mpMRI alone. Moreover, the authors proposed a 5-point scale (primary score) to evaluate the PSMA uptake pattern in the prostate gland to standardize and objectify the reported results. The use of PSMA-ligand PET for the guidance of prostate biopsy is a new indication added in the latest joint European Association of Nuclear Medicine procedure guidelines/Society of Nuclear Medicine and Molecular Imaging procedure standard for PCa imaging 2.0, but it should be combined with mpMRI (2). Currently, this procedure is considered as a possible option after one previous negative biopsy and existing or rising clinical suspicion for PCa, based on imaging findings and laboratory results. Recently, PSA density has gained considerable clinical application and has been correlated with the PI-RADS score

derived from mpMRI in the decision to perform a prostate biopsy. According to the risk data table in the recent European Association of Urology Guideline 2023 on PCa (3), biopsy is strongly recommended in patients with a PSA density >0.2 ng/mL² and PI-RADS score >4. Still, there is a gray area with PSA density between 0.1 and 0.2 ng/mL² and intermediate PI-RADS 3 score, where the decision for biopsy remains controversial and subjective. Based on our recent clinical experience with a larger patient cohort, we believe that in this clinical scenario PSMA PET could be a useful tool not only for diagnostic management but also for the detection of additional lesions missed by mpMRI to improve the detection rate, as demonstrated in the case presented.

Ethics

Informed Consent: The patient consent was obtained.

Footnote

Authorship Contributions

Surgical and Medical Practices: Y.G., V.Y., N.H., Concept: Y.G., P.N., Design: Y.G., M.I., V.Y., Data Collection or Processing: Y.G., V.Y., Analysis or Interpretation: Y.G., P.N., Literature Search: Y.G., V.H., Writing: Y.G., M.I., V.H.

Conflict of Interest: No conflicts of interest were declared by the authors.

Financial Disclosure: The authors declare that this study has received no financial support.

References

1. Emmett L, Papa N, Buteau J, Ho B, Liu V, Roberts M, Thompson J, Moon D, Sheehan-Dare G, Alghazo O, Agrawal S, Murphy D, Stricker P, Hope TA, Hofman MS. The PRIMARY Score: Using Intraprostatic 68Ga-PSMA PET/CT Patterns to Optimize Prostate Cancer Diagnosis. J Nucl Med. 2022;63:1644-1650.
2. Fendler WP, Eiber M, Beheshti M, Bomanji J, Calais J, Ceci F, Cho SY, Fanti S, Giesel FL, Goffin K, Haberkorn U, Jacene H, Koo PJ, Kopka K, Krause BJ, Lindenberg L, Marcus C, Mottaghy FM, Oprea-Lager DE, Osborne JR, Piert M, Rowe SP, Schöder H, Wan S, Wester HJ, Hope TA, Herrmann K. PSMA PET/CT: joint EANM procedure guideline/SNMMI procedure standard for prostate cancer imaging 2.0. Eur J Nucl Med Mol Imaging. 2023;50:1466-1486.
3. EAU Guidelines. Edn. presented at the EAU Annual Congress Milan 2023. ISBN 978-94-92671-19-6.

Interesting Image

Mol Imaging Radionucl Ther 2025;34:149-151 *DOI:10.4274/mirt.galenos.2024.56689*

The Poor Prognostic Stigma of Hepatic Superscan on ^{18}F-FDG PET Imaging

^{18}F-FDG PET Görüntülemede Hepatik Superscan Görünümünün Kötü Prognoz Damgası

Dhuha Al-Adhami[1], Malik Juweid[2], Akram Al-Ibraheem[1]

[1]King Hussein Cancer Center (KHCC), Department of Nuclear Medicine and PET/CT, Al-Jubeiha, Amman, Jordan
[2]University of Jordan, Department of Radiology and Nuclear Medicine, Division of Nuclear Medicine, Amman, Jordan

Abstract

Pancreatic exocrine carcinoma (PEC) is a lethal malignancy with high mortality rates because of its aggressive nature and frequent late-stage diagnosis. When histopathological diagnosis becomes unfeasible because of patient deterioration, clinicians must rely on clinical, biochemical, and radiological findings. This case report describes a 78-year-old woman with aggressive PEC visualized through ^{18}F-fluorodeoxyglucose (^{18}F-FDG) positron emission tomography/computed tomography. The imaging revealed an intensely hypermetabolic head mass, hepatic superscan, and hypermetabolic abdominal lymphadenopathy. Despite strong clinical indicators suggesting stage IV PEC, rapid disease progression and patient demise precluded histopathological confirmation, emphasizing the poor prognosis associated with hepatic superscan in this context.

Keywords: Pancreatic carcinoma, hepatic superscan, fulminant metastasis, ^{18}F-FDG, PET/CT

Öz

Pankreas ekzokrin karsinomu (PEK), agresif doğası ve sıklıkla geç evrede tanı alması nedeniyle yüksek ölüm oranlarına sahip ölümcül bir malignitedir. Hastanın kötüleşmesi nedeniyle histopatolojik tanı olanaksız hale geldiğinde, klinisyenler klinik, biyokimyasal ve radyolojik bulgulara güvenmelidir. Bu olgu bildiriminde, ^{18}F-florodeoksiglukoz (^{18}F-FDG) pozitron emisyon tomografisi/bilgisayarlı tomografi ile görüntülenen agresif PEK'li 78 yaşında bir kadın hasta bildirilmektedir. Görüntülemede, yoğun bir şekilde hipermetabolik pankreas başı kitlesi, hepatik superscan görünümü ve hipermetabolik abdominal lenfadenopati saptanmıştır. Evre IV PEK'yi düşündüren güçlü klinik göstergelere rağmen, hastalığın hızlı ilerlemesi ve hastanın ölümünün histopatolojik doğrulamayı mümkün kılmaması, bu bağlamda hepatik superscan görünümü ile ilişkili kötü prognozu vurgulamıştır.

Anahtar kelimeler: Pankreas karsinomu, hepatik superscan, fulminan metasta, ^{18}F-FDG, PET/BT

Address for Correspondence: Akram Al-Ibraheem, Prof. MD, King Hussein Cancer Center (KHCC), Department of Nuclear Medicine and PET/CT, Al-Jubeiha, Amman, Jordan
E-mail: akramalibrahim@gmail.com **ORCID ID:** orcid.org/0000-0002-0978-4716
Received: 15.08.2024 **Accepted:** 08.09.2024 **Publication Date:** 03.05.2025

Cite this article as: Al-Adhami D, Juweid M, Al-Ibraheem A. The poor prognostic stigma of hepatic superscan on ^{18}F-FDG PET imaging. Mol Imaging Radionucl Ther. 2025;34:149-151.

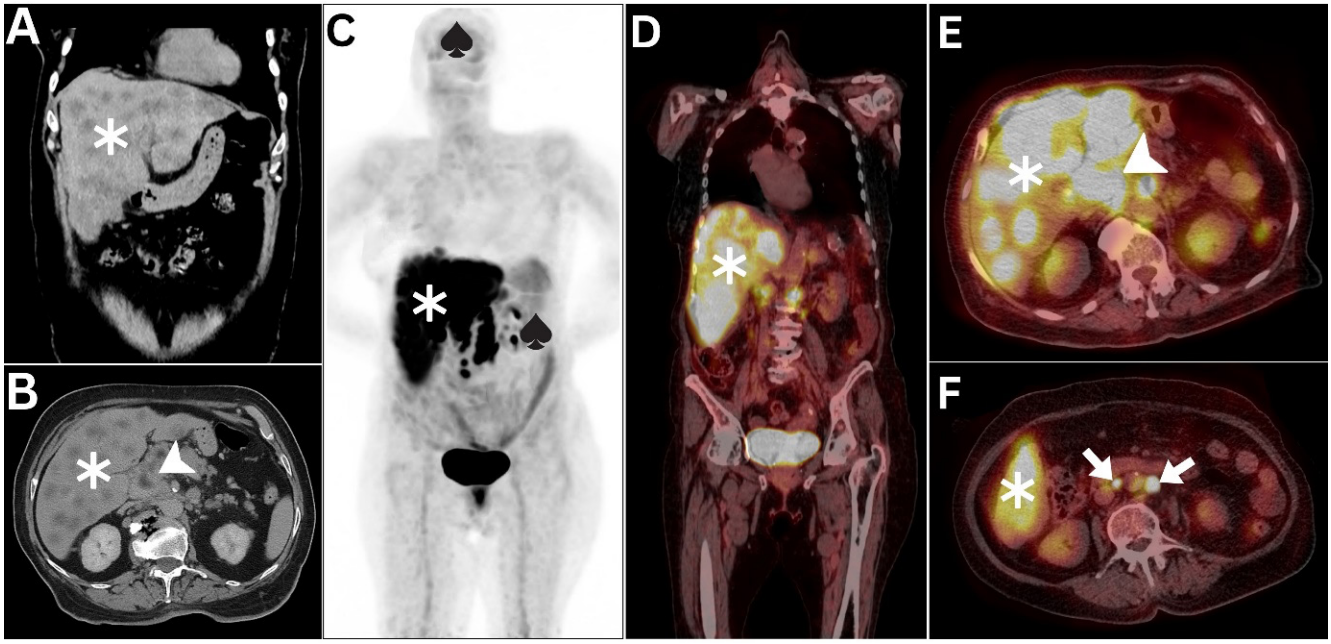

Figure 1. A 78-year-old female non-smoker with long-standing hypertension and no history of familial malignancy presented with a 3-month history of diffuse abdominal pain radiating to the shoulder that was accompanied by generalized weakness, anorexia, and weight loss. Multiple emergency visits for fluid and electrolyte replacement due to dehydration were reported. Financial constraints initially prevented the patient from undergoing definitive clinical, biochemical, and radiological tests for provisional diagnosis. The decision to seek a comprehensive evaluation was delayed until the patient experienced unbearable pain, frequent unresolved episodes of nausea and vomiting, and weight loss of 12 kg. Physical examination revealed a tired, pale patient in pain, with yellowish skin discoloration and tender hepatomegaly. Comprehensive hematologic, hepatic, renal, and tumor marker profiles were obtained. Results were normal except for anemia (hemoglobin 7.1 g/dL), elevated total bilirubin (4.5 mg/dL), elevated hepatic transaminases (aspartate transaminase 111 IU/L, alanine transaminase 137 IU/L), and an elevated carbohydrate antigen 19-9 (CA 19-9) level of 1397 U/mL. Initial diagnostic workup (Figure 1) included abdominal computed tomography (CT), which revealed widespread liver hypodensities suggesting fulminant hepatic metastasis (A, B; asterisks), in addition to a large multicystic pancreatic head tumor (B; arrowhead). Subsequent ^{18}F-fluorodeoxyglucose (^{18}F-FDG) positron emission tomography/computerized tomography (PET/CT) imaging demonstrated a hepatic superscan on maximum intensity projection (MIP) image, characterized by diffuse intensely hypermetabolic hepatomegaly (C; asterisks) and suppressed ^{18}F-FDG activity in the brain and pelvicalyceal system (C; spades). Coronal and axial fused PET/CT images revealed evidence of widespread hepatic hypodensities (D-F; asterisk). Furthermore, axial fused PET/CT images depict an intensely hypermetabolic neoplastic process involving the pancreatic head tumor (E; arrowhead). In addition, few hypermetabolic metastatic abdominal lymph nodes were observed (F; arrows). Due to rapid clinical deterioration, worsening performance status, and admission to intensive care unit (ICU), a definitive histopathologic diagnosis could not be established. The patient succumbed to multiorgan failure 14 days after ICU admission. A clinical diagnosis of stage IV pancreatic exocrine cancer was provisionally made.

Hepatic superscan is a rare molecular imaging entity observed in aggressive hematologic and solid malignancies (1,2). To our knowledge, its occurrence in pancreatic carcinoma has not been previously reported. The distinct pattern of hepatic superscan characterized by intensely hypermetabolic hepatomegaly and suppressed ^{18}F-FDG activity in organs with normally intensified ^{18}F-FDG metabolism can be observed on MIP images (1). Recent observations have highlighted the prognostic significance of hepatic superscan, associating it with poor prognosis and rapid onset of disease, often before management can be initiated. Such cases frequently receive delayed diagnosis because of neglect, delayed diagnosis, or misdiagnosis (2,3,4,5). Therefore, recognition of this unique neoplastic pattern should prompt immediate clinical and oncologic intervention to achieve the best possible outcome.

Ethic

Informed Consent: The patient consent was obtained.

Footnote

Authorship Contributions

Surgical and Medical Practices: D.A., M.J., A.A., Concept: D.A., M.J., A.A., Design: D.A., M.J., A.A., Data Collection or Processing: D.A., M.J., A.A., Analysis or Interpretation: D.A., A.A., Literature Search: M.J., A.A., Writing: D.A., A.A.

Conflict of Interest: No conflicts of interest were declared by the authors.

Financial Disclosure: The authors declare that this study has received no financial support.

References

1. Basu S, Nair N. Unusually elevated liver radioactivity on F-18 FDG PET in Hodgkin's disease: hepatic 'superscan'. Clin Nucl Med. 2004;29:626-628.
2. Abdlkadir AS, Al-Adhami D, Alsyouf B, Alhouwari R, Al-Rasheed U, Jaber O, Mohamad I, Al-Ibraheem A. Hepatic Superscan in Medullary Thyroid Carcinoma: A Rare Presentation in [^{18}F]FDG PET/CT. Nucl Med Mol Imaging. 2024;58:147-149.
3. Abdlkadir AS, Almasri N, Estrada E, Fani Bozkurt M, Al-Ibraheem A. 18 F-FDG PET/CT Unveils Coexistent Myelomatous Hepatosplenic and Thyroid Cartilage Involvement : A Rare Presentation in Multiple Myeloma. Clin Nucl Med. 2024;49:897-898.
4. Taneja S, Achong DM. Hepatic superscan on PET/CT due to Richter's transformation of chronic lymphocytic leukemia. Clin Nucl Med. 2010;35:644-645.
5. Yang G, Nie P, Wang Z, Xing X. (18)F-FDG hepatic superscan caused by a non-germinal center subtype of diffuse large B-cell lymphoma. Eur J Nucl Med Mol Imaging. 2016;43:1928.

Interesting Image

Mol Imaging Radionucl Ther 2025;34:152-155 *DOI:10.4274/mirt.galenos.2024.99267*

Molecular Perspectives on Meningioma with Osseous Infiltration Revealed by ^{68}Ga-DOTA TOC PET-CT

^{68}Ga-DOTA TOC PET-CT ile Saptanan Kemik İnfiltrasyonlu Menenjiyomlar Üzerine Moleküler Perspektifler

Sharjeel Usmani[1], Anjali Jain[1], Khulood Al Riyami[1], Syed Furqan Hashmi[2], Jamsari Khalid[2], Subhash Kheruka[1]

[1]*Sultan Qaboos Comprehensive Cancer Care and Research Centre, Department of Radiology and Nuclear Medicine, Muscat, Oman*
[2]*Sultan Qaboos Comprehensive Cancer Care and Research Centre, Department of Radiation Oncology, Muscat, Oman*

Abstract

Meningiomas express the somatostatin receptor (SSTR). The utilization of SSTR ligands, specifically Gallium-68 (^{68}Ga) isotope, a radioactive isotope (^{68}Ga)-DOTA-labeled peptides, has demonstrated exceptional diagnostic precision for the detection of meningiomas, primarily due to the absence of normal brain and bone activity. We report a case of a 48-year-old woman with sphenoid wing meningioma who underwent ^{68}Ga-DOTA TOC positron emission tomography (PET) for tumor delineation. ^{68}Ga-DOTA TOC PET shows SSTR-avid meningioma in the right sphenoid/anterior temporal region with significant hyperostosis with high expression of SSTR in the bone. ^{68}Ga-DOTA TOC uptake in the hyperostosis signifies bone infiltration rather than reactive changes. ^{68}Ga-DOTA PET provides a better assessment of osseous involvement and provides additional information in terms of meningioma extent and planning for further management.

Keywords: ^{68}Ga-DOTA, positron emission tomography/computed tomography, meningioma, SSTR, hyperostosis

Öz

Menenjiyomlar somatostatin reseptörü (SSTR) ekprese eder. SSTR ligandlarının, özellikle Gallium-68 (^{68}Ga)-DOTA etiketli peptitlerin kullanımı, öncelikle normal beyin ve kemik aktivitesinin olmaması nedeniyle menenjiyomları tespit etmede olağanüstü tanısal hassasiyet göstermiştir. Tümör tanımlaması için ^{68}Ga-DOTA TOC pozitron emisyon tomografisi (PET)'e tabi tutulan sfenoid kanat menenjiyomu olan 48 yaşında bir kadın olgusunu bildiriyoruz. ^{68}Ga-DOTA TOC PET, kemikte yüksek SSTR ekspresyonu ile belirgin hiperostozisli sağ sfenoid/ön temporal bölgede SSTR avid menenjiyomu göstermiştir. Hiperostozisteki ^{68}Ga-DOTA TOC tutulumu, reaksiyonel değişikliklerden ziyade kemik infiltrasyonunu ifade eder. ^{68}Ga-DOTA PET, kemik tutulumunun daha iyi değerlendirilmesini sağlar ve menenjiyomun içeriği ve daha ileri tedavi planlaması açısından ek bilgi sağlar.

Anahtar kelimeler: ^{68}Ga-DOTA pozitron emisyon tomografisi/bilgisayarlı tomografi, menenjiyom, SSTR, hiperostoz

Address for Correspondence: Sharjeel Usmani MD, Sultan Qaboos Comprehensive Cancer Care and Research Centre, Department of Radiology and Nuclear Medicine, Muscat, Oman
E-mail: dr_shajji@yahoo.com **ORCID ID:** orcid.org/0000-0001-9274-7571
Received: 01.04.2024 **Accepted:** 13.10.2024 **Publication Date:** 03.05.2025

Cite this article as: Usmani S, Jain A, Al Riyami K, Hashmi SF, Khalid K, Kheruka S. Molecular perspectives on meningioma with osseous infiltration revealed by ^{68}Ga-DOTA TOC PET-CT. Mol Imaging Radionucl Ther. 2025;34:152-155.

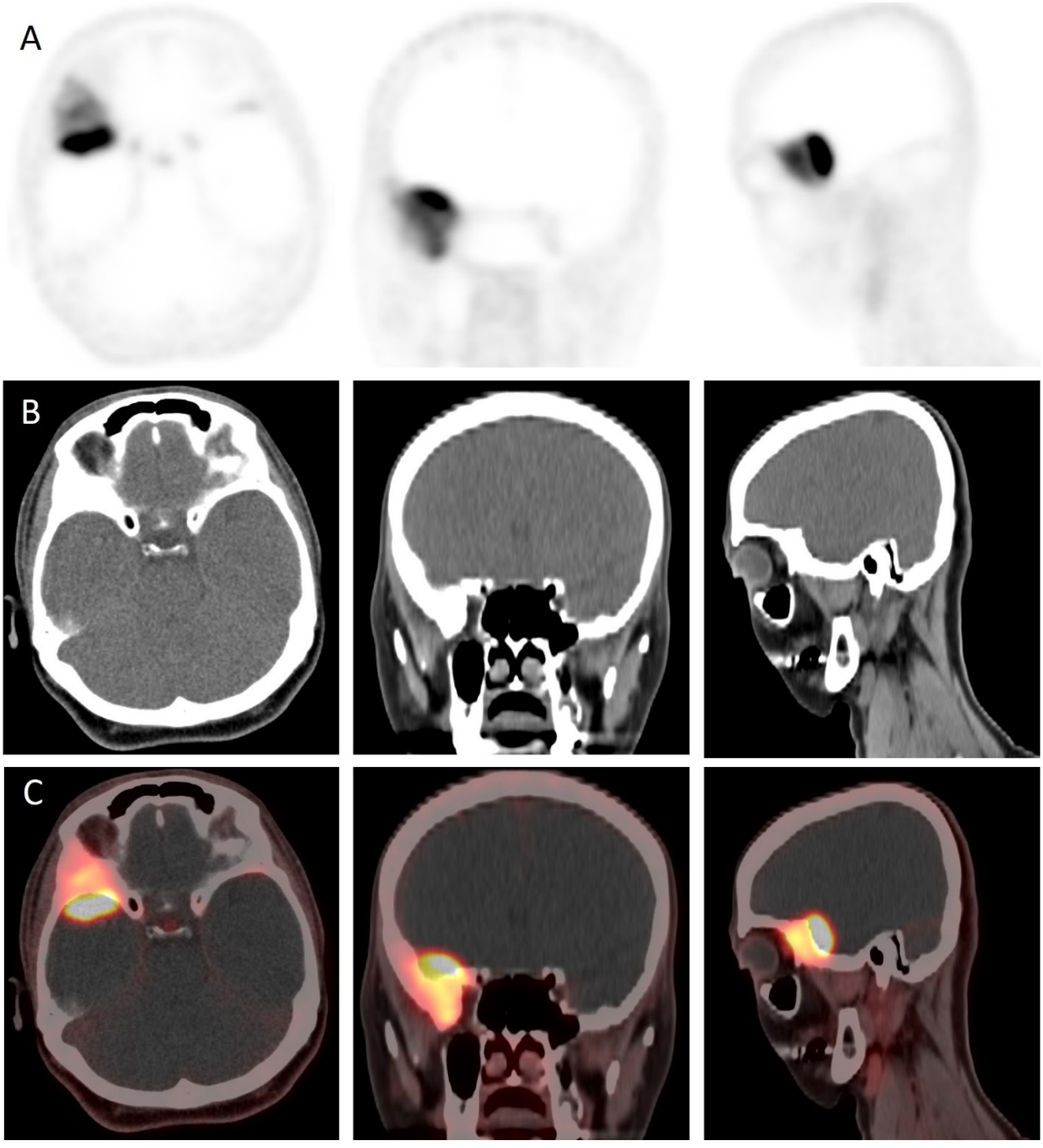

Figure 1: A 48-year-old woman with right orbital pain and swelling was diagnosed with meningioma of the right sphenoid wing on magnetic resonance imaging (MRI). Gallium-68 (^{68}Ga)-DOTA positron emission tomography/computed tomography (PET/CT) was performed for tumor delineation and lesion characterization. A-C ^{68}Ga-DOTA TOC PET/CT images demonstrate an extraaxial focal area of increased tracer uptake (SUV_{max}: 17.5) along the right sphenoid region/right anterior temporal region.

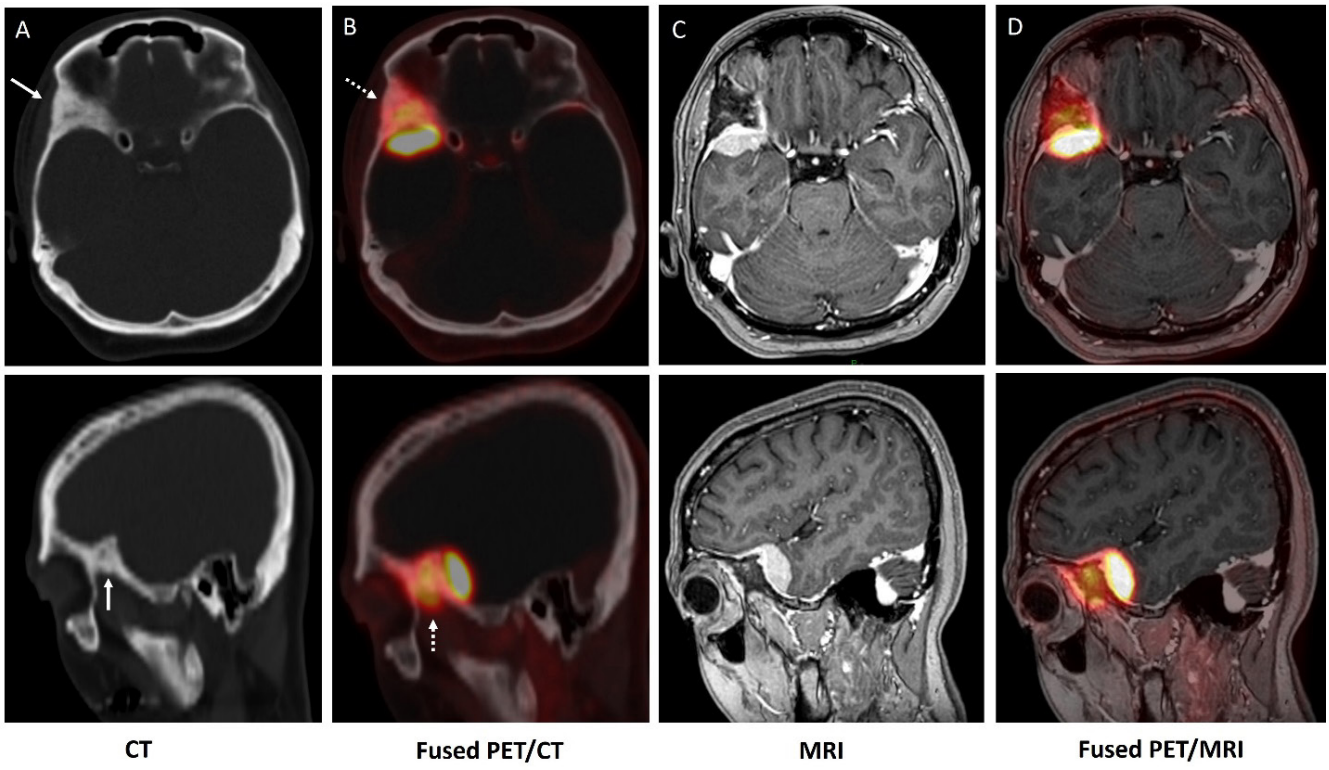

Figure 2: A. CT bone window showing expansile sclerosis (hyperostosis) mainly involving the right wing of the sphenoid bone (solid arrow), right lateral orbital wall, anterior clinoid process, and lateral wall of right sphenoid hemisinus with diffuse increased ^{68}Ga-DOTA TOC uptake of SUV_{max} 8.4 on fused images B (dashed arrow). C. MRI showing a well-defined lobulated dural-based mass arising from the greater wing of the sphenoid extending to the orbital apex. The lesion was better delineated on fused PET/MRI images (D). Findings are consistent with somatostatin receptor-avid meningioma with significant hyperostosis of the underlying bone, suggesting meningioma with bone infiltration.

Meningiomas are the most common primary brain tumors, accounting for approximately 30% of intracranial tumors (1). Bony involvement in intracranial meningiomas is uncommon and is believed to occur due to hyperostosis, which is reported to occur in 4.5%-17% of cases. Neoplastic infiltration of intracranial bone and primary intraosseous meningioma are other causative factors for bone involvement (2). It is more frequently observed in meningiomas with plaque, with an occurrence rate of 13%-49% (3). Transosseous extension of intracranial meningiomas is associated with a high risk of tumor recurrence and mortality and often requires gross total resection and cranial reconstruction (4). There is no clear mechanism underlying the hyperostotic changes that have been described in the literature. Hyperostosis may occur due to irritation from an adjacent tumor, leading to bone invasion by meningiomatosis cells, resulting in secondary hypervascularity in the diploe of the surrounding skull. Some authors have suggested that the infiltration of bone by tumor cells causes secondary changes in osteoblast and osteoclast activity, leading to increased bone deposition. A small cohort study by Matschke J et al. (5) suggests that there is high expression of somatostatin receptor 2A (SSR2A) during the histogenesis of hyperostosis in meningioma. They found that the osseous part of the tumor exhibited the same strong SSR2A reactivity as the extraosseous part of the tumor, which possibly favors bone infiltration rather than reactive changes.

Somatostatin receptor (SSTR) is a ^{68}G-protein-coupled receptor that is highly expressed in the majority of meningiomas, with subtype 2 being the most abundant (6). ^{68}Ga-DOTA PET imaging with radiolabeled somatostatin agonists offers high diagnostic accuracy for assessing meningiomas because of the high density of SSTRs. This modality provides additional information for patients exhibiting ambiguous or equivocal results on MRI. ^{68}Ga-DOTA PET delineates tumor extent more accurately than MRI with contrast, particularly in regions such as the skull base, orbital area, and parasagittal regions, where bone invasion or involvement of the dural sinuses is frequently observed (7). ^{68}Ga-DOTA PET is also more proficient in detecting osseous involvement than MRI, as the detection of osseous infiltration relies on morphologic features such as hyperostosis and intraosseous contrast enhancement (8). It is difficult to precisely define the degree of infiltration on CT and MRI images. ^{68}Ga-DOTA PET provides a better assessment of osseous involvement and has great potential to improve target delineation for surgical resection and radiation treatment planning (9). ^{68}Ga-DOTA PET can accurately determine tumor margins for radiotherapy**.** A recent study by Kowalski ES et al. (10) reported the value of ^{68}Ga-DOTATATE PET/CT in the diagnosis, radiation treatment planning, and evaluation of the response of meningiomas to radiotherapy.

Ethics

Informed Consent: Patient consent was not required for this study.

Authorship Contributions

Surgical and Medical Practices: S.F.H., J.K., Concept: S.U., A.J., K.A.R., S.F.H., S.K., Design: S.U., A.J., S.K., J.K., Data Collection or Processing: S.U., J.K., Analysis or Interpretation: S.U., S.F.H., A.J., K.A.R., S.K., Literature Search: S.U., Writing: S.U., A.J., K.A.R.

Conflict of Interest: No conflicts of interest were declared by the authors.

Financial Disclosure: The authors declare that this study has received no financial support

References

1. Ostrom QT, Gittleman H, Truitt G, Boscia A, Kruchko C, Barnholtz-Sloan JS. CBTRUS statistical report: Primary brain and other central nervous system tumors diagnosed in the united states in 2011-2015. Neuro Oncol. 2018;20(suppl_4):iv1-86.
2. Pieper DR, Al-Mefty O, Hanada Y, Buechner D. Hyperostosis associated with meningioma of the cranial base: secondary changes or tumor invasion. Neurosurgery. 1999;44:742-746
3. Akutsu H, Sugita K, Sonobe M, Matsumura A. Parasagittal meningioma en plaque with extracranial extension presenting diffuse massive hyperostosis of the skull. Surg Neurol. 2004;61:165-169.
4. Ildan F, Erman T, Göçer AI, Tuna M, Bağdatoğlu H, Cetinalp E, Burgut R. Predicting the probability of meningioma recurrence in the preoperative and early postoperative period: a multivariate analysis in the midterm follow-up. Skull Base. 2007;17:157-171.
5. Matschke J, Addo J, Bernreuther C, Zustin J. Osseous changes in meningioma en plaque. Anticancer Res. 2011;31:591-596.
6. Theodoropoulou M, Stalla GK. Somatostatin receptors: from signaling to clinical practice. Front Neuroendocrinol. 2013;34:228-252.
7. Rachinger W, Stoecklein VM, Terpolilli NA, Haug AR, Ertl L, Pöschl J, Schüller U, Schichor C, Thon N, Tonn JC. Increased 68Ga-DOTATATE uptake in PET imaging discriminates meningioma and tumor-free tissue. J Nucl Med. 2015;56:347-353.
8. Kunz WG, Jungblut LM, Kazmierczak PM, Vettermann FJ, Bollenbacher A, Tonn JC, Schichor C, Rominger A, Albert NL, Bartenstein P, Reiser MF, Cyran CC. Improved detection of transosseous meningiomas using 68Ga-DOTATATE PET/CT compared with contrast-enhanced MRI. J Nucl Med. 2017;58:1580-1587.
9. Perlow HK, Siedow M, Gokun Y, McElroy J, Matsui J, Zoller W, Beyer S, Arnett A, Blakaj D, Boulter D, Fritz J, Miller E, Raval R, Kleefisch C, Bovi J, Palmer JD. 68Ga-DOTATATE PET-Based Radiation Contouring Creates More Precise Radiation Volumes for Patients With Meningioma. Int J Radiat Oncol Biol Phys. 2022;113:859-865.
10. Kowalski ES, Khairnar R, Gryaznov AA, Kesari V, Koroulakis A, Raghavan P, Chen W, Woodworth G, Mishra M. 68Ga-DOTATATE PET-CT as a tool for radiation planning and evaluating treatment responses in the clinical management of meningiomas. Radiat Oncol. 2021;16:151.

Interesting Image

Mol Imaging Radionucl Ther 2025;34:156-158 *DOI:10.4274/mirt.galenos.2024.26879*

Neurolymphomatosis: The Sinister Face of Lymphoma

Nörolenfomatozis: Lenfomanın Kötü Yüzü

Sana Munir Gill[1], Aamna Hassan[1], Pir Abdul Ahad Aziz Qureshi[2], Humayun Bashir

[1]*Shaukat Khanum Memorial Cancer Hospital and Research Centre, Clinic of Nuclear Medicine, Lahore, Pakistan*
[2]*Landspítali -The National University Hospital, Clinic of Nuclear Medicine, Reykjavik, Iceland*
[3]*East Kent Hospitals University NHS Foundation Trust, Department of Nuclear Medicine, Canterbury, United Kingdom*

Abstract

Neurolymphomatosis (NL) is a rare clinical condition characterized by the infiltration of malignant lymphocytes into the cranial or peripheral nerves, nerve roots, or plexus. Diagnosis can be clinically challenging due to its variable presentation. It usually occurs in B cell lymphoma; however, a few cases of extranodal killer/T cell lymphoma. Most cases present at a secondary site in patients with primary site in remission. ^{18}Fluorine fluorodeoxyglucose positron emission tomography/computed tomography plays an important role in the early detection of NL, resulting in timely treatment. We present a case of a 24-year-old male with nasal natural killer T cell lymphoma who initially responded to treatment but relapsed with NL based on clinical and radiological findings.

Keywords: Neurolymphomatosis, natural killer T cell lymphoma, ^{18}Fluorine fluorodeoxyglucose positron emission tomography/computed tomography, lymphom

Öz

Nörolenfomatozis (NL), nadir görülen bir klinik durumdur ve kranial veya periferik sinirlerin, sinir köklerinin veya pleksusların malign lenfositler tarafından enfiltrasyonudur. Değişken klinik sunumu nedeniyle tanısı zor olabilir. Genellikle B hücreli lenfoma ile birlikte görülür; ancak, ekstra nodal doğal öldürücü/T hücreli lenfomalı birkaç olguda bildirilmiştir. Çoğu zaman, birincil bölge remisyonda olan hastalarda ikincil bir bölgede ortaya çıkar. ^{18}Flor florodeoksiglukoz pozitron emisyon tomografisi/bilgisayarlı tomografi, NL'nin erken tespitinde önemli bir rol oynar ve zamanında tedavi edilmesini sağlar. Klinik ve radyolojik bulgulara dayanarak, başlangıçta tedaviye yanıt veren ancak daha sonra NL ile birlikte tekrarlayan 24 yaşında bir erkek nazal doğal öldürücü T hücreli lenfomalı olguyu sunuyoruz.

Anahtar kelimeler: Nörolenfomatozis, doğal öldürücü T hücreli lenfoma, ^{18}Flor florodeoksiglukoz pozitron emisyon tomografisi/bilgisayarlı tomografi, lenfoma

Address for Correspondence: Aamna Hassan, Shaukat Khanum Memorial Cancer Hospital and Research Centre, Clinic of Nuclear Medicine, Lahore, Pakistan
E-mail: aamnah@skm.org.pk **ORCID ID:** orcid.org/0000-0003-0026-0729
Received: 20.08.2024 **Accepted:** 23.12.2024 **Epub:** 23.05.02025 **Publication Date:** 03.05.2025

Cite this article as: Gill SM, Hassan A, Qureshi PAAA, Bashir H. Neurolymphomatosis: the sinister face of lymphoma. Mol Imaging Radionucl Ther. 2025;34:156-158.

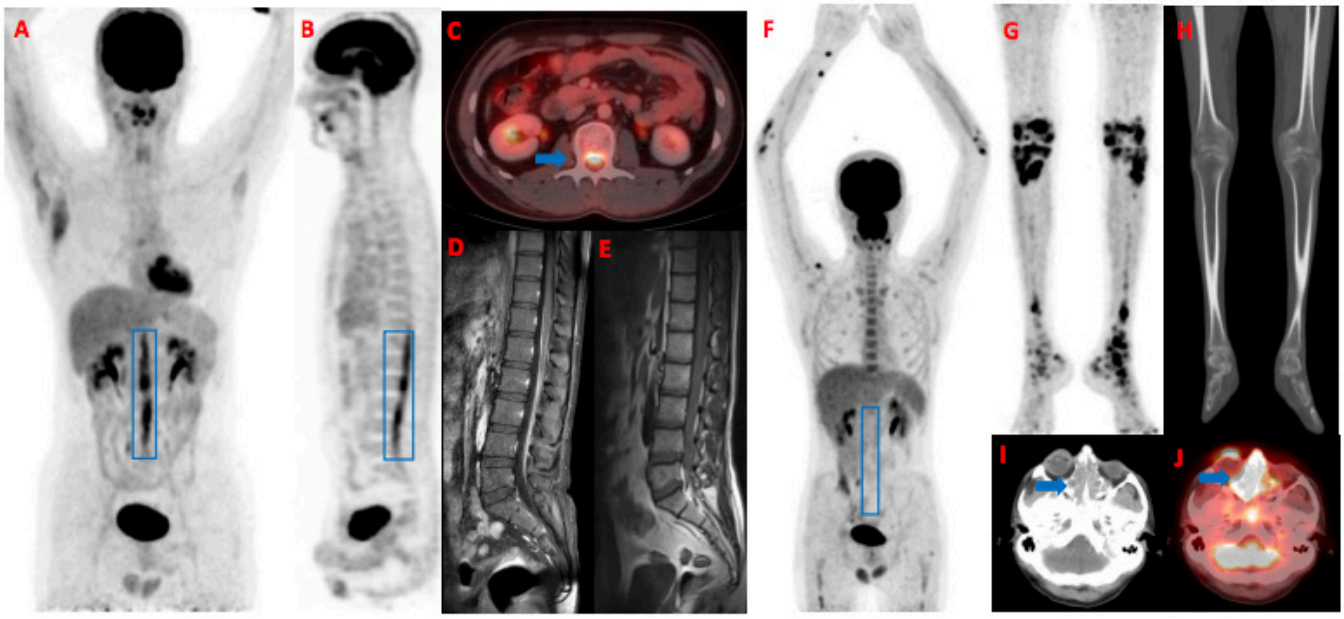

Figure 1. A 24-year-old male patient diagnosed with natural killer T cell lymphoma (NKTL) presented to our department for ^{18}Fluorine fluorodeoxyglucose 2-deoxy-glucose positron emission tomography/computed tomography (^{18}F-FDG-PET/CT). There was clinical suspicion of disease relapse due to complaints of backache, heavy headedness, and diplopia for 1 week. On examination, his glascow coma scale score was 15/15; power in upper limbs was unremarkable; however, power in lower limbs was reduced to 1/5 along with decreased tone and reflexes. His fundoscopy findings were unremarkable. Contrast-enhanced brain magnetic resonance imaging (MRI) of the patient was unremarkable. His ^{18}F-FDG PET/CT showed hypermetabolic mild thickening of the conus medullaris and cauda equina [standardized uptake value (SUV) 6.6, liver SUV 2.9] highly concerning for neurolymphomatosis (NL) [A,B maximum intensity projection (MIP) and sagittal PET blue boxes and C fused PET/CT blue arrow]. The primary tumor site (i.e., nasal cavity) showed minimal thickening along the nasal turbinate without significant FDG uptake. Contrast-enhanced spine MRI also revealed diffuse thickening, edema and abnormal enhancement of the conus medullaris and cauda equina, suggestive of lymphomatous infiltration [C and D, Sagittal pre- and post-contrast T1-weighted imaging (T1WI) MRI]. Cerebrospinal fluid analysis revealed cluster of differentiation 56+ malignant cells, and flow cytometry confirmed central nervous system relapse. He was then treated with high-dose chemotherapy and radiotherapy. Response evaluation ^{18}F-FDG PET/CT showed interval resolution of FDG uptake in the conus medullaris (F, MIP image blue box); however, there was progression at multiple sites, including bone marrow (G and H, MIP and coronal CT), preseptal region, and nasopharynx (I and J, axial CT and fused images, blue arrows). At this point, the patient was referred for palliative treatment; and after a period of about 2 months on palliative treatment, the patient succumbed to the complications of disease.

NL is a rare condition. Diagnosis can be clinically challenging due to its variable presentation. Literature review shows that, most commonly, it is associated with non-hodgkin lymphoma (1,2). Approximately 80% of the cases are associated with B cell lymphoma compared with T cell lymphoma. Among T cell lymphomas, NKTL is a rare entity that occurs at unusual sites, such as the central nervous system, skin, and nasopharynx. Despite aggressive treatment, it usually follows a rapidly progressive course (3). It is important to differentiate NL from non-cancerous conditions, such as the Miller Fischer variant of Guillain-Barre Syndrome, inflammatory radiculopathy, neuropathies, and chemoradiotherapy-induced damage to the nerves. That history proves to be of paramount importance in making definitive diagnosis. Although histopathology remains the gold standard for diagnosing NL, due to its limitations, MRI and PET-CT play a major role in the diagnosis of NL, with sensitivity of 87.5% and 100%, respectively (4,5,6). Biopsy is associated with an increased risk of permanent nerve damage, and it is usually reserved for cases that are not diagnosed on history and imaging. Within our institution, over a span of the last 15 years, there are 9 reported cases of NL on ^{18}F-FDG PET/CT (7,8), of which only our patient was of NKTL. Therefore, clinicians reporting PET scans should be cognizant of the fact that NL is likely to represent the aggressive extra-nodal lymphoma spectrum.

Ethics

Informed Consent: An informed consent was obtained from the patient.

Footnotes

Authorship Contributions:

Concept: S.M.G., P.A.A.A.Q., Design: S.M.G., A.H., P.A.A.A.Q., H.B., Data Collection or Processing: S.M.G., P.A.A.A.Q., Analysis or Interpretation: S.M.G., A.H., P.A.A.A.Q., H.B., Literature Search: S.M.G., Writing: S.M.G., A.H., P.A.A.A.Q.

Conflict of Interest: No conflicts of interest were declared by the authors.

Financial Disclosure: The authors declare that this study has received no financial support.

References

1. Pan Q, Luo Y. Recurrence of nasal type NK/T cell lymphoma presenting as neurolymphomatosis on 18F-FDG PET/CT: a case report and literature review. Medicine (Baltimore). 2020;99:e18640.
2. DeVries AH, Howe BM, Spinner RJ, Broski SM. B-cell peripheral neurolymphomatosis: MRI and ^{18}F-FDG PET/CT imaging characteristics. Skeletal Radiol. 2019;48:1043-1050.
3. Lee J, Suh C, Park YH, Ko YH, Bang SM, Lee JH, Lee DH, Huh J, Oh SY, Kwon HC, Kim HJ, Lee SI, Kim JH, Park J, Oh SJ, Kim K, Jung C, Park K, Kim WS. Extranodal natural killer T-cell lymphoma, nasal-type: a prognostic model from a retrospective multicenter study. J Clin Oncol. 2006;24:612-618.
4. Choi YJ, Shin JA, Kim YH, Cha SJ, Cho JY, Kang SH, Yi SY, Lee HR. Neurolymphomatosis of brachial plexus in patients with non-hodgkin's lymphoma. Case Rep Oncol Med. 2013;2013:492329.
5. Baehring JM, Batchelor TT. Diagnosis and management of neurolymphomatosis. Cancer J. 2012;18:463-468.
6. Soni N, Ora M. FDG PET/CT in neurolymphomatosis. Radiology. 2021;298:36.
7. Yaseen MT, Aziz PAA, Siddique K, Tariq TA. Neurolymphomatosis of the sciatic and tibial nerves. J Coll Physicians Surg Pak. 2019;29:S86-S88.
8. Riaz S, Naz F, Bashir H, Niazi IK. "Bottle brush sign"- Spinal meningeal disease on 18F-FDG PET-CT scan. Clin Nucl Med. 2016;41:726-727.

Interesting Image

Mol Imaging Radionucl Ther 2025;34:159-161 *DOI:10.4274/mirt.galenos.2025.46693*

Incidentally Detected High-Grade Follicular Derived Non-Anaplastic Thyroid Carcinoma on ^{68}Ga-PSMA PET-CT

^{68}Ga-PSMA PET-BT'de Tesadüfen Tespit Edilen Yüksek Dereceli Foliküler Kaynaklı Non-Anaplastik Tiroid Karsinomu

Parneet Singh[1], Srijani Mandal[1], Amit Kumar Adhya[2], Girish Kumar Parida[1], Kanhaiyalal Agrawal[1]

[1]*All India Institute of Medical Sciences, Clinic of Nuclear Medicine, Bhubaneswar, India*
[2]*All India Institute of Medical Sciences, Clinic of Pathology, Bhubaneswar, India*

Abstract

^{68}Ga–prostate-specific membrane antigen (PSMA)-11 positron emission tomography/computed tomography (PET/CT) is currently routinely used for the evaluation of prostate cancer. However, due to its whole-body imaging capability, it can incidentally identify pathologies beyond prostate cancer. Herein, we describe a case of a 67-year-old man who was recently diagnosed with prostate carcinoma (PCa). The patient had a high PSMA-avid thyroid carcinoma detected incidentally during the initial staging of PCa with ^{68}Ga-PSMA-11 PET-CT.

Keywords: Thyroid carcinoma, incidental, prostate-specific membrane antigen, neovasculature

Öz

^{68}Ga-prostat-spesifik membran antijeni (PSMA)-11 pozitron emisyon tomografisi/bilgisayarlı tomografi (PET-BT), prostat kanserinin değerlendirilmesinde standart görüntüleme yöntemi haline gelmiştir. Ancak, tüm vücudu görüntüleyebilme kapasitesi sayesinde prostatın ötesinde önemli patolojileri tesadüfen tespit edebilir. Bu yazıda, yakın zamanda prostat karsinomu teşhisi konmuş 67 yaşında bir erkek hastayı bildiriyoruz. Hastada, ^{68}Ga-PSMA-11 PET-BT kullanılarak prostat kanserinin ilk evrelemesi sırasında tesadüfen yüksek PSMA-avid tiroid karsinomu saptandı.

Anahtar kelimeler: Tiroid karsinomu, tesadüfi, prostat spesifik membran antijeni, neovaskülatür

Address for Correspondence: Kanhaiyalal Agrawal MD, All India Institute of Medical Sciences, Department of Nuclear Medicine, Bhubaneswar, India
E-mail: nucmed_kanhaiyalal@aiimsbhubaneswar.edu.in **ORCID ID:** orcid.org/0000-0003-4855-8938
Received: 20.08.2024 **Accepted:** 08.01.2025 **Epub:** 23.05.2025 **Publication Date:** 03.05.2025

Cite this article as: Singh P, Mandal S, Adhya AK, Parida GK, Agrawal K. Incidentally detected high-grade follicular derived non-anaplastic thyroid carcinoma on [^{68}Ga] PSMA PET-CT. Mol Imaging Radionucl Ther. 2025;34:159-161.

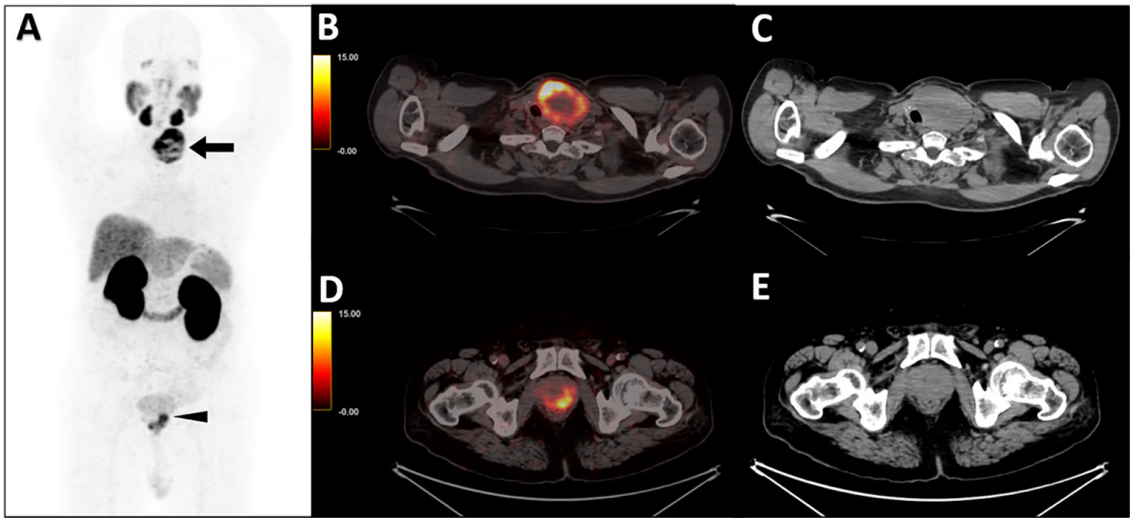

Figure 1. A 67-year-old gentleman with recently diagnosed prostate carcinoma (PCa) (Gleason's score: 5+4=9) and serum prostate-specific antigen level 106 ng/mL underwent ^{68}Ga-prostate-specific membrane antigen (PSMA)-11 positron emission tomography/computed tomography for staging. A) maximum intensity projection image showing a large focus of abnormal tracer uptake in the neck (arrow) and focal tracer uptake in the pelvis (arrowhead). B-C) The uptake in the neck localized to a large heterogeneous density mass with central necrosis and foci of calcification, replacing almost the entire left lobe of the thyroid and displacing the trachea toward the right measuring 6.8x5.4x7.1 cm with SUV_{max} 27.0 B-C). Pelvic PSMA uptake localized to an ill-defined lesion involving the bilateral peripheral zone of the prostate suggestive of known primary malignancy. D-E) The patient underwent ultrasonography (USG) neck which revealed a large thyroid mass on the thyroid imaging reporting and data system IV. Subsequently, the patient underwent USG-guided fine needle aspiration, which revealed a follicular neoplasm (Bethesda category-IV). Subsequently, the patient underwent total thyroidectomy, and histopathology revealed a high-grade follicular-derived non-anaplastic thyroid carcinoma.

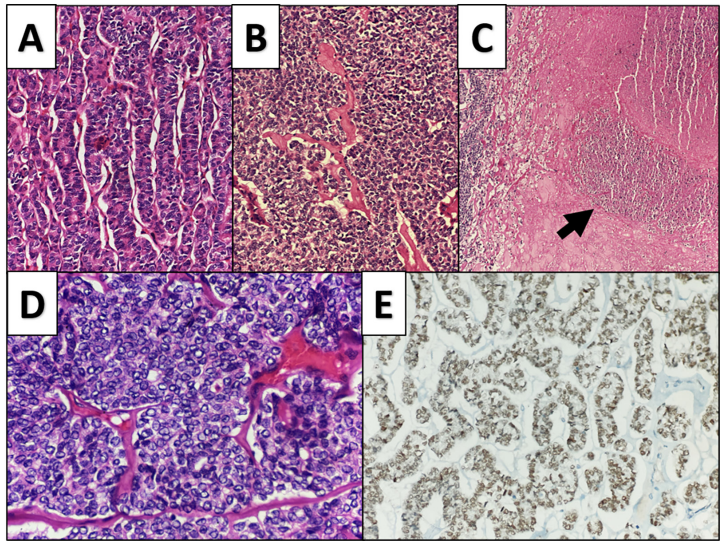

Figure 2. Histopathological images of thyroid tissue showing follicular cells arranged in a; A) trabecular growth pattern; B) solid, nested growth pattern H & E stain, 200x. C) Foci of necrosis are noted within the tumor. H & E stain, 40x. D) Nuclear features of papillary carcinoma of the thyroid, e.g., nuclear crowding, clearing, orphan annie nucleus and grooves H&E stain, 400x. E) Tumor cells showing immunoreactivity for Thyroid transcription factor-1, 200x. The features are suggestive of high-grade follicular-derived non-anaplastic thyroid carcinoma. PSMA is a type II transmembrane glycoprotein. This is overexpressed in prostate carcinoma (PCa) cells, more so in hormone-refractory PCa. PSMA overexpression is not restricted to the prostate and is also expressed in other normal tissues like salivary glands and duodenum. Further, it is overexpressed in endothelial cells of tumor neovasculature in different cancers of kidney, colon, melanoma, breast, etc. and also in benign diseases like endochondroma (1,2,3,4). PSMA is proven to be overexpressed on the endothelial cells of the neovasculature where it expedites endothelial cell sprouting and invasion to cleave the extracellular matrix by lytic proteases (5). It is necessary to be aware of these pitfalls and to evaluate the incidental PSMA uptake apart from its physiological distribution, as in the present case in which abnormal tracer accumulation in the thyroid helped in the diagnosis of thyroid malignancy.

Ethics

Informed Consent: Informed consent was taken.

Footnotes

Authorship Contributions

Surgical and Medical Practices: P.S., S.M., A.K.A., G.K.P., K.A., Concept: P.S., S.M., A.K.A., Design: P.S., K.A., Data Collection or Processing: P.S., S.M., A.K.A., Analysis or Interpretation: P.S., S.M., A.K.A., K.A., Literature Search: P.S., S.M., Writing: P.S., S.M., A.K.A., G.K.P., K.A.

Conflict of Interest: No conflicts of interest were declared by the authors.

Financial Disclosure: The authors declare that this study has received no financial support.

References

1. Hofman MS, Hicks RJ, Maurer T, Eiber M. Prostate-specific membrane antigen PET: clinical utility in prostate cancer, normal patterns, pearls, and pitfalls. Radiographics. 2018;38:200-217.
2. de Galiza Barbosa F, Queiroz MA, Nunes RF, Costa LB, Zaniboni EC, Marin JFG, Cerri GG, Buchpiguel CA. Nonprostatic diseases on PSMA PET imaging: a spectrum of benign and malignant findings. Cancer Imaging. 2020;20:23.
3. Singh P, Kandula KK, Patel RK, Parida GK, Agrawal K. Incidental 68 Ga-PSMA uptake in the benign enchondroma-a rare finding on 68 Ga-PSMA PET/CT. Clin Nucl Med. 2024;49:e525-e527.
4. Lauri C, Chiurchioni L, Russo VM, Zannini L, Signore A. psma expression in solid tumors beyond the prostate gland: ready for theranostic applications? J Clin Med. 2022;11:6590.
5. Van de Wiele C, Sathekge M, de Spiegeleer B, De Jonghe PJ, Debruyne PR, Borms M, Beels L, Maes A. PSMA expression on neovasculature of solid tumors. Histol Histopathol. 2020;35:919-927.

Interesting Image

Mol Imaging Radionucl Ther 2025;34:162-164 *DOI:10.4274/mirt.galenos.2025.94557*

^{68}Ga-PENTIXAFOR PET/CT Captures Superscan in Refractory Multiple Myeloma

^{68}Ga-PENTIXAFOR PET/BT Refrakter Multiple Miyelomada Süper Scan Paternini Gösterir

Siven Kar, Harshita Gupta, Nusrat Shaikh, Vikram R Lele

Jaslok Hospital and Research Centre, Clinic of Nuclear Medicine and PET-CT, Mumbai, India

Abstract

We present a case of a 40-year-old male with refractory multiple myeloma, assessed using ^{68}Gallium-PENTIXAFOR positron emission tomography/computed tomography (^{68}Ga-PENTIXAFOR PET/CT), revealing widespread and intense C-X-C motif chemokine receptor 4 (CXCR4) expression in multiple osteolytic lesions across axial and appendicular skeletons, including bone marrow deposits. Despite undergoing autologous hematopoietic stem cell transplantation and multiple lines of maintenance therapy, the patient experienced disease relapse and progression. The term "superscan" typically refers to diffuse skeletal uptake in conventional bone scans, primarily seen in advanced metastatic cancers or metabolic bone diseases. CXCR4, crucial for tumor growth and metastasis, binds C-X-C motif chemokine 12 (CXCL12) to promote cancer progression. PENTIXAFOR, a CXCR4-targeted PET agent, facilitates imaging of such malignancies. While superscans using PET/CT are rare, our case underscores the utility of ^{68}Ga-PENTIXAFOR PET/CT in evaluating CXCR4 expression in multiple myeloma, highlighting its potential as a diagnostic and prognostic tool in refractory disease management.

Keywords: PENTIXAFOR, C-X-C motif chemokine receptor 4, positron emission tomography/computed tomography, superscan, multiple myeloma

Öz

^{68}Galyum-PENTIXAFOR pozitron emisyon tomografisi/bilgisayarlı tomografi (^{68}Ga-PENTIXAFOR PET/BT) kullanılarak değerlendirilen, kemik iliği tutulumları da dahil olmak üzere aksiyel ve apendiküler iskeletlerde çoklu osteolitik lezyonlarda yaygın ve yoğun C-X-C motif kemokin reseptörü 4 (CXCR4) ekspresyonu gösteren, refrakter multipl miyelomlu 40 yaşında bir erkek hastayı sunuyoruz. Otolog hematopoietik kök hücre nakli ve çoklu idame tedavisine rağmen hastalık nüksetti ve progrese oldu. "süper scan" terimi genellikle konvansiyonel kemik taramalarında yaygın iskelet tutulumunu ifade eder ve öncelikli olarak ileri metastatik kanserlerde veya metabolik kemik hastalıklarında görülür. Tümör büyümesi ve metastaz için kritik öneme sahip olan CXCR4, kanser ilerlemesini desteklemek için C-X-C motif kemokin 12'ye (CXCL12) bağlanır. CXCR4 hedefli bir PET ajanı olan PENTIXAFOR, bu tür malignitelerin görüntülenmesini kolaylaştırır. PET/BT kullanan süper scanler nadir olsa da, olgumuz ^{68}Ga-PENTIXAFOR PET/BT'nin multipl miyelomda CXCR4 ekspresyonunu değerlendirmedeki faydasını vurgulayarak, dirençli hastalık yönetiminde tanı ve prognoz aracı olarak potansiyelini vurgulamaktadır.

Anahtar kelimeler: PENTIXAFOR, C-X-C motif kemokin reseptörü 4, pozitron emisyon tomografisi/bilgisayarlı tomografi, süper scan, multiple miyelom

Address for Correspondence: Siven Kar MBBS, Jaslok Hospital and Research Centre, Clinic of Nuclear Medicine and PET-CT, Mumbai, India
E-mail: siven.kar@gmail.com **ORCID ID:** orcid.org/0000-0001-6173-679X
Received: 03.07.2024 **Accepted:** 10.02.2025 **Epub:** 23.05.2025 **Publication Date:** 03.05.2025

Cite this article as: Kar S, Gupta H, Shaikh N, Lele VR. ^{68}Ga-PENTIXAFOR PET/CT captures superscan in refractory multiple myeloma. Mol Imaging Radionucl Ther. 2025;34:162-164.

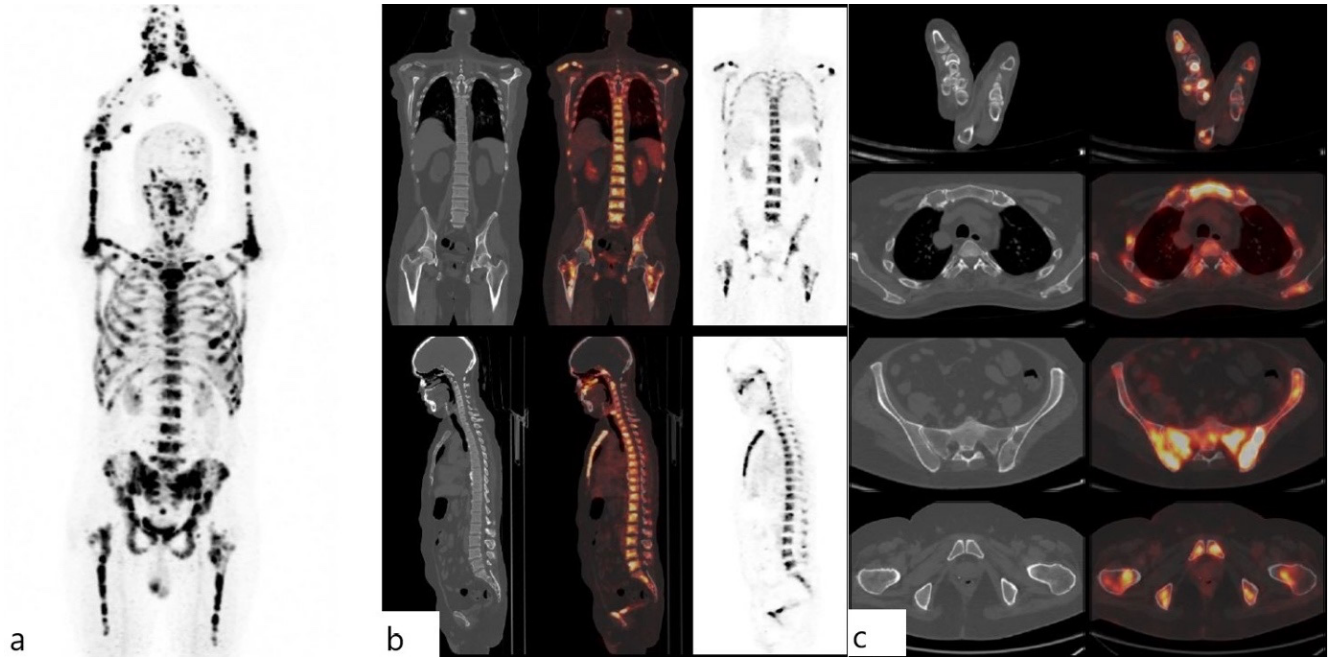

Figure 1. ^{68}Gallium-PENTIXAFOR positron emission tomography/computed tomography (^{68}Ga-PENTIXAFOR PET/CT)-maximum intensity projection image (a), coronal and sagittal (b) and axial sections (c) showing diffuse intensely increased C-X-C motif chemokine receptor 4 (CXCR4) expression in multiple osteolytic lesions throughout the visualised axial (including skull) and appendicular skeleton (including small bones of hands and feet) and bone marrow deposits in a 40-year-old male, known case of multiple myeloma, with renal impairment. He underwent autologous hematopoietic stem cell transplantation in 2021. Afterwards, he has been on multiple lines of maintenance therapy. He has had relapses and disease progression despite continuing therapy. The term "Superscan" (also "beautiful bone scan") is generally used for ^{99m}Technetium-methylenediphosphonate bone scan when there is diffuse increased osseous activity noted in the bones, with reduced or faint visualisation of the bladder and kidneys. It is usually seen in diffuse metastatic carcinoma of the prostate or in the setting of metabolic bone disease (e.g. hyperparathyroidism, osteomalacia, Paget's disease, etc.). CXCR4 is a chemokine receptor, which is widely expressed in hematopoietic cells (1). The abnormal expression of which is associated with tumor growth, dissemination, metastasis, and disease progression (2). CXCR4 binds specifically to C-X-C motif chemokine 12 (CXCL12) and this CXCL12/CXCR4 axis is critical for tumour growth. PENTIXAFOR is a novel PET agent that binds with high affinity to CXCR4. Hence, it has been useful in imaging multiple myeloma, myeloproliferative neoplasms, and aldosterone adenomas (3,4,5). It has been proven to show a greater extent of disease involvement than ^{18}F-fluorodeoxyglucose (^{18}F-FDG) (3). A recent study by Chen et al. (6), demonstrated similar findings, demonstrating the ability of ^{68}Ga-PENTIXAFOR to more effectively predict disease progression (progression-free survival) in newly diagnosed multiple myeloma patients than ^{18}F-FDG. These developments have paved the way for possible use of alternative therapeutic strategies such as ^{177}[Lu]Pentixather for managing relapsed and refractory multiple myeloma in the future. Few superscans have been reported using PET/CT, but we found only two cases for multiple myeloma - one with fluorodeoxyglucose and one with PENTIXAFOR (7,8).

Ethics

Informed Consent: Patient consent was obtained for this study.

Footnotes

Authorship Contributions

Concept: V.R.L., Design: S.K., H.G., Data Collection or Processing: S.K., N.S., Analysis or Interpretation: N.S., Literature Search: S.K., H.G., Writing: S.K.

Conflict of Interest: No conflicts of interest were declared by the authors.

Financial Disclosure: The authors declare that this study has received no financial support.

References

1. Jacobson O, Weiss ID. CXCR4 chemokine receptor overview: biology, pathology and applications in imaging and therapy. Theranostics. 2013;3:1-2.
2. Chen J, Xu-Monette ZY, Deng L, Shen Q, Manyam GC, Martinez-Lopez A, Zhang L, Montes-Moreno S, Visco C, Tzankov A, Yin L, Dybkaer K, Chiu A, Orazi A, Zu Y, Bhagat G, Richards KL, Hsi ED, Choi WW, van Krieken JH, Huh J, Ponzoni M, Ferreri AJ, Zhao X, Møller MB, Farnen JP, Winter JN, Piris MA, Pham L, Young KH. Dysregulated CXCR4 expression promotes lymphoma cell survival and independently predicts disease progression in germinal center B-cell-like diffuse large B-cell lymphoma. Oncotarget. 2015;6:5597-614.
3. Shekhawat AS, Singh B, Malhotra P, Watts A, Basher R, Kaur H, Hooda M, Radotra BD. Imaging CXCR4 receptors expression for staging multiple myeloma by using 68Ga-Pentixafor PET/CT: comparison with 18F-FDG PET/CT. Br J Radiol. 2022;95:20211272.
4. Kraus S, Dierks A, Rasche L, Kertels O, Kircher M, Schirbel A, Zovko J, Steinbrunn T, Tibes R, Wester HJ, Buck AK, Einsele H, Kortüm KM,

Rosenwald A, Lapa C. ^{68}Ga-Pentixafor PET/CT for Detection of Chemokine Receptor CXCR4 Expression in Myeloproliferative Neoplasms. J Nucl Med. 2022;63:96-99.

5. Hu J, Xu T, Shen H, Song Y, Yang J, Zhang A, Ding H, Xing N, Li Z, Qiu L, Ma L, Yang Y, Feng Z, Du Z, He W, Sun Y, Cai J, Li Q, Chen Y, Yang S. Chongqing Primary Aldosteronism Study (CONPASS) Group. Accuracy of Gallium-68 Pentixafor Positron Emission Tomography-Computed Tomography for Subtyping Diagnosis of Primary Aldosteronism. JAMA Netw Open. 2023;6:e2255609.
6. Chen Z, Yang A, Chen A, Dong J, Lin J, Huang C, Zhang J, Liu H, Zeng Z, Miao W. [^{68}Ga]Pentixafor PET/CT for staging and prognostic assessment of newly diagnosed multiple myeloma: comparison to [^{18}F]FDG PET/CT. Eur J Nucl Med Mol Imaging. 2024;51:1926-1936.
7. Fu Z, Chen X, Yang X, Li Q. Skeletal Superscan on 18F-FDG PET/CT in a Patient With Multiple Myeloma. Clin Nucl Med. 2019;44:169-170.

Case Report

Mol Imaging Radionucl Ther 2025;34:165-167 *DOI:10.4274/mirt.galenos.2025.93276*

Disseminated candidiasis on FDG-PET/CT

FDG-PET/BT'de Yaygın Kandidiyazis

Yassir Benameur[1], Adnane Hammani[2], Kamal Doghmi[2], Abderrahim Doudouh[1]

[1]*Mohammed V Military Teaching Hospital, Clinic of Nuclear Medicine; Mohamed V University Faculty of Medicine and Pharmacy, Rabat, Morocco*

[2]*Mohammed V Military Teaching Hospital, Clinic of Hematology; Mohamed V University Faculty of Medicine and Pharmacy, Rabat, Morocco*

Abstract

Disseminated candidiasis presents a significant diagnostic and therapeutic challenge in immunocompromised patients, particularly those with hematological malignancies like leukemia. ^{18}F-fluorodeoxyglucose positron emission tomography/computed tomography (^{18}F-FDG-PET/CT) is a crucial imaging modality in oncology and infection, outperforming conventional imaging in diagnosing and managing fungal infections, especially in cases of fever of unknown origin. We present a compelling case of a young leukemia patient with persistent fever, demonstrating FDG-avid lesions in various organs, including the liver, spleen, and left kidney, indicative of disseminated candidiasis.This highlights the critical role of ^{18}F-FDG-PET/CT in situations where invasive procedures like liver biopsy are challenging or contraindicated. Such instances underscore the paramount importance of utilizing advanced imaging techniques for accurate diagnosis and treatment, especially in the complex clinical setting of immunocompromised individuals, with hematological malignancies. This case emphasizes the significant contribution of ^{18}F-FDG-PET/CT as a non-invasive diagnostic tool, enhancing patient care and enabling more effective management strategies amidst challenging medical circumstances.

Keywords: Candidiasis, fluorodeoxyglucose, positron emission tomography/computed tomography, fever of unknown origin

Öz

Yaygın kandidiyazis, özellikle lösemi gibi hematolojik maligniteleri olan immün sistemi baskılanmış hastalarda önemli bir tanı ve tedavi zorluğu sebebidir. ^{18}F-florodeoksiglukoz pozitron emisyon tomografisi/bilgisayarlı tomografi (^{18}F-FDG-PET/BT), onkolojide ve enfeksiyon hastalıklarında önemli bir görüntüleme yöntemidir ve özellikle sebebi bilinmeyen ateş vakalarında mantar enfeksiyonlarının teşhisinde ve yönetiminde geleneksel görüntülemeyi geride bırakır. Karaciğer, dalak ve sol böbrek dahil olmak üzere çeşitli organlarda yaygın kandidiyazis ile uyumlu ^{18}FDG-avid lezyonları saptanan, inatçı ateşi olan genç bir lösemili hasta sunulmaktadır. Bu olgu, karaciğer biyopsisi gibi invaziv prosedürlerin zor veya kontrendike olduğu durumlarda F-FDGPET/BT kritik rolünü vurgulamaktadır. Bu tür durumlar, özellikle immün sistemi baskılanmış ve hematolojik maligniteleri olan hastalarda doğru tanı ve tedavi için gelişmiş görüntüleme tekniklerinin kullanılmasının son derece önemli olduğunu vurgular. Bu olgu, ^{18}F-FDG-PET/BT'nin invaziv olmayan bir tanı aracı olarak önemli katkısını, hasta bakımını geliştirmesini ve zorlu tıbbi koşullar altında daha etkili yönetim stratejilerine olanak sağlamasını vurgular.

Anahtar kelimeler: Kandidiyazis, florodeoksiglukoz, pozitron emisyon tomografisi/bilgisayarlı tomografi, sebebi bilinmeyen ateş

Address for Correspondence: Yassir Benameur MD, Mohammed V Military Teaching Hospital, Clinic of Nuclear Medicine; Mohamed V University Faculty of Medicine and Pharmacy, Rabat, Morocco

E-mail: benameur.yassir@gmail.com **ORCID ID:** orcid.org/0000-0003-4611-1753

Received: 09.10.2023 **Accepted:** 28.01.2025 **Publication Date:** 03.05.2025

Cite this article as: Benameur Y, Hammani A, Doghmi K, Doudouh A. Disseminated candidiasis on FDG-PET/CT. Mol Imaging Radionucl Ther. 2025;34:165-167.

Introduction

The prevalence of disseminated candidiasis has steadily increased over the last thirty years, emerging as a notable complication in neutropenic patients and those undergoing cancer treatments (1). This infection constitutes a significant contributor to morbidity and mortality among individuals at high risk (1). According to several studies, ^{18}F-fluorodeoxyglucose positron emission tomography/computed tomography (^{18}F-FDG-PET/CT) proves valuable in identifying sites of disseminated candidiasis and evaluating the effectiveness of antifungal treatment (2,3).

Case Report

An 18-year-old man was admitted to the hematology department with Philadelphia chromosome-negative acute lymphoblastic leukemia. He underwent chemotherapy protocol using idarubicin and aracytine. On the 16th day of treatment, the patient developed a fever along with severe neutropenia and thrombocytopenia. As a precaution, he was isolated, and we initiated treatment with broad-spectrum antibiotics targeting gram-negative bacteria. Physical examination revealed no abnormalities, except for mild hepatomegaly. Blood cultures yielded negative results. After 72 hours, the patient continued to experience fever despite antibiotic treatment and developed abdominal pain. Repeated bone marrow aspiration and immunophenotyping of bone marrow cells revealed no blasts. A CT scan revealed multiple low-density lesions in the liver. A liver biopsy was not performed due to the patient's very low platelet count and the associated risk of bleeding.

The patient underwent an ^{18}F-FDG PET/CT to identify the cause of persistent fever, revealing multiple lesions with high metabolic activity in the liver, spleen, and left kidney (Figure 1). At that time, serum beta-d-glucan (BDG) were measured at 65 pg/mL (normal range: 60 to 79 pg/mL). Despite the absence of clinical symptoms and the borderline serum BDG levels, the exceptional pattern observed on the PET/CT, characterized by intense ^{18}F-FDG avid lesions in the liver, spleen, and left kidney, suggested hepatic, splenic, and left renal candidiasis. Antifungal treatment was initiated, leading to a gradual resolution of symptoms. Unfortunately, the patient's condition deteriorated dramatically, marked by the onset of cerebral hemorrhage, and the patient succumbed.

Discussion

Fungal infections can impact mucous membranes, giving rise to conditions such as esophagitis, vulvovaginitis, or keratitis, all of which may entail significant complications.

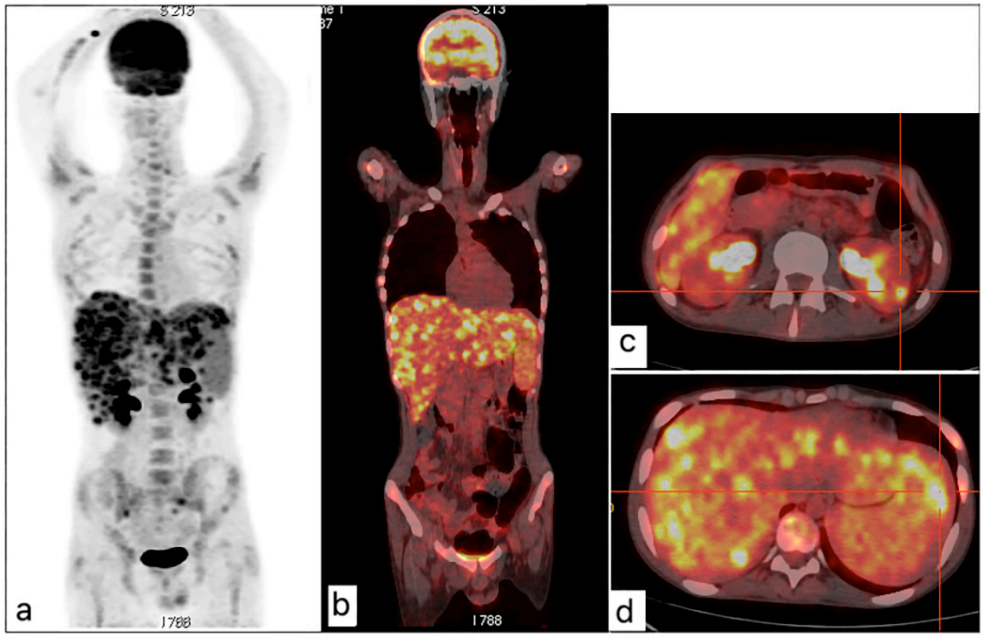

Figure 1. FDG-PET/CT images (a: MIP Maximum intensity projection, b: coronal, c, d: the transaxial) revealed intense FDG avid foci disseminated in the liver, spleen, and cortex of the upper pole of the left kidney, this activity is distinct from the normal tracer activity observed in the medulla and collecting system
FDG: Fluorodeoxyglucose, PET/CT: Positron emission tomography/computed tomography, MIP: Maximum intensity projection

If the fungal infection advances into the deeper tissues of the body, it can result in invasive fungal disease, posing a substantial risk of morbidity and mortality (4). Disseminated candidiasis is a severe and feared invasive fungal disease, often seen in patients undergoing intensive chemotherapy for acute leukemia (5). The liver is the organ most frequently affected given its exposure to the largest inoculum through the portal system (6). The primary clinical manifestation of disseminated candidiasis in neutropenic patients is an isolated fever that does not respond to broad-spectrum antibacterial therapy (7). The diagnostic challenge arises from the atypical clinical presentation, often marked by fever of unknown origin and a decline in general condition in immunocompromised patients. These conditions contraindicate certain invasive explorations, notably biopsies, as was the case with our patient. In such scenarios, FDG-PET/CT proves valuable as a whole-body imaging modality, playing a crucial role in the initial diagnosis. It provides comprehensive information from various body sites, allowing for a metabolic map that accurately delineates the disease burden and identifies concealed lesions of invasive fungal disease (8). Studies have shown that FDG-PET/CT has the capability to detect all infectious sites, particularly deep-seated ones, with a sensitivity superior to that of other conventional imaging modalities (9,10). It is also valuable in therapeutic assessment, aiding in the identification of the most effective antifungal treatment. In this context, FDG-PET/CT for monitoring therapy probably represents the most potent use of PET/CT, acting as a non-invasive marker of disease. It utilizes standard uptake value and other metabolic indices to offer a semi-quantitative assessment of disease activity within lesions (8). In disseminated candidiasis, FDG-PET/CT typically reveals FDG-avid focal and small lesions in the liver and spleen, and exceptionally in the kidneys (11), as observed in our case. Indeed, FDG-PET/CT lacks specificity and has its limitations, particularly due to the physiological accumulation of tracer in certain anatomical sites (such as the brain, heart, and FDG excretion by the kidneys). Nontheless, it remains a valuable whole-body examination, facilitating the identification of suitable biopsy sites in cases of diagnostic uncertainty or avoiding it when contraindicated, as seen in this patient's case. The diagnosis of disseminated candidiasis was established by evaluating the appearance on the PET-FDG scan, the hypodense lesions in the liver observed on the CT scan, and the blood level of D-glucan.

Conclusion

This particular case is noteworthy, illustrating the use of ^{18}F-FDG PET/CT in the diagnosis of fungal infection to identify the sites of disseminated Candida infection. Additionally, it highlights its utility in guiding subsequent patient management, particularly in situations where a biopsy may not be feasible. However, further studies are needed to assess its precise role in the management algorithm.

Ethics

Informed Consent: Written informed consent was obtained from the patient for publication of this case report and accompanying images.

Footnotes

Authorship Contributions

Surgical and Medical Practices: Y.B., A.H., K.D., A.D., Concept: Y.B., A.D., Design: Y.B., A.D., Data Collection or Processing: Y.B., A.D., Analysis or Interpretation: Y.B., A.D., Literature Search: Y.B., Writing: Y.B.

Conflict of Interest: No conflicts of interest were declared by the authors.

Financial Disclosure: The authors declare that this study has received no financial support.

References

1. Mohammadi R, Foroughifar E. Candida infections among neutropenic patients. Caspian J Intern Med. 2016;7:71-77.
2. Avet J Jr, Granjon D, Prevot-Bitot N, Isnardi V, Berger C, Stephan JL, Dubois F. Monitoring of systemic candidiasis by 18F-FDG PET/CT. Eur J Nucl Med Mol Imaging. 2009;36:1900.
3. Xu B, Shi P, Wu H, Guo X, Wang Q, Zhou S. Utility of FDG PET/CT in guiding antifungal therapy in acute leukemia patients with chronic disseminated candidiasis. Clin Nucl Med. 2010;35:567-570.
4. Köhler JR, Casadevall A, Perfect J. The spectrum of fungi that infects humans. Cold Spring Harb Perspect Med. 2014;5:a019273.
5. Thaler M, Pastakia B, Shawker TH, O'Leary T, Pizzo PA. Hepatic candidiasis in cancer patients: the evolving picture of the syndrome. Ann Intern Med. 1988;108:88-100.
6. Albano D, Bosio G, Bertoli M, Petrilli G, Bertagna F. Hepatosplenic candidiasis detected by (18)F-FDG-PET/CT. Asia Ocean J Nucl Med Biol. 2016;4:106-108.
7. Rammaert B, Desjardins A, Lortholary O. New insights into hepatosplenic candidosis, a manifestation of chronic disseminated candidosis. Mycoses. 2012;55:e74-84.
8. Ankrah AO, Lawal IO, Dierckx RAJO, Sathekge MM, Glaudemans AWJM. Imaging of invasive fungal infections- the role of PET/CT. Semin Nucl Med. 2023;53:57-69.
9. Douglas AP, Thursky KA, Worth LJ, Drummond E, Hogg A, Hicks RJ, Slavin MA. FDG PET/CT imaging in detecting and guiding management of invasive fungal infections: a retrospective comparison to conventional CT imaging. Eur J Nucl Med Mol Imaging. 2019;46:166-173.
10. Leroy-Freschini B, Treglia G, Argemi X, Bund C, Kessler R, Herbrecht R, Imperiale A. 18F-FDG PET/CT for invasive fungal infection in immunocompromised patients. QJM. 2018;111:613-622.
11. Teyton P, Baillet G, Hindié E, Filmont JE, Sarandi F, Toubert ME, Moretti JL. Hepatosplenic candidiasis imaged with F-18 FDG PET/CT. Clin Nucl Med. 2009;34:439-440.